THE ROLE OF PIK3R1 IN THE REGULATION OF ADIPOSE TISSUE INSULIN SENSITIVITY

by

ZACHARY STEPHEN CLAYTON

A DISSERTATION

Presented to the Department of Human Physiology
and the Graduate School of the University of Oregon
in partial fulfillment of the requirements
for the degree of
Doctor of Philosophy

June 2018

DISSERTATION APPROVAL PAGE

Student: Zachary Stephen Clayton

Title: The Role of *Pik3r1* in the Regulation of Adipose Tissue Insulin Sensitivity

This dissertation has been accepted and approved in partial fulfillment of the requirements for the Doctor of Philosophy degree in the Department of Human Physiology by:

Carrie E. McCurdy, PhD	Advisor
John R. Halliwill, PhD	Core Member
Hans C. Dreyer, PhD	Core Member
Annie Zemper, PhD	Institutional Representative

and

Sara D. Hodges	Interim Vice Provost and Dean of the Graduate School

Original approval signatures are on file with the University of Oregon Graduate School.

Degree awarded June 2018.

DISSERTATION ABSTRACT

Zachary Stephen Clayton

Doctor of Philosophy

Department of Human Physiology

June 2018

Title: The Role of *Pik3r1* in the Regulation of Adipose Tissue Insulin Sensitivity

Obesity is a burgeoning health crisis in the United States. Obesity is associated with an earlier and greater risk for developing metabolic diseases. Insulin resistance is a central and defining feature of the metabolic diseases associated with obesity.

Class 1a Phosphatidylinositol 3-kinase (PI3K) is integral in canonical insulin signaling. PI3K contains regulatory (p85α/β, p55α/γ, p50α) and catalytic (p110α/β/δ) subunits. The α regulatory subunits are encoded by *Pik3r1*. Increased *Pik3r1* abundance has been observed in obese white adipose tissue (WAT). Furthermore, obese mice with heterozygous (HZ) knockout of *Pik3r1* remain insulin sensitive, despite marked obesity.

Taken together, it is crucial to understand the role of WAT *Pik3r1* in regulating insulin sensitivity. Recently, literature has demonstrated that standard vivarium temperature (~22°C) is a thermal stress for mice, as their thermoneutral zone is ~30°C. Considering mice are a preclinical model for studying metabolic disease, it is critical to understand cellular and systemic responses to high fat diet (HFD) at 22°C and 30°C.

To determine the role of AT *Pik3r1* in regulating insulin sensitivity, mice with constitutive and inducible adipocyte specific hetero/homozygous knockout of *Pik3r1* were studied following acute (three days) and chronic (12 week) HFD, respectively. Furthermore, insulin sensitivity was assessed in mice with adipocyte specific

overexpression (OX) of p55α. To determine the influence of short-term (8 and 12 days) thermoneutral housing on insulin sensitivity, mice were studied following one and five days of HFD at 22°C and 30°C (one week acclimation at 30°C prior to starting HFD).

Visceral WAT p85α abundance was increased (2-fold) following acute HFD in wild-type mice, with a parallel increase in systemic insulin resistance. HZ knockout of adipocyte *Pik3r1* prevented acute HFD induced systemic insulin resistance. Furthermore, HZ knockout of adipocyte *Pik3r1* reversed obesity induced glucose intolerance and enhanced systemic insulin sensitivity and adipocyte insulin signaling. Moreover, OX of adipocyte p55α enhanced (40%) glucose tolerance, energy expenditure (30%: light cycle; 45%: dark cycle) and markers of AT thermogenesis in brown AT. Lastly, housing temperature had a significant impact on the cellular pathways that regulate glucose metabolism in response to HFD exposure. This dissertation includes previously published co-authored material.

CURRICULUM VITAE

NAME OF AUTHOR: Zachary Stephen Clayton

GRADUATE AND UNDERGRADUATE SCHOOLS ATTENDED:

University of Oregon, Eugene, OR
San Diego State University, San Diego, CA

DEGREES AWARDED:

Doctor of Philosophy, Human Physiology, 2018, University of Oregon
Master of Science, Exercise Physiology, 2013, San Diego State University
Master of Science, Nutritional Science, 2013 San Diego State University
Bachelor of Science, Foods and Nutrition, 2012, San Diego State University

AREAS OF SPECIAL INTEREST:

The role of adipose tissue in maintaining metabolic health throughout lifespan

The role of food as medicine

PROFESSIONAL EXPERIENCE:

Graduate Employee, Dr. Carrie E. McCurdy, Department of Human Physiology, University of Oregon 2014-2018

Graduate Employee, Dr. Mark Kern, Department of Exercise and Nutritional Science, San Diego State University, 2012-2013

Undergraduate Research Assistant, Dr. Mark Kern, Department of Exercise and Nutritional Science, San Diego State University, 2010-2012

GRANTS, AWARDS, AND HONORS:

International Union of Physiological Sciences travel award for the American Physiological Society for the 38th annual IUPS Congress, Rio de Janeiro, Brazil, 2017. Not accepted

Food Studies Graduate Research Grant, University of Oregon, 2016

Eugene and Clarissa Evonuk Memorial Graduate Fellowship in Environmental, Cardiovascular, or Stress Physiology, The role of *pik3r1* in the regulation of adipose tissue insulin sensitivity, University of Oregon, 2016

Campbell Poster Award Finalist, American Physiological Society, Endocrinology and Metabolism Section, Experimental Biology, 2015

Kasch-Boyer Endowed Scholarship in Exercise and Nutritional Sciences. San Diego State University, 2013

Gatorade Sports Science Institute's Student Grant Program, L-glutamine supplementation: Ergogenic potential and its effect on plasma glutamine throughout repeated bouts of exercise, 2013

PUBLICATIONS:

Clayton ZS, McCurdy CE. Thermoneutral housing influences glucose metabolism and markers of adipose tissue browning in response to short-term overfeeding in lean mice. In Press.

Ely BR, **Clayton ZS**, McCurdy CE, Pfeiffer J, Minson CT. Meta-inflammation and cardiometabolic disease in obesity: Can heat therapy help? *Temperature*. 2017 Nov 10; 5(1):9-21

Clayton ZS, Fusco E, Kern M. Egg consumption and heart health: A review. *Nutrition.* 2017 May 37:79-85

Clayton ZS, Wilds GP, Mangum JE, Hocker AD, Dawson S. Do targeted written comments and rubric method of delivery affect performance on future human physiology lab reports? *Advances in Physiology Education.* 2016 Sep 40(3):359-364

Clayton ZS, Hobb K, Schelechi M, Hernandez LM, Barber A, Petrisko Y, Hooshmand S, Kern M. Influence of resistance training combined with daily consumption of an egg-based or bagel-based breakfast on risk factors of chronic diseases in healthy untrained individuals. *Journal of the American College of Nutrition*. 2015 Mar 18:1-7

ACKNOWLEDGMENTS

I wish to express sincere appreciation to Dr. Carrie E. McCurdy for her scientific mentorship and guidance. You provided me with immense opportunities, and I am forever grateful. I would like to thank the members of the McCurdy lab for their insightful input throughout my doctoral studies. The day-to-day friendly banter made things more exciting and enhanced comradery in the lab. I would like to thank Dr. Simon Schenk for allowing me to volunteer in his lab at the University of California San Diego, while I was pursuing my MS degrees at San Diego State University. His patients in teaching me how to perform oral glucose tolerance tests in mice will never be forgotten. Furthermore, I would like to thank Dr. Schenk for connecting me with Dr. McCurdy. I would like to express sincere gratitude to Drs. Shirin Hooshmand and Mark Kern for believing in an undergraduate nutrition student that, at the time, just wanted to see what research was all about. You both instilled in me a passion for my work, as well as the awareness to cherish all the relationships I build along the way. I would not be where I am today without the love and encouragement from my mother and father. Mom, you are two wings short of being an angel and I am forever grateful for the blessings you have brought and continue to bring to my life. Dad, although you are gone, your love, strength and encouragement will remain with me forever. Thank you for showing me what it means to work for everything you want in life. I could not have completed this work without the support of my loving wife, Marissa. You are my favorite person to do science with, train with, dog parent with and do life with.

My dissertation is dedicated to my wife, Marissa, mother, Cindy, and my late father, Jerry. You are all my heroes.

TABLE OF CONTENTS

LIST OF FIGURES

Figure Page

Figure Page

CHAPTER I

INTRODUCTION AND LITERATURE REVIEW

Introduction

Obesity is a progressive disease that is a result of prolonged positive energy balance. The increased prevalence of obesity has directed attention on a worldwide problem that is one of surplus, rather than one of famine or virus. In the United States, obesity is a burgeoning health crisis, with only 30% of adults considered to be of 'normal weight' (16), and similar trends are being observed worldwide (1). Considering obesity increases the risk of complex and costly metabolic diseases including type 2 diabetes, cardiovascular disease, stroke and non-alcoholic fatty liver disease as well as certain cancers (31), it is one of the greatest public health challenges in the United States (14). At the turn of this century, 171 million individuals were estimated to have diabetes; this is expected to increase to 366 million by 2030 (46).

Insulin resistance is a central and defining feature of obesity (31) that is proposed to be a consequence of increased adipose tissue inflammation. Insulin resistance is defined as an inadequate response by insulin target tissues, such as skeletal muscle, liver, and white adipose tissue, to the physiologic effects of circulating insulin. The hallmarks of impaired insulin sensitivity in these three target tissues are decreased insulin-stimulated glucose uptake into skeletal muscle, impaired insulin-mediated suppression of hepatic glucose production, and a reduced ability of insulin to inhibit lipolysis and increase glucose uptake in adipose tissue. In type 2 diabetes, it has been widely established that insulin resistance precedes the development of evident hyperglycemia (37). Thus, targeting interventions

that regulate insulin sensitivity may be crucial in preventing the progression of other metabolic diseases.

Although the pathogenesis of insulin resistance in obesity is multifactorial, it is clear that chronic, low-grade inflammation is a major contributor, with the proinflammatory macrophage identified as the primary stimulus (28). Mechanistically, the current model for insulin resistance in obesity suggests that adipose tissue macrophage (ATM) infiltration and proinflammatory cytokine release activates inflammatory pathways such as inhibitor of kappa B kinase β (IKKβ) and Jun NH_2-terminal kinase (JNK), which impinge upon the insulin signaling cascade by inhibiting tyrosine phosphorylation of insulin receptor substrate 1 (IRS1), leading to impaired insulin activation of Phosphatidylinositol 3-Kinase (PI3K) and Akt (28).

PI3K, a heterodimeric enzyme composed of a regulatory subunit (p85α/β, p55α/γ, p50α) and a catalytic subunit (p110α/β), is an essential component of the canonical insulin signaling cascade in adipose tissue (15). Insulin-stimulated PI3K activity is decreased in obese adipose tissue in parallel with a 1.5, 4, and 3 -fold increase in p85α, p55α and p50α abundance, respectively (26); heterozygous deletion of *Pik3r1* limits regulatory subunit expression, enhances adipocyte insulin signaling and protects against adipose tissue macrophage accumulation (26). Additionally, genetic deletion of p55α/ p50α in mice has been shown to increase adipocyte insulin-stimulated glucose uptake and systemic insulin sensitivity (8).

The developmental niche, anatomical distribution, and abundance of particular white adipose tissue depots have been shown to influence systemic glucose tolerance, insulin sensitivity and inflammation (32). Furthermore, brown fat and the propensity of

white adipose tissue to adopt a brown-like phenotype has been shown to influence systemic glucose tolerance and insulin sensitivity. Standard mouse vivarium temperature is set below the murine thermoneutral zone (30°C), which may be a thermal stress. Housing temperature has been shown to influence brown adipose tissue development, white adipose tissue browning, inflammation and energy expenditure. Thus, it is critical to understand the relationship between environmental temperature and adipose tissue browning, inflammation and insulin sensitivity.

Background and Significance

Obesity and insulin resistance.

In Western cultures, obesity is one of the most common acquired factors causing insulin resistance (31). Glucose levels may remain relatively normal in an insulin resistant state due to the presence of a robust compensatory insulin secretory response. However, when insulin-producing pancreatic β cells can no longer compensate for the decreased tissue insulin sensitivity, glucose homeostasis deteriorates and impaired glucose tolerance and eventually type 2 diabetes develop. Insulin resistance is marked by impaired cellular insulin action in its target tissues (30).

Obesity is a progressive disease that develops due to prolonged positive energy balance. Interestingly however, brief (3 and 7 d) caloric overfeeding rapidly induces systemic glucose intolerance and insulin resistance (22; 9; 45) independent of significant changes in body weight. Conversely, calorie restriction without significant changes in body weight, enhances skeletal muscle (7; 19) and liver (19) insulin sensitivity. Thus, significant changes in insulin action can occur with small changes in energy balance, without substantial weight change, and within a relatively short period of time. The fact that insulin sensitivity can be modulated so quickly raises important questions, such as, why and how are these tissues so sensitive to slight perturbations in nutritional cues?

In skeletal muscle and adipose tissue, an increase in insulin promotes glucose uptake by activating a complex cascade of signaling events (38; 41). Briefly, binding of insulin to the insulin receptor leads to downstream tyrosine phosphorylation of protein substrates that then engage and activate PI3K. This leads to downstream signaling through Akt, which results in GLUT4 translocation from its intracellular pool to the plasma

membrane and glucose transport into the cell (41). In adipose tissue, insulin is also anti-lipolytic, whereby it inhibits the release of fatty acids and glycerol from adipocytes by decreasing the activity of hormone-sensitive lipase (11). In the liver, insulin decreases the release of glucose by inhibiting hepatic glycogenolysis (glycogen breakdown to glucose) and the expression of key gluconeogenic enzymes (44).

ii. White adipose tissue biology as it relates to obesity and insulin resistance.

White adipose tissue was once thought to be strictly a sight for triacylglycerol storage and maintenance of energy equilibrium, but is now considered to function as an endocrine organ (43). Adipocyte functionality is lost during obesity and has been related to adipocyte hyptertrophy, imbalance between lipolysis and lipogenesis leading to lipotoxicity and an inability to respond to external signals, such as insulin (32). Furthermore, the specific site of white adipocyte dysfunction plays a significant role in the development of associated metabolic diseases (32).

White adipose tissue develops in multiple discrete depots throughout the body. The most common classification scheme of white adipose tissue distinguishes between subcutaneous and visceral adipose tissue (32). There is a wealth of literature supporting the positive association of visceral adipose tissue with metabolic disease, whereas less is known about the role of subcutaneous adipose tissue, but it may be inversely related (21). Important to note, many adipose tissue depots in mice do not have defined correlates in humans, and vice versa; for example, visceral fat in humans is commonly stored in the omentum, which is hardly present in rodents. Conversely, the epididymal fat pads in male mice that are commonly assayed for visceral adipose tissue metabolism and inflammation, do not exist in humans (32).

Despite the distinctions between human and rodents, there are clearly regional differences in adipocyte function, such as secretory profiles and rates of insulin stimulated suppression of lipolysis and triglyceride storage (40). Two hypotheses have emerged as a means of explaining the differences between subcutaneous and visceral adipose tissue: either (1) each depot has a specific relationship with circulation or (2) physiology is predicated on cell autonomous differences. For example, gene signatures of pre adipocytes are specific to their tissue of origin, even after multiple passages (23; 39). Furthermore, transplantation studies have directly assessed this by placing visceral adipose tissue in the subcutaneous space, which had minimal effect, but transplantation of subcutaneous adipose tissue to the visceral space results in decreased adiposity and enhanced glucose metabolism (42). Taken together, there are clear molecular and physiological distinctions between visceral and subcutaneous adipose tissue, demonstrating the importance to study each depot individually when implementing interventions that have a profound effect on adiposity and glucose metabolism, such as high fat diet treatment.

Recently, the developmental niche of adipose tissue has been a topic of investigation in an attempt to better understand the innate differences between the distinct depots. All adipocytes develop from pre-adipocytes, which initially develop from hematopoietic precursors (32). In a state of energy surplus, subcutaneous adipocytes expand through both hyperplasia and hypertrophy (17), while epididymal adipocytes expand strictly through hypertrophy (17). Relative to hyperplasia, adipocyte hypertrophy is associated with increased metabolic dysfunction due to larger adipocytes having greater rates of lipolysis, macrophage chemotaxis and insulin resistance (17).

Distinct from white adipose tissue, brown adipose tissue (BAT) is multilocular rather than unilocular, and shares a development lineage with skeletal muscle (originate from $Pax7^{+}/Myf5^{+}$ stem cells) and not WAT (originate from $Pax7^{-}/Myf5^{-}$ stem cells) (34). BAT has been highly studied as a therapeutic target to offset obesity due to expression of uncoupling protein-1 (UCP1), which circumvents ATP synthase to generate heat from glucose and lipid oxidation (20). UCP1 ablation induces obesity and abolishes diet-induced thermogenesis (13). BAT is positively associated with energy expenditure (5), glucose tolerance (36) and insulin sensitivity (36). Cold exposure in rodents has been shown to increase brown fat abundance, *Ucp1* expression in brown and white adipose tissue and increase the number of multilocular cells in white adipose tissue (5). Interestingly, subcutaneous WAT appears to be more susceptible than epdidymal WAT to cold-induced browning (35).

Taken together, it is clear there are cell autonomous roles of each adipose tissue depot (subcutaneous WAT, epididymal WAT and BAT), and it is imperative to understand these differences when studying adipose tissue. Furthermore, considering the adiponectin-Cre mouse is commonly used to cross with transgenic and knockout (KO) mouse models to determine adipocyte specific roles of genes and proteins, it is important to be mindful that adiponectin is also expressed in BAT. Considering the dynamic role of BAT in regulating obesity and insulin sensitivity, BAT must not be overlooked when interpreting findings from AT specific OX and KO models.

Adipocyte specific mouse models.

The study of adipose tissue has been significantly advanced through use of genetic mouse models. The use of the Cre/lox system for gene targeting has

revolutionized the study of tissue specific functions *in vivo*. Cre recombinase may be integrated downstream of an endogenous promotor, or it can be placed under control of a promoter fragment which is then integrated into the genome at a random site. Additionally, temporal control over gene expression can be gained by use of tamoxifen-sensitive Cre. When applying these techniques, it is imperative to keep in mind the limitations of these approaches including variable expression of Cre transgenes and the varying sensitivity of different genomic sites to Cre-mediated loxP recombination (5, 8).

To facilitate the study of adipocyte specific functions *in vivo*, several adipocyte-specific promotors have been generated to drive the expression of Cre recombinase in adipose tissue. Of these, commonly used Cre transgenes were generated from the promotor of the fatty acid binding protein 4 (*Fabp4*) gene which encodes adipocyte protein 2 (aP2) (3). However, aP2-Cre has been shown to have Cre activity in other tissues and cell types, including brain, endothelial cells, macrophages, adipocyte precursors and embryonic tissues (6, 7, 9, 12). The discovery of white adipose tissue's capacity to secrete a variety of hormones, including adiponectin, has guided further development of adipocyte-specific Cre mouse models. Adiponectin has been shown to selectively localize to the adipocyte (1), making it a potential target for creating adipocyte-specific Cre mouse models.

Adiponectin (encoded by *Adipoq)* has been used to generate Cre lines to study adipocyte function (13). These Adiponectin-Cre lines have been shown by multiple groups to be highly specific to adipose tissue (2, 6, 7). Utilization of the membrane-Tomato/membrane-GFP (mT/mG) dual fluorescent reporter has been used to determine tissue specific recombination (4). Using the mT/mG further supported previous findings

(6, 7, 9, 12) that aP2-Cre does not label the majority of adipocytes in white adipose tissue depots (4). These data may be explained by a shift in the Cre expression pattern in these lines over generations (5), which demonstrates the need to monitor the level of recombination over time. Furthermore, these data highlight the importance of determining tissue specificity within any Cre model system. Alternatively, adipocyte specific recombination was shown in the Adipoq-Cre mouse line, when using the mT/mG reporter (4). Furthermore, the Adiponectin-CreER line was shown to be efficient in targeting adipocytes in an inducible manner (4). However, recent reports have shown adiponectin to also be expressed in intestinal epithelial paneth cells (11).

When using constitutive Cre mouse models, the development of the target promotor must be considered to ensure developmental differences are considered when interpreting results. Adipoq-Cre is active during fetal inguinal white adipose tissue adipocyte differentiation and in fully mature adipocytes (not pre-adipocytes) in adult animals (10). Taken together, one should consider how the protein under investigation may influence adipocyte differentiation, if differences in adipose tissue mass and/or distribution are observed.

Phosphatidylinositol 3-Kinase.

Class 1a PI3K is lipid kinase that catalyzes the production of plasma membrane-bound phosphatidylinositol-3,4,5-triphosphate from phosphatidylinositol-4,5-biphosphate **(6)**. The enzyme contains a catalytic (p110 α, β, δ) and regulatory (p85α a/β, p55 α/ϒ, p50α) subunits. Class 1a regulatory subunits are encoded by the *Pik3r1* gene. (Figure 1.) Of the Class 1a PI3K regulatory subunits, p85α is the most abundant (12), thus it has historically been the primary focus of the studies assessing the role of the regulatory

subunits in insulin signaling (4; 18). Whole body knockout of p85α results in significantly improved systemic insulin sensitivity and protects against HFD induced insulin resistance (3; 27). Alternatively, increased expression of p85 α triggers severe insulin resistance (3). Taken together, it is theorized that the regulatory subunits exist as either monomers or as heterodimers bound to the p110 catalytic subunit (p85-p110, p55-p110, p50-p110) (8; 24). During insulin stimulation, when functional PI3K heterodimers bind to Insulin Receptor Substrate-1 (IRS-1), normal insulin signaling occurs, however; the theory suggests that when monomeric regulatory subunits bind to IRS-1, insulin signaling is competitively inhibited (8; 24). Thus, excess regulatory subunits of PI3K may cause decreased insulin sensitivity and are indeed elevated in obese skeletal muscle and adipose tissue (2; 26). To date however, over-expression of the specific Class 1a PI3K regulatory subunits has not been directly tested *in vivo*.

Clinical studies have shown a significant induction of p85α in skeletal muscle after as little as three days of positive energy balance with a parallel decrease in systemic insulin sensitivity as measured by hyperinsulinemic-euglycemic clamps (10). Moreover, three days of high-fat diet significantly impairs systemic glucose tolerance and insulin sensitivity in rodents, but the effect on PI3K is unknown (22). Alternatively, caloric restriction in rodents enhances skeletal muscle glucose transport in parallel with decreased abundance of p55α/p50α and enhanced PI3K activity (25; 33). Caloric restriction has also shown to significantly improve insulin-stimulated glucose uptake in primary adipocytes (29). Thus, perturbations in the PI3K ratio of regulatory to catalytic subunit abundance may be the molecular mechanism connecting cellular insulin sensitivity to cellular energy status.

Specific Aims

<u>AIM 1.</u> Investigate *in vivo* if increased adipocyte *pik3r1* abundance is necessary to drive adipocyte and systemic insulin resistance. The primary research question addressed in AIM1 is: Can heterozygous knockout of adipose tissue *pik3r1* prevent initiation of adipose tissue insulin resistance with acute high-fat diet?

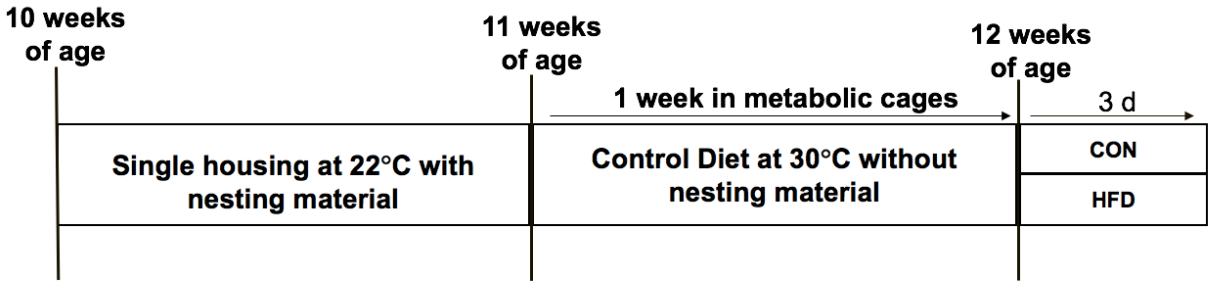

<u>AIM 2.</u> Investigate *in vivo* if temporal heterozygous knockout of adipocyte *pik3r1* reverses obesity induced insulin resistance and adipose tissue inflammation. The primary research question addressed in AIM2 is: Following the development of obesity, can heterozygous knockout of adipocyte *pik3r1* reverse obesity induced insulin resistance, independent of weight and adiposity, as well as enhance adipocyte and systemic insulin sensitivity?

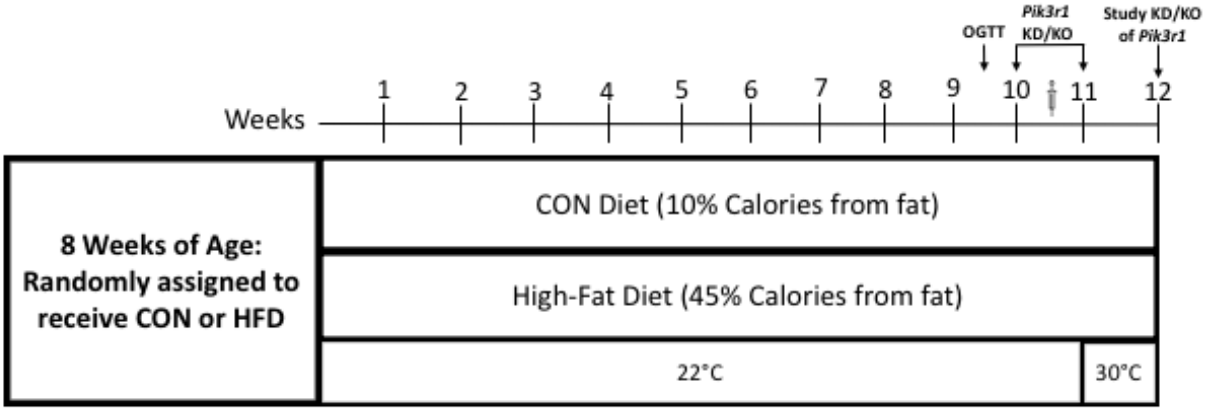

<u>AIM 3.</u> Investigate *in vivo* if adipocyte overexpression of PI3K p55alpha drives insulin resistance in lean mice. The primary research question addressed in AIM3 is: Is overexpression of adipocyte PI3K p55α sufficient to drive adipose tissue and systemic insulin resistance in chow fed mice, lean mice?

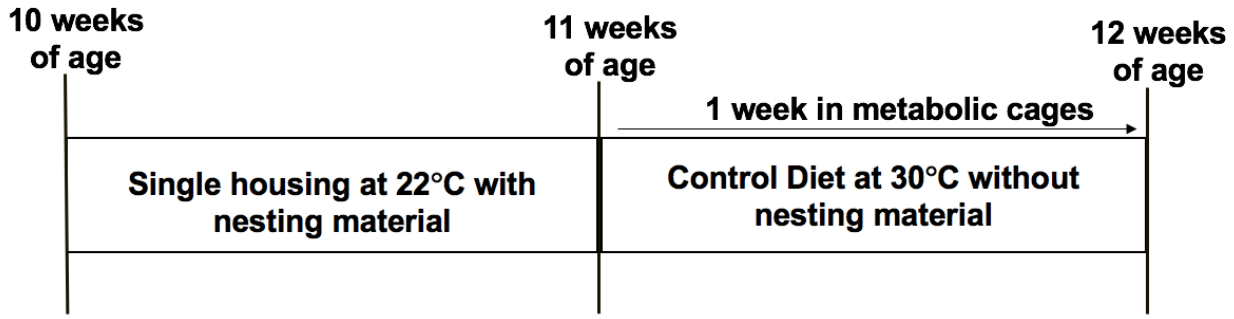

<u>AIM4.</u> Investigate the role of housing temperature in the regulation of glucose metabolism and markers of adipose tissue browning in response to short-term overfeeding in lean wild type mice. The primary research question addressed in AIM4 is: Does housing temperature influence glucose metabolism and inflammation following short-term high-fat diet feeding.

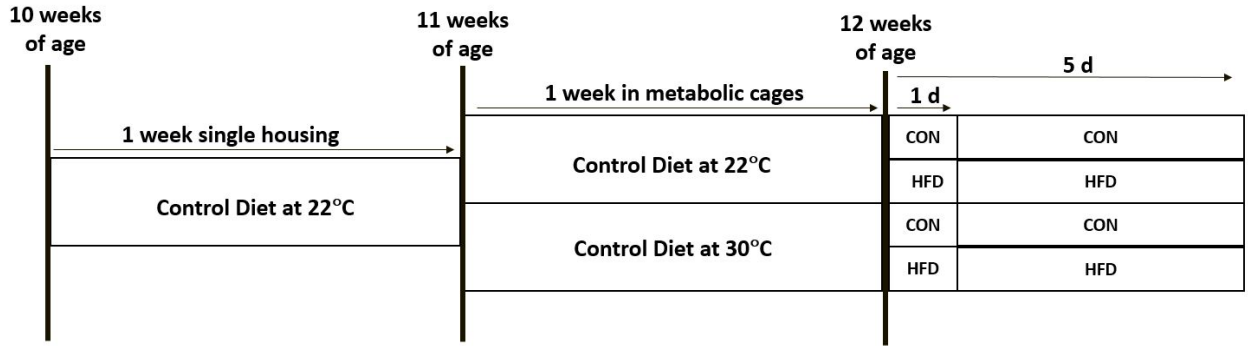

Chapter V of this dissertation has previously been published.

CHAPTER II

HETEROZYGOUS KNOCKOUT OF PIK3R1 PROTECTS AGAINST ACUTE HIGH FAT DIET INDUCED GLUCOSE INTOLERANCE AND INSULIN RESISTANCE

Introduction

Obesity and its reciprocal metabolic diseases are a burgeoning health crisis in the United States, with approximately 40% of US adults classified as obese (8). Insulin resistance, a central and defining component of obesity, has been identified as a primary contributor to the increase in a multitude of metabolic diseases (6). Brief (3 and 7 day) caloric overfeeding, resulting in a positive energy balance, rapidly induces systemic glucose intolerance and insulin resistance, independent of changes in body weight or adiposity (5; 9; 20). Thus, changes in insulin sensitivity can be modulated quickly, but the driving mechanism is unknown. Phosphotidylinositol 3-kinase (PI3K) is a critical node in canonical insulin signaling, and is essential for a multitude of cellular functions and is critical for nearly all of insulin's metabolic actions including glucose transport, lipid metabolism, and glycogen and protein synthesis (3). In adipocytes, PI3K plays a key role in regulating insulin-stimulated glucose uptake and inhibition of lipolysis (15). A variety of impairments in the aforementioned PI3K-linked pathways are found in obesity (2; 12), suggesting PI3K plays a major role in the progression of insulin resistance.

PI3K is an obligate heterodimer consisting of a regulatory subunit (p85α/β, p55α, p50α) and a catalytic subunit (p110α/β) (19). The regulatory subunits p85α, p55α, p50α are encoded by the *Pik3r1* gene, while p85β is encoded by the *Pik3r2* gene. Studies conducted in cell culture and transgenic mouse models have shown that complete

deletion of the regulatory isoforms (p85α only, p85β only, and p55α/p50α double knockout) or heterozygous (HZ) *Pik3r1* deletion enhances PI3K activity and subsequent insulin sensitivity (4; 7; 18; 17; 12). Furthermore, inhibiting p85α expression improves insulin signaling and glucose homeostasis in obese mice (16), and mice with genetically induced insulin resistance via heterozygous deletion of the insulin receptor (IR) or insulin receptor substrate-1 (IRS1) (11). Global HZ knockout of *Pik3r1,* but not *Pik3r2*, has been shown to enhance PI3K enzyme activity and improve systemic and adipocyte insulin sensitivity, despite marked obesity (12). Taken together, there is a clear link between adipose tissue *Pik3r1* abundance and insulin sensitivity.

Here, we investigated the hypothesis that adipocyte specific HZ knockout of *Pik3r1* maintains glucose tolerance and systemic insulin sensitivity, following three-day HFD treatment. To accomplish this, we studied free living metabolic profiles, glucose tolerance and systemic insulin sensitivity in mice with adipocyte specific hetero/homozygous knockout of *Pik3r1* under the control of the constitutive adiponectin promoter. Our results demonstrate that HZ mice, but not KO, maintain glucose tolerance and insulin sensitivity following three-day HFD treatment. Furthermore, KO mice demonstrate decreased energy expenditure during the light and dark cylces, independent of diet treatment. Together, these data support the notion that adipose tissue PI3K is a key step in regulating energy and glucoses homeostasis, as well as insulin sensitivity.

Methods

Experimental Design. All experiments were approved by Institutional Animal Care and Use Committee at the University of Oregon. Mice with a mixed B6/129S background and homozygous for *loxP* sites flanking exon 8 of the *Pik3r1* gene (*Pik3r1*^{tm1Lca}/J; Jackson Laboratory, #012871) (Pik3r1 flox) were used in these studies. Mice with the targeted allele compared to wild type show no difference p85α abundance in the absence of recombinant cre (**1, 10**). To generate mice with adipocyte specific hetero/homozygous knockout of *Pik3r1*, we crossed *Pik3r1* flox mice with mice expressing Cre recombinase (Cre) under the control of the adipose tissue adiponectin promoter (adipo Cre). After Cre-mediated recombination, exon8 of the *Pik3r1* gene is cleaved, specifically in adipocytes. *Pik3r1* flox mice that lacked adipo Cre are referred to herein as wild-type (WT) and were used as controls for all studies. All mice were housed at standard vivarium temperature (22°C) with a 12:12-h light-dark cycles (Light Cycle: 6:00- 18:00; Dark Cycle: 18:00-6:00) and fed chow diet with 13% fat (Picolab Rodent Diet 20; LabDiet) until 10 weeks of age. At ten weeks of age, male mice were singly housed in standard-sized cages and placed within an environmental cabinet set to mouse thermoneutral temperature (30°C) and fed a control diet (CON: 10% Calories from fat; 3.85 kcals/g, D1245OH, Research Diets, New Brunswick, NJ) for one week. After a one week acclimation period, mice were randomly assigned to remain on the CON diet or were provided a high fat diet (HFD; 45% Calories from fat; 4.73 kcals/g, D12451, Research Diets, New Brunswick, NJ). Both the CON and HF diets were matched for sucrose (17%).

Body Composition. Body composition (lean tissue, fat and free fluid) was measured by time domain (TD)-NMR using the Minispec LF50 mouse NMR (Bruker BioSpin,

Billerica MA, state) in un-anaesthetized mice before and after the 3 day period. Percentages were calculated from body weight measured on a standard scale (Mettlor-Toledo, Columbus, OH) using the Minispec Software.

Food Intake and Total Energy Expenditure. Using a metabolic monitoring system (Promethion, Sable Systems, Las Vegas, NV), we measured cage behavior (food intake, water intake and activity), oxygen, carbon dioxide and water vapor during the 12:12-h light-dark cycles (Light Cycle: 6:00- 18:00; Dark Cycle: 18:00-6:00) following three full light and dark cycles. The metabolic cages were kept inside an environmental cabinet allowing temperature control throughout the study. Metascreen software (Sable Systems Inc.) was used for data collection and data was processed with ExpeData (Sable Systems Inc.) proprietary macros. Energy expenditure (kcals/hour) was calculated relative to bodyweight (kg). Food intake (g/day) was converted to kcals/day and made relative to bodyweight (kg).

Oral Glucose Tolerance Test. Glucose tolerance tests were performed in conscious mice following 3d diet treatment. Mice were fasted for 4 h (6-10 AM) before testing to normalize glucose and insulin levels. Tails were nicked with sterile scissors and ~2-5 µl of blood was analyzed with a handheld glucometer (Bayer Contour). After the fasting glucose measurements, the animals were given 5g/kg bodyweight dextrose by oral gavage. Glucose was measured again at 10, 20, 30, 45, 60, 75, 90 and 120 minutes. Glucose area under the curve (AUC) was calculated from baseline glucose values using GraphPad Prsim 7.0.

Insulin Tolerance Test. Insulin tolerance tests were performed in conscious mice following the 3d diet treatment. Mice were fasted for 4h (6-10 AM) before testing to normalize glucose and insulin levels. Tails were nicked with sterile scissors and ~2-5 µl of

blood was analyzed with a handheld glucometer (Bayer Contour). After the fasting glucose measurements, the animals received an intraperitoneal (I.P.) injection of 0.25 U insulin (Humulin-R, Eli Lilly and Company, Indianapolis, IN)/kg bodyweight. Glucose was measured from tail blood again at 10, 20, 30, 40, 50 and 60 minutes.

Immunoblotting. Perigonadal eWAT was homogenized with a BDC 2002 (Compact Digital, Caframo Lab Solutions, Ontario, Canada) at 100mg tissue/ 300μL of homogenization buffer (20mM Tris-HCl pH 7.4, 150mM NaCl, 1% Igepal/NP-40, 20mM NaF, 2mM EDTA pH 8.0, 2.5mM NaPP, 20mM β-glycerophosphate, 10% glycerol with added protease inhibitors (1mg/mL Aprotinin, 1mg/mL Leupeptin, 1mg/mL Pepstatin, 6mg/mL Pefabloc SC, Phosphatase Inhibitor Cocktail 2 and 3 (Sigma Aldrich, San Jose, CA)). Samples were solubilized at 4°C for 1 hour with rotation and centrifuged at 4°C at a speed of 12,000 x g for 15min. Protein abundance was measured by bicinchoninic acid (BCA) assay (Thermo Fisher Scientific, Eugene, OR). Target proteins were measured in tissue homogenates (1 mg/mL) by capillary electrophoresis using a Wes instrument (Protein Simple, Biotechne) with PI3-Kinase p85 (1:25, ABS233; EMD Millipore; Burlington, MA) and with GAPDH (1:1K, 25778; Santa Cruz Biotechnology; Santa Cruz, CA) as a loading control. Data was quantitated using Compass Software (Protein Simple, Biotechne) with target proteins expressed relative to the loading control.

Statistical Analysis. Data were analyzed by a two-way analysis of variance (ANOVA) for main effects of diet and genotype except for the oral glucose tolerance test, which used a repeated measures 2-way ANOVA for main effects of group and genotype. A Sidak's multiple comparisons post hoc test was performed when significant main effect differences were detect using a p-value of ≤ 0.05. All data are presented as the mean ±

standard error of the mean (SEM). Statistics were calculated using Graph Pad Prism version 7 (Graph Pad Software; La Jolla, CA).

Results

Hetero and homozygous knockout of adipocyte Pik3r1 exacerbates three-day high fat diet induced increases in body weight and adiposity. KO mice had a 7.5-fold decrease in eWAT p85α abundance relative to WT, while no difference was detected between WT and HZ mice (Fig. 1*A*). Relative to WT, body weights of HZ and KO mice following CON and HFD diet treatment were 20% and 25% higher, respectively. Furthermore, HZ and KO mice had a 9% increase in body weight between CON and HFD, while no difference was detected in WT mice (Fig. 1*B*). No differences in percent fat mass were detected between genotypes following CON diet treatment; however, relative to WT, HZ and KO mice had a 30% increase in percent fat mass following HFD treatment. Furthermore, HZ and KO mice had a 50% and 30% increase in percent fat mass between CON and HFD, respectively, while no difference was detected in WT mice (Fig. 1*C*). No differences in inguinal scWAT mass were detected between genotypes following CON diet treatment; however, relative to WT, HZ and KO mice had 25% greater inguinal scWAT mass following HFD treatment. No within genotype diet differences were detected in scWAT mass (Fig. 1*D*). Perigonadal eWAT mass increased in KO mice, relative to WT and HZ, independent of diet (Fig. 1*E*). Furthermore, KO mice had 20% lower brown AT (BAT) mass, independent of diet treatment.

Heterozygous and homozygous knockout of adipocyte Pik3r1 alters the mouse behavior and the metabolic and circadian response to HFD. Mouse feeding behavior was changed by both diet and genotype. Specifically, relative to WT and KO mice on CON, HZ CON mice had 2.6 and 1.5-fold greater food intake, respectively (Fig. 2*A*). Relative to WT and KO mice on HFD, HZ mice had 1.5 and 1.8-fold greater food intake,

respectively (Fig. 2*A*). During the dark cycle, WT mice had 1.8-fold greater food intake following HFD treatment (Fig. 2*B*). Furthermore, relative to WT and HZ mice, KO mice had 1.2-fold greater food intake following CON diet treatment during the dark cycle (Fig. 2*B*). RER was lower in WT, HZ and KO mice on HFD during the light cycle (WT: 0.90±0.10 vs. 0.80±0.10; HZ: 0.89±0.20 vs. 0.83±0.10; KO: 0.88±0.10 vs. 0.81±0.20) (Fig. 2*C*). RER was lower in WT, HZ and KO mice on HFD during the dark cycle (WT:0.91±0.01 vs. 0.82±0.01; HZ: 0.94±0.01 vs. 0.81±0.01; KO: 0.90±0.01 vs. 0.81±0.02) (Fig. 2*D*). Furthermore, relative to WT and KO mice on CON diet, HZ mice on CON diet had greater RER (HZ:0.94±0.01 vs. WT:0.91±0.01 and KO:0.90±0.01) (Fig. 2*D*). There were no differences in total activity during the light cycle by diet or genotype (Fig.2, *E-F*). Relative to WT and HZ mice on HFD, energy expenditure was 40% lower in KO mice on HFD during the light cycle (Fig.2, *G*). Furthermore, relative to WT and HZ mice on CON and HFD, energy expenditure was 30% lower in KO mice during the dark cycle (Fig.2, *H*).

Glucose intolerance and insulin resistance is associated with perigonadal eWAT p85α abundance. Following 3d HFD treatment, there was a 2-fold increase in perigonadal eWAT p85α abundance in WT mice (Fig. 3*A*). Relative to CON, fasting blood glucose increased following 3d HFD treatment, by 20% and 25% in WT mice and KO mice, respectively (Fig. 3*B*). Following CON diet treatment, fasting blood glucose was 20% higher in HZ mice, relative to WT (Fig. 3*B*). Furthermore, following HFD treatment, fasting blood glucose was increased by 16% in KO mice, relative to WT and HZ mice (Fig. 3*B*). Relative to CON, glucose clearance was reduced at the 20, 30, 45, 60, 75, 90 and 120-minute time-points during a two-hour oral glucose tolerance test in WT

mice following HFD treatment (Fig. 3*C*). No differences in glucose clearance were detected at any time-point in HZ mice following HFD treatment, relative to CON (Fig. 3*D*). Glucose clearance was reduced at the 30, 45, 60, 75, 90 and 120 minute time-points during a two hour oral glucose tolerance test in KO mice following HFD treatment, relative to CON (Fig. 3*E*). Glucose area under the curve, calculated from oral glucose tolerance tests, was increased by 1.5 and 2.2-fold in WT and KO mice, respectively, following HFD treatment (Fig. 3*F*). Following HFD treatment, insulin induced decrease in blood glucose was reduced at 40, 50 and 60 minutes, throughout a one hour insulin tolerance test, in WT mice (Fig. 3*G*). No differences in insulin tolerance were detected in HZ mice following HFD treatment (Fig. 3*H*). Insulin induced decrease in blood glucose was reduced at 40, 50, 60 minutes throughout a one hour insulin tolerance test, in KO mice following HFD treatment (Fig. 3*I*).

Discussion

The most salient findings of this study are that HZ mice maintain glucose tolerance and insulin sensitivity following three day HFD treatment, despite having marked increases in body weight and percent fat mass. Furthermore, KO mice had decreased BAT mass and energy expenditure which was associated with an exacerbated glucose intolerant phenotype. This is the first study to assess the effect of adipocyte specific hetero/homozygous knockout of *Pik3r1* on the regulation of *in vivo* energy homeostasis, glucose metabolism and insulin sensitivity following acute HFD treatment.

Acute HFD treatment had a significant and rapid impact on the phenotype and metabolism of the mice, which was in part influenced by AT *Pik3r1* expression. Specifically, AT *Pik3r1* expression influenced food intake, energy expenditure and RER resulting in altered fat accretion and adipose tissue distribution. KO mice had decreased food intake during light cycle, independent of diet treatment, which was likely to offset the decreased energy expenditure observed during the light cycle. During the dark cycle, normal circadian patterns (elevated food intake, activity and energy expenditure) are disrupted in KO mice. Recent literature suggests PI3K regulates BMAL1/CLOCK-mediated circadian transcription, (13) thus KO of PI3K could disrupt normal rhythmicity of these genes. Furthermore, HZ mice had elevated RER following CON diet treatment during the dark cycle, which is most likely due to elevated fasting blood glucose observed in HZ mice following the CON diet. KO mice had decreased energy expenditure at both the light and dark cycles, independent of differences in total activity, which is aligned with previous finding in mice with adipose tissue specific knockout of

PI3K p110α (14). In further support of the observed energy expenditure phenotype in KO mice, KO mice had decreased BAT mass, relative to WT and HZ mice, independent of diet. Taken together, it is clear that PI3K is critical for maintaining energy homeostasis.

Increased perigonadal eWAT p85α abundance in WT HFD treated mice was associated with impaired glucose tolerance and insulin sensitivity. These data are similar to what has been previously shown in obese mice, in which obesity decreased insulin-stimulated eWAT PI3K enzyme activity and glucose uptake (12). HZ mice in the present study were protected from HFD induced impairments in glucose tolerance and insulin sensitivity, which is aligned with previous findings in obese mice with whole-body HZ knockout of *Pik3r1* (αHZ) (12). eWAT p85α abundance was not increased in αHZ mice, which was associated with maintained insulin-stimulated eWAT PI3K enzyme activity and glucose uptake, despite marked obesity (12). Thus, there is a clear connection between adipose tissue *Pik3r1* expression, glucose homeostasis and insulin sensitivity. In the present study, we reason that the glucose intolerant phenotype was exacerbated by adipose tissue KO following HFD treatment, most likely due to impaired PI3K enzyme activity. PI3K functions as a heterodimer, in which the α regulatory subunits all contain bindings sites for the p110α catalytic subunit (3). The regulatory subunits also contain an inter-SH2 (iSH2) domain which recognize upstream phosphorylated tyrosine residues on insulin receptor substrate-1 (IRS-1) (3). Taken together, by lacking both the catalytic subunit binding domains and iSH2 domains, PI3K enzyme activity would be impaired in *Pik3r1* KO mice and result in decreased glucose uptake in adipose tissue, and ultimately decreased glucose clearance overall.

From the data presented here, it is evident that glucose intolerance and insulin resistance can occur rapidly, and prior to a significant gain in body weight and adiposity. Furthermore, adipocyte *Pik3r1* undoubtedly plays a role in regulating systemic glucose homeostasis and energy balance; thus, *Pik3r1* may be used as a therapeutic target to attenuate the progression of metabolic diseases brought about by increased gain in weight and adiposity.

To follow up on the results presented here and to determine the role of adipocyte *Pik3r1* in regulating adipose tissue insulin sensitivity and insulin signaling, future experiments should assess insulin stimulated suppression of plasma glycerol to assess adipocyte insulin sensitivity as well as insulin activation of Insulin receptor substrate-1(p-Y896), Akt (s473) and Hormone Sensitive Lipase (s660). By addressing these questions, we will be able to determine whether differences in systemic glucose metabolism are associated with specific differences in adipose tissue insulin sensitivity.

CHAPTER III

INDUCIBLE HETEROZYGOUS KNOCKOUT OF ADIPOCYTE PIK3R1 REVERSES OBESITY INDUCED GLUCOSE INTOLERANCE AND ENHANCES ADIPOCYTE INSULIN SENSITIVITY

Introduction

Obesity is a growing health crisis in the United States, with ~40% of adults classified as obese (6). Obesity is associated with an earlier and greater risk for developing hypertension, coronary heart disease, type 2 diabetes and certain cancers (4). Treating obesity and its associated complications costs ~$230 billion/year, and startlingly, this economic burden is anticipated to more than double in the next 25 years (20). Insulin resistance is a central and defining feature of the metabolic diseases associated with obesity (5). Much attention has focused on the role of immune cells in exacerbating insulin resistance in obesity (15). However, therapies that chronically target the immune system in order to improve insulin sensitivity could have unwanted consequences on overall health, such as reducing one's ability to fight infection (7). Furthermore, enhancing insulin sensitivity, independent of bodyweight, has been shown to reduce the incidence of metabolic diseases (17).

Phosphatidylinositol 3-kinase (PI3K) is an essential component of insulin signaling, and is comprised of regulatory subunits (p85, p55, p50) and a catalytic subunit (p110) (2). In insulin activated cells, the regulatory-catalytic complex recognizes phospho-tyrosines (insulin receptor and insulin receptor substrate-1) by means of the Src homology 2 (SH2) domains in the regulatory subunits, which bring the p110 catalytic subunit in proximity to its lipid substrates. PI3K then catalyzes the reaction of PI-3,4,5-

triphosphate (PIP3) from PI-4,5-bisphosphate (PIP2). PIP3 recruits PDK-1 (3-phosphoinositide-dependent protein kinase) and mTORC2 (mammalian target of rapamycin complex 2) to the plasma membrane, which activate Akt, which, depending on the cell type, has a multitude of downstream effects (2). In adipose tissue, insulin signaling results in glucose uptake and inhibition of lipolysis (13).

PI3K signaling is required for several key inflammatory functions, including cytokine production, proliferation and chemotaxis (14). PI3K activity is decreased in obese adipose tissue, which has been associated with increased NFκB activation and cytokine secretion (11). Inversely, maintaining PI3K activity in adipose tissue, despite marked obesity, has been shown to reduce NFκB activation and cytokine secretion (11).

The *Pik3r1* gene encodes the p85α, p55α, p50α isoforms of the regulatory subunits (2). It is well documented that global knockout of p85α (1) or p55α and p50α (3) improves insulin action in mice. However, there is no difference in insulin sensitivity in mice with liver specific deletion of *Pik3r1* (19) and mice with skeletal muscle specific deletion of *Pik3r1* have impaired insulin sensitivity (9). Furthermore, global deletion of the PI3K catalytic subunit has opposite effects on insulin sensitivity, relative to deletion of the regulatory subunit (1). Moreover, global heterozygous knockout (αHZ) of *Pik3r1* protects against obesity induced systemic and tissue specific insulin resistance, as well as adipose tissue inflammation, despite marked obesity (11). Interestingly, αHZ mice are protected against obesity induced insulin resistance in both adipose tissue and skeletal muscle. Considering adipose tissue inflammation is proposed to contribute to skeletal muscle insulin resistance (15), it is necessary to understand the independent role of adipose tissue *Pik3r1* in obesity.

Here, we investigated the hypothesis that inducible heterozygous knockout of adipocyte *Pik3r1* would reverse obesity induced insulin resistance, enhance adipocyte insulin signaling and decrease the abundance of pro-inflammatory immune cells in white adipose tissue. To do this, we studied adipose tissue immune cell infiltration and cytokine profiles, systemic glucose tolerance and insulin sensitivity, adipocyte insulin sensitivity and adipocyte insulin signaling in a mouse model with inducible adipocyte specific hetero/homozygous knockout of *Pik3r1*. Our results demonstrate that glucose intolerance is reversed following αHZ knockout of adipocyte *Pik3r1*. Furthermore, systemic insulin sensitivity, adipocyte insulin sensitivity and adipocyte insulin signaling are enhanced in obese HZ mice.

Methods

Mouse model. All experiments were approved by and conducted in accordance with the Animal Care Program at the University of Oregon. All studies were conducted in male mice on a C57BL/6J background. To generate inducible adipocyte (iAdipo) specific *Pik3r1* hetero/homozygous knockout mice, mice with a mixed B6/129S background and homozygous for *loxP* sites flanking exon 8 of the *Pik3r1* gene (*Pik3r1*^{tm1Lca}/J; Jackson Laboratory, #012871) were crossed with Adipo-CreER^{T2} (graciously donated by Dr. Stefan Offeremans) (16). To manipulate adipocyte *Pik3r1* expression, 100μL of tamoxifen was administered daily for five consecutive days, at a dose of 10 mg/mL (resuspended in peanut oil) via oral gavage. Cre negative flox/flox mice also received tamoxifen, and were used as controls for the study.

Experimental Design. At eight weeks of age, mice were individually housed at standard vivarium temperature (22-23°C) with access to nesting material and randomized to the control (CON: 10% Calories from fat; 3.85 kcals/g) (D1245OH, Research Diets, New Brunswick, NJ) or high-fat diet (HFD; 45% Calories from fat; 4.73 kcals/g) (D12451, Research Diets, New Brunswick, NJ) group. Following 10 weeks of diet treatment, mice underwent an oral glucose tolerance test (details described below), which served as assessment of obesity induced glucose intolerance. All mice were then administered tamoxifen (100μL; 10 mg/mL) for five consecutive days. From 19-20 weeks of age, mice remained on the assigned diet and were transferred to our metabolic monitoring system (Promethion, Sable Systems, Las Vegas, NV), which was set to 30°C, void of nesting material. This week served as an acclimation period to the new living conditions. One to two weeks following the final dose of tamoxifen, we determined total energy expenditure

during the 12:12-h light-dark cycles (Light Cycle: 6:00-18:00; Dark Cycle: 18:00-6:00) by monitoring oxygen consumption and carbon dioxide production. The metabolic monitoring system is within a thermal cabinet, allowing us to monitor mice throughout the experiment. We then conducted follow up OGTT experiments two weeks following the final dose of tamoixfen, as well as other metabolic testing (details described below) to determine the role of hetero/homozygous knockout of adipocyte *Pik3r1* in obesity induced glucose intolerance. Between one and two weeks from the final dose of tamoxifen, mice were euthanized by cervical dislocation following isolfluorane anesthesia between 10am and 1pm and tissues (inguinal scWAT, interscapular BAT and perigonadal eWAT) were rapidly dissected, snap-frozen in liquid nitrogen and stored at -80°C until analysis.

Metabolic Monitoring. Throughout these studies, the thermal cabinet remained set to 30°C, void of nesting material. Food intake, total activity, and energy expenditure were assessed following three full light and dark cycles. The measures of O_2 consumption and CO_2 production were used to calculate energy expenditure and the respiratory exchange ratio (RER), which is an index of the relative reliance on carbohydrate vs. fat oxidation. Metascreen software (Sable Systems Inc.) was used for data collection and data was processed with ExpeData (Sable Systems Inc.) proprietary macros. Energy expenditure (kcals/hour) was calculated relative to bodyweight (kg). Food intake (g/day) was converted to kcals/day and made relative to bodyweight (kg).

Oral Glucose Tolerance Tests. Glucose tolerance tests were performed in conscious mice prior to tamoxifen administration, and following the three day data collection period in the metabolic monitoring system. Mice were fasted for 4 h (6-10 AM) before testing, to normalize glucose and insulin levels. Tails were nicked with

sterile scissors and ~2-5 µl of blood was analyzed with a handheld glucometer (Bayer Contour). After the fasting glucose measurements, the animals were given 5g/kg bodyweight dextrose by oral gavage. Glucose was measured again at 10, 20, 30, 45, 60, 75, 90 and 120 minutes. Glucose area under the curve (AUC) was calculated from baseline glucose values.

Insulin Tolerance Test. Insulin tolerance tests were performed in conscious mice following the 1d and 5d diet treatment. Mice were fasted for 4h (6-10 AM) before testing to normalize glucose and insulin levels. Tails were nicked with sterile scissors and ~2-5 µl of blood was analyzed with a handheld glucometer (Bayer Contour). After the fasting glucose measurements, the animals received an intraperitoneal (I.P.) injection of 0.25 U insulin (Humulin-R, Eli Lilly and Company, Indianapolis, IN)/kg bodyweight. Glucose was measured from tail blood again at 10, 20, 30, 40, 50 and 60 minutes.

Insulin Suppression of Plasma Glycerol. Mice were fasted for 4h (6-10AM). Following the 4h fasting period, venous blood was collected from the tail vein through an EDTA coated capillary tube, transferred to EDTA coated blood collection tubes and stored on ice. Mice were then received an IP injection of 1.0 U/kg insulin (Humulin), and a second blood sample was collected 15 minutes following insulin injection. Plasma was separated by spinning tubes at 12,000 x g for 15 minutes at 4°C. Glycerol was assessed by colorimetric assay as previously described (11).

Adipocyte Insulin Signaling. Primary adipocytes were isolated from perigonadal eWAT by collagenase (1 mg/mL) digestion (10). Digest was passed through a 100µM filter and spun at 150 x g for 5 minutes. The floating adipocyte layer was carefully removed and resuspended in AT wash buffer (1:10 adipocytes: wash buffer) (10). Two tubes (basal and

insulin-stimulated conditions) per mouse, of isolated adipocytes (100 μL packed cell volume per tube) were incubated for two hours at 37°C in AT wash buffer (buffer described in (10)), with light rocking. Following the two-hour incubation, cells were treated with (insulin-stimulated condition) or without (basal condition) 1.2nM insulin for 5 minutes and immediately flash frozen.

Immunoblotting. Adipocytes were homogenized with a BDC 2002 (Compact Digitial, Caframo Lab Solutions, Ontario, Canada) at 1:1 cell volume/ homogenization buffer (20mM Tris-HCl pH 7.4, 150mM NaCl, 1% Igepal/NP-40, 20 mM NaF, 2mM EDTA pH 8.0, 2.5mM NaPP, 20mM β-glycerophosphate, 10% glycerol with added protease and phosphatase inhibitors (1 mg/mL Aprotinin, 1 mg/mL Leupeptin, 1 mg/mL Pepstatin, 6 mg/mL Pefabloc SC, Phosphatase Inhibitor Cocktails 2 and 3 (Sigma Aldrich)). A bicinchoninic acid (BCA) assay was ran on individual tissue lysates and 1 mg/mL was loaded per lane on the WES (Protein Simple). Antibodies: 1:25 PI3K p85α (Millipore Sigma ABS233); 1:25 pIRS1 Y896 (Abcam ab46800); 1:25 total IRS1 (Cell Signaling 2382); 1:25 pAkt S473 (Cell Signaling 9271); 1:25 pan Akt (Cell Signaling 4691) 1:1K GAPDH (Millipore Sigma G9545).

Statistical Analysis. Data were analyzed by a two-way analysis of variance (ANOVA) for main effects of diet and genotype except for the oral glucose tolerance test, which used a repeated measures 2-way ANOVA for main effects of group and genotype. A Sidak's multiple comparisons post hoc test was performed when significant main effect differences were detect using a p-value of ≤ 0.05. All data are presented as the mean ± standard error of the mean (SEM). Statistics were calculated using Graph Pad Prism version 7 (Graph Pad Software; La Jolla, CA).

Results

Validation of inducible adipocyte Pik3r1 KO mouse. Following tamoxifen treatment, there is a 5-fold decrease in WAT adipocyte p85α and p55α protein abundance in KO mice, relative to WT (Fig. 1*A*). There is no difference in WAT adipocyte p85α and p55α protein abundance between WT and HZ mice (Fig. 1*A*). Furthermore, there is no difference in p85α protein abundance between WT, HZ and KO WAT SVF (Fig. 1*B*), gastrocnemius (Fig. 1*C*) and liver (Fig. 1*D*).

Body weight and body composition in CON and HFD fed WT, HZ and KO mice following tamoxifen treatment. Body weight (Fig. 2*B*), percent fat mass (Fig. 2*C*), perigonadal eWAT mass (Fig. 2*D*) and scWAT mass (Fig. 2*E*) significantly increased following 12 weeks of HFD in WT, HZ and KO mice. Interscapular BAT mass increased with 12 weeks HFD only in WT and KO mice (Fig. 2*F*). No differences between genotypes were detected following CON treatment.

Adipocyte Pik3r1 HZ and KO alters mouse behavior as well as the metabolic and circadian response to HFD. Mouse feeding behavior was changed by HFD, but there were no differences between genotypes. Specifically, HFD resulted in greater food intake across all genotypes in the light cycle (Fig. 3*A*); however, food intake only increased in HFD fed KO mice during the dark cycle (Fig. 3*B*). There was a significant effect of diet and genotype in assessment of RER during the light and dark cycles (Fig. 3, *C-D*). During the light cycle, RER was higher in KO mice on CON relative to HFD (0.90±0.04 vs. 0.80±0.02), while this difference was not observed in WT and HZ mice. During the dark cycle, RER was higher in HZ and KO mice on CON, relative to HFD (HZ: 0.88±0.05 vs. 0.75±0.02; KO: 0.88±0.03 vs. 0.80±0.03), while no difference was

observed in WT. No differences between diet or genotype were observed in total activity during the light cycle (Fig. 3*E*). During the dark cycle, total activity was higher in KO mice on CON, relative to WT; however, no differences were observed in total activity throughout HFD feeding (Fig. 3*F*). No differences in energy expenditure were observed between diet or genotype during the light and dark cycles (Fig. 3, *G-H*).

Inducible HZ knockout of adipocyte Pik3r1 reverses obesity induced glucose intolerance. Following 10 weeks of HFD, prior to tamoxifen treatment (hetero/homozygous knockout of adipocyte *Pik3r1*), glucose intolerance was significantly increased in all mice, regardless of genotype (Fig. 4, *A-D*). Following hetero/homozygous knockout of adipocyte *Pik3r1*, glucose intolerance was ameliorated in HFD fed HZ mice, but not in HFD fed WT or KO mice, despite no improvement in fasting glucose (Fig. 4, *E-H*).

Inducible heterozygous knockout of adipocyte Pik3r1 improves systemic and adipocyte insulin sensitivity. Following hetero/homozygous knockout of adipocyte *Pik3r1*, HZ mice are protected from obesity induced impairments in insulin tolerance, which was not observed in obese WT and KO mice (Fig. 5, *A-D*). Furthermore, HZ mice are protected against obesity induced impairments in adipocyte insulin sensitivity, as measured by insulin-stimulated stimulated suppression of plasma glycerol. This protective phenotype was not observed in in obese WT and KO mice (Fig. 5*E*).

Inducible heterozygous knockout of adipocyte Pik3r1 influences adipocyte insulin signaling upstream and downstream of PI3K. Adipocyte insulin-stimulated phosphorylation of IRS1(Y896) and Akt(S473) were reduced 2-fold in WT obese, independent of changes in total IRS1 or total Akt *(*Fig. 6, *B-E)*. Changes in pIRS1 and

pAkt were not observed in HZ or KO obese mice; however, insulin-stimulated pIRS1 and pAkt were reduced in KO CON relative to WT CON, despite elevated abundance of total Akt (Fig. 6, *B*-*E*).

Discussion

The most salient findings of this study are that heterozygous knockout of adipocyte *Pik3r1* reverses obesity induced impairments in glucose tolerance, prevents obesity induced systemic and adipocyte insulin resistance and enhances adipocyte insulin signaling. This study expands upon previous findings from our laboratory which demonstrated that systemic and adipose tissue insulin sensitivity were enhanced in mice with whole-body heterozygous knockout (αHZ) of *Pik3r1*, despite marked obesity (11). αHZ mice also had enhanced skeletal muscle and liver insulin sensitivity, so the present study has identified an independent role for adipocyte *Pik3r1* in regulating adipocyte and systemic insulin sensitivity.

Adipose tissue insulin sensitivity has and continues to be a therapeutic target to treat obesity related metabolic diseases (22). The current dogma for which obesity results in insulin resistance suggests that obesity is a state of chronic low-grade inflammation, which is associated with AT macrophage infiltration, and secondary to this infiltration, AT insulin resistance manifests (15). In contrast, however, several studies have shown dissociation between AT macrophage and the development of insulin resistance. Lee et al. (8) demonstrated that despite knockout of peritoneal macrophage, three days of HFD treatment was sufficient to drive insulin resistance; however, the same study revealed that inflammation was necessary for obesity induced insulin resistance. Furthermore, findings in αHZ mice suggest that it is not obesity, *per* se, that drives adipose tissue inflammation as obese αHZ mice have reduced AT macrophage infiltration, along with enhanced insulin sensitivity (11). Although we did not measure AT inflammation in the present

study, it is clear from the present study and previous work from our laboratory (11) that AT *Pik3r1* expression is involved in regulating AT inflammation and insulin sensitivity.

PI3K functions as a heterodimer, in which the α regulatory subunits (*Pik3r1*) all contain binding sites for the p110α catalytic subunit (2). The regulatory subunits also contain an inter-SH2 (iSH2) domain which recognize upstream phosphorylated tyrosine residues on insulin receptor substrate-1 (IRS-1) (2). Thus, we hypothesized that adipocyte insulin signaling would only be impaired downstream of PI3K in HZ and KO obese mice, which aligns with data from αHZ mice (11). Contrary to our hypothesis, we found that HZ obese mice have enhanced adipocyte insulin signaling upstream of PI3K (IRS-1 Y896) relative to WT obese mice, and are protected from an obesity induced decrease downstream of PI3K (Akt S473). Unpublished data from our laboratory suggests that HZ mice maintain M2-like (anti-inflammatory) macrophage following three days of HFD, relative to WT. Furthermore, considering the role of PI3K in regulating inflammation (14; 18; 21), we reason that insulin-stimulated phosphorylation of IRS1 is maintained in HZ obese mice potentially due to the influence of adipocyte *Pik3r1* on adipose tissue inflammation in obesity.

Obesity is strongly associated with insulin resistance, incidence of type 2 diabetes mellitus and cardiovascular disease (12). Furthermore, insulin resistance, independent of obesity is an independent predictor of type two diabetes mellitus, hypertension, coronary heart disease, stroke and some cancers (4). Thus, insulin resistance is a logical therapeutic target in obesity. The findings in the present study provide evidence that adipocyte *Pik3r1* can serve as a therapeutic target to attenuate metabolic diseases associated with obesity, independent of changes in body weight and adiposity.

Future experiments should assess insulin activation of adipocyte hormone sensitive lipase (pHSL Ser660) to assess a critical node in the molecular regulation of insulin-stimulated suppression of lipolysis. Data regarding activation of pHSL would support our data regarding insulin-stimulated suppression of plasma glycerol. Furthermore, considering αHZ mice are protected against obesity induced AT pro-inflammatory macrophage accumulation, analysis of AT macrophage accumulation is warranted in the present study. Taken together, the proposed experiments, in combination with previously collected data will allow us to determine the role of adipocyte *Pik3r1* in regulating both AT insulin sensitivity and AT inflammation.

CHAPTER IV

ADIPOSE TISSUE OVEREXPRESSION OF PI3-KINASE P55α IMPROVES SYSTEMIC GLUCOSE METABOLISM AND ENHANCES BROWN ADIPOSE TISSUE THERMOGENIC ACTIVATION

Introduction

Class 1a phosphatidylinositol 3-kinases (PI3K) play an essential role in insulin stimulation of glucose transport, lipid and protein synthesis, and cell growth and differentiation (6) (8); (15). The class 1a PI3 kinases are obligate heterodimers, which consist of regulatory subunits (p85, p55, p50) and a catalytic subunit (p110), and exist in multiple isoforms (18). The group of regulatory subunits includes p85α, p85β, p55α, p55γ, p50α. The group of catalytic subunits includes p110α, p110β, and p110δ (18).

The regulatory subunits p85α, p55α, p50α are all encoded by the *Pik3r1* gene and have identical C-terminal regions that include one proline-rich domain and two SH2 domains flanking the p110 binding site (5). These individual regulatory subunits, however, differ in their N termini. p85α has a large N terminus containing one SH3 domain, a second proline-rich region, and BCR homology domain; p55α contains a unique 34 amino acid extension; and p50α has a shorter 6 amino acid extension (2); (9) (10); (11). These regulatory subunits have discrete, but overlapping, tissue distributions, such that p85α and p85β are ubiquitously expressed (9), and p50α/p55α are present in insulin-responsive tissues including skeletal muscle, liver and brain (2); (10) (11). Mice with complete knockout of p85α up-regulate p50α/p55α in skeletal muscle and adipose tissue and have enhanced insulin sensitivity, suggesting p50α/p55α are important signaling molecules for insulin action (19).

While much attention has focused on p85α, little is known about the physiological role of p55α or p50α abundance. The structure and function of p55α and p50α has not been rigorously investigated (9), although some evidence exists for unique signaling capabilities (20). For example, p50α can form a heterodimer with p110 catalytic subunit that is not sensitive to wortmannin, while p85α and p55α have been shown to associate with a wortmannin-sensitive p110 subunit (11). Furthermore, mice with a global p55α/p50α deletion have enhanced systemic, skeletal muscle and adipocyte insulin sensitivity. Interestingly, however, insulin-stimulated PI3K activity is only increased in skeletal muscle suggesting that adipocyte p55α and p50α may have PI3K-independent roles that influence adipocyte metabolism (7). Obese wild type mice display increased abundance of adipose tissue p55α and p50α with a parallel decrease in adipocyte insulin sensitivity (13). Obese mice with global heterozygous deletion of *Pik3r1* do not upregulate adipose tissue p55α and p50α and maintain adipocyte insulin sensitivity (13), demonstrating a link between increased adipose tissue p55α/p50α abundance and adipocyte insulin resistance. By mimicking conditions in lean mice that have been observed in obesity, we can determine whether overexpression of adipocyte p55α is sufficient to cause adipocyte insulin resistance, independent of obesity.

Here, we investigated the hypothesis that adipocyte specific over expression of p55α would result in systemic and adipose tissue insulin resistance. To test this, we studied systemic glucose tolerance, insulin sensitivity, and adipose tissue insulin signaling in male mice with adipocyte specific overexpression of p55α (adipo-p55 OX) and WT (Cre negative; $p55^{flox/flox}$) littermates. Contrary to our hypothesis, our results

demonstrate that adipo-p55 OX mice have enhanced glucose tolerance, adipose tissue insulin sensitivity and adipose tissue insulin signaling, relative to WT mice.

Methods

Mouse Model. All experiments were approved by and conducted in accordance with the Animal Care Program at the University of Oregon. Studies were conducted in male and female mice on a C57BL/6J background. To generate mice with adipose tissue specific p55α overexpression, we created p55α knock-in at the ROSA26 locus by recombinase-mediated cassette exchange (RMCE). A p55α recombination cassette was made by flanking the cDNA of p55α and a floxed PGK-Puro selection marker followed by 4x SV40 polyA STOP signal with FRT and F3. This cassette together with pCAG-Flpe were electroporated into ROSA-FNF3-1F1 ES cells (an ES cell line targeted with FRT-PGK-neo-F3 at the ROSA26 locus). The exchange of neo for p55α at the ROSA26 locus was facilitated by Flp-recombinase mediated site specific recombination so that the recombinants would become G418 sensitive and Puro resistant. The correct exchange was confirmed by PCR. The 4x SV40 polyA STOP signal along with the selection marker PGK-Puro is removed by Cre recombinase. This puts the p55α cDNA under the expression of the endogenous ROSA26 promoter. To generate adipose tissue specific overexpression, $p55\alpha^{flox/flox}$ mice were crossed with mice expressing Cre recombinase (Cre) under the control of the adipose tissue adiponectin promotor (adipo Cre). After cre mediated recombination, the STOP signal was removed, resulting in adipose tissue specific p55α overexpression. Herein, Cre negative, $p55\alpha^{flox/flox}$ mice were used as wild type (WT) controls for this study.

Experimental Design. At ten weeks of age, all mice were singly housed and remained on standard mouse chow (Lab Diets, Pico Lab, Rodent Diet 20, 5053), housed at 22°C with access to nesting material. At eleven weeks of age, mice remained singly housed and were

placed in our metabolic monitoring system (Promethion, Sable Systems, Las Vegas, NV.) set to 30°C. Mice were euthanized by cervical dislocation following isolfluorane anesthesia between 10am and 1pm and tissues (inguinal scWAT, interscapular BAT and perigonadal eWAT) were rapidly dissected, snap-frozen in liquid nitrogen and stored at -80°C until analysis.

Metabolic Monitoring. The metabolic monitoring system is within a thermal cabinet, allowing us to monitor mice throughout the experiment. Throughout the acclimation period and data collection, the thermal cabinet was set to 30°C, and cages were free of nesting material. At twelve weeks of age, we determined total energy expenditure during the 12:12-h light-dark cycles (Light Cycle: 6:00-18:00; Dark Cycle: 18:00-6:00) by monitoring oxygen consumption and carbon dioxide. Food intake and energy expenditure were assessed following three full light and dark cycles. The measures of O_2 consumption and CO_2 production in individual chambers were used to calculate energy expenditure and the respiratory exchange ratio (RER), which is an index of the relative reliance on carbohydrate vs. fat oxidation. Metascreen software (Sable Sytems Inc.) was used for data collection and data was processed with ExpeData (Sable Systems Inc.) proprietary macros. Energy expenditure (kcals/hour) data were calculated relative to bodyweight (kg). Food intake (g/day) data were converted to kcals/day and made relative to bodyweight (kg).

Body Composition. Body composition (lean tissue, fat and free fluid) was measured by time domain (TD)-NMR using the Minispec LF50 mouse NMR (Bruker BioSpin, Billerica MA, state) in anaesthetized mice before and after the 1 and 5 day period.

Percentages were calculated from body weight measured on a standard scale (Mettlor-Toledo, Columbus, OH) using the Minispec Software.

Food Intake and Total Energy Expenditure. Using a metabolic monitoring system (Promethion, Sable Systems, Las Vegas, NV), we measured cage behavior (food intake, water intake and activity), oxygen, carbon dioxide and water vapor during the 12:12-h light-dark cycles (Light Cycle: 6:00- 18:00; Dark Cycle: 18:00-6:00) following one and five full light and dark cycles. The metabolic cages were kept inside an environmental cabinet allowing temperature control throughout the study. Metascreen software (Sable Systems Inc.) was used for data collection and data was processed with ExpeData (Sable Systems Inc.) proprietary macros. Energy expenditure (kcals/hour) was calculated relative to bodyweight (kg). Food intake (g/day) was converted to kcals/day and made relative to bodyweight (kg).

Oral Glucose Tolerance Test. Glucose tolerance tests were performed in conscious mice following the 1d and 5d diet treatment. Mice were fasted for 4 h (6-10 AM) before testing to normalize glucose and insulin levels. Tails were nicked with a sterile scissors and ~2-5 µl of blood was analyzed with a handheld glucometer (Bayer Contour). After the fasting glucose measurements, the animals were given 5g dextrose/kg bodyweight by oral gavage. Glucose was measured from the tail blood at 10, 20, 30, 45, 60, 75, 90 and 120 minutes. Glucose area under the curve (AUC) was calculated from baseline glucose values using Graphpad Prism 7.0.

Insulin Tolerance Test. Insulin tolerance tests were performed in conscious mice following the 1d and 5d diet treatment. Mice were fasted for 4h (6-10 AM) before testing to normalize glucose and insulin levels. Tails were nicked with sterile scissors and ~2-5 µl

of blood was analyzed with a handheld glucometer (Bayer Contour). After the fasting glucose measurements, the animals received an intraperitoneal (I.P.) injection of 0.25 U insulin (Humulin-R, Eli Lilly and Company, Indianapolis, IN)/kg bodyweight. Glucose was measured from tail blood again at 10, 20, 30, 40, 50 and 60 minutes.

Insulin Suppression of Plasma Glycerol. Mice were fasted for 4h (6-10AM). Following the 4h fasting period, venous blood was collected from the tail vein through an EDTA coated capillary tube, transferred to EDTA coated blood collection tubes and stored on ice. Mice were then received an IP injection of 1.0 U insulin (Humulin-R, Eli Lilly and Compnay, Indianapolis, IN)/kg bodyweight, and a second blood sample was collected 15 minutes following insulin injection. Plasma was separated by spinning tubes at 4°C at a speed of 12,000 x g for 15 minutes. Glycerol was assessed by colorimetric assay as previously described (13).

RNA isolation and quantitative real-time PCR. Interscapular BAT was homogenized using the Bead Ruptor Elite, Bead Mill Homogenizer (OMNI International, Kennesaw, GA) at (5 m/second for 30 seconds x 2) in 100 mg/ 1mL Qiazol (Qiagen, Valencia, CA). Total RNA was isolated using a Pure Link RNA Kit (Invitrogen, Eugene, OR) according to the manufacturer's protocol and quantified with a nanodrop spectrophotometer. cDNA was synthesized from total RNA using iScript reverse transcriptase (BioRad) and gene expression was measured by quantitative real-time PCR in CFX384 instrument (BioRad). Gene expression was calculated as the $2^{-\Delta\Delta CT}$ with target genes normalized to beta actin and an internal reference sample (CON diet at 22°C). Mouse PCR primers (BioRad) were used for *Actb, Ucp1*and *Prdm16*.

In vivo insulin signaling. Mice were fasted for 4h (6-10AM), and anesthetized with an IP injection of a Ketamine/Xylazine/Acepromazine cocktail. Once mice were non-responsive, the left perigonadal eWAT depot was removed and immediately flash frozen, which served as basal conditions. Insulin (10 U/kg) was then injected into the inferior vena cava and the contralateral eWAT depot was removed 5 minutes following the insulin injection and immediately flash frozen, which served as insulin stimulated conditions.

Immunoblotting. eWAT, BAT, liver and skeletal muscle (gastrocnemius) samples were homogenized using the Bead Ruptor Elite, Bead Mill Homogenizer (OMNI International, Kennesaw, GA) at (5 m/second for 30 seconds x 2) in (20mM Tris-HCl pH 7.4, 150mM NaCl, 1% Igepal/NP-40, 20mM NaF, 2mM EDTA pH 8.0, 2.5mM NaPP, 20mM β-glycerophosphate, 10% glycerol with added protease inhibitors (1mg/mL Aprotinin, 1mg/mL Leupeptin, 1mg/mL Pepstatin, 6mg/mL Pefabloc SC, Phosphatase Inhibitor Cocktail 2 and 3 (Sigma Aldrich, San Jose, CA); eWAT and BAT: 100 mg tissue/300μL of Homogenization Buffer; Liver: 100 mg tissue/500μL of Homogenization Buffer; gastrocnemius: 100 mg tissue/200μL of Homogenization Buffer). Samples were solubilized at 4°C for 1 hour with rotation and spun at 4°C at a speed of 12,000 x g for 15min. Protein abundance was measured by bicinchoninic acid (BCA) assay (Thermo Fisher Scientific, Eugene, OR). Target proteins were measured in tissue homogenates (1 mg/mL) by capillary electrophoresis using a Wes instrument (Protein Simple, Biotechne) with N-SH2 PI3-Kinase (1:100, Millipore Sigma ABS233), pIRS1 Y896 (1:100, Abcam ab46800); 1:100 total IRS1 (1:100, Cell Signaling 2382); pAkt S473 (1:100, Cell Signaling 9271); pan Akt (1:100, Cell Signaling 4691); GAPDH (1:1K, Santa Cruz Biotechnology 25778); PRDM16 (1:25, Thermo Fisher A5-20872. Data was quantitated using Compass

Software (Protein Simple, Biotechne) with target proteins expressed relative to the loading control.

Results

Tissue abundance of p55α. Adipo-p55OX mice do not have greater p55α abundance is eWAT (Fig. 2*A*), relative to WT mice; however, p85α was decreased by 35%, and there was no difference in p50α (Fig. 2*B*). BAT p55α abundance was increased 4.5-fold (Fig. 2*C*), while no difference in p85α or p50α were detected. No differences in p85α (data not shown), p55α or p50α (data not shown) were detected in gastrocnemius (p50α WT: 0.15±0.03 v. OX: 0.16±0.04; p85α WT: 0.67±0.05 vs. OX:0.51±0.13; Fig. 2*D*) and liver (p50α WT: 0.71±0.13 vs. OX: 0.69±0.13; p85α WT: 0.91±0.13 vs. OX: 0.95±0.09; Fig. 2*E*) from adipo-p55 OX and WT mice.

Adipocyte OX of p55α influences perigonadal eWAT mass and interscapular BAT mass. No difference in body weight was observed between adipo-p55 OX and WT mice (Fig. 3*A*). No difference was observed in percent fat mass (Fig. 3*B*), percent lean mass (data not shown: WT: 76±0.3 vs. OX:76±0.3) or inguinal scWAT mass (Fig. 3*C*) between adipo-p55 OX and WT mice. Adipo-p55 OX mice had lower perigonadal eWAT mass (Fig. 3*D*) and greater interscapular BAT mass (Fig. 3*E*), relative to WT mice.

Adipocyte OX of p55α influences kilocalorie intake, substrate oxidation and energy expenditure. Kilocalorie intake was greater during the dark cycle, independent of group. No difference in kilocalorie intake was observed during the light cycle, however; adipo-p55 OX mice consumed 25% more kilocalories than WT during the darky cycle (Fig. 4*A*). RER was greater during the dark cycle, independent of group. RER was greater in adipo-p55OX relative to WT mice during the light (0.79 vs. 0.74) and dark (0.83 vs. 0.77) cycles (Fig. 4*B*). No difference in activity between adipo-p55OX and WT mice was detected during the light cycle; however, adipo-p55OX mice recorded less activity during the dark

cycle relative to WT mice (Fig. 4*C*). Energy expenditure was greater during the dark cycle independent of group. Adipo-p55OX mice had greater energy expenditure, relative to WT mice, during the light and dark cycles (Fig. 4*D*).

Adipocyte OX of p55α enhances glucose tolerance but not insulin sensitivity. Glucose tolerance was enhanced in adipo-p55OX mice relative to WT, demonstrating decreased blood glucose concentrations at 20, 30, 45, 60, 75 and 90 minutes throughout a 2h oral glucose tolerance test (Fig. 5*A*). Glucose AUC, quantified from individual oral glucose tolerance tests, was reduced in adipo-p55OX mice (Fig. 5*B*) relative to WT. No difference in insulin tolerance was detected between WT and OX mice (Fig. 5*C*). No difference in insulin-stimulated suppression of plasma glycerol was detected between WT and OX mice (Fig. 5*D*).

Adipocyte OX of p55α do not have impaired adipose tissue insulin signaling. No differences in maximal insulin-stimulated phosphorylated IRS1(Y896) (Fig. 6*A*), phosphorylated AKT(S473) (Fig. 6*B*), total IRS1 (Fig. 6*C*) or total AKT (Fig. 6*D*) were detected between WT and adipo-p55OX mice.

Adipocyte OX of p55α increases markers of adipose tissue thermogenesis in BAT. BAT *Ucp1* gene expression was increased in adipo-p55OX mice (Fig. 7*A)*. BAT UCP1 protein abundance increased in adipo-p55OX mice (Fig. 7*B*). BAT *Prdm16* gene expression was increased in adipo-p55OX mice (Fig. 7*C*). BAT PRDM16 protein abundance was increased in adipo-p55OX mice (Fig. 7*D*).

Discussion

The most salient findings in the present study are that adipo-p55αOX mice have decreased eWAT p85α abundance, enhanced glucose tolerance, which was associated with increased BAT mass, energy expenditure, lipid utilization and markers of adipose tissue thermogenesis in BAT. This is the first study to assess the role of adipocyte specific p55α OX *in vivo* and demonstrates a novel role of BAT p55α in the regulation of adipose tissue thermogenesis and glucose metabolism.

Given the inverse association of adipose tissue p55/p50α abundance with systemic and adipocyte insulin sensitivity in lean (7) and obese (13) mice, we investigated whether overexpression of adipocyte p55α is sufficient to decrease glucose tolerance and adipose tissue insulin sensitivity. Contrary to our hypothesis, we found that adipo-p55 OX mice have enhanced glucose tolerance. Furthermore, enhanced glucose tolerance was associated with elevated BAT mass, lipid utilization and energy expenditure. Changes in glucose tolerance occurred independent of differences in perigonadal eWAT insulin signaling or insulin sensitivity, but were associated with increased BAT UCP1 and PRDM16 gene and protein expression. PRDM16 is necessary for increased uncoupling in adipose tissue (17), thus PRDM16 serves as a crucial target in adipose tissue thermogenic programming.

Increased PI3K p85α is a potent negative regulator of insulin sensitivity (3) due to the resulting decrease in PI3K enzyme activity. Furthermore, PI3K p110α catalytic subunit deletion has opposite effects on insulin sensitivity, compared to p85α regulatory subunit deletion (4). Interestingly, mice with adipose tissue specific (WAT and BAT) deletion of p110α have decreased insulin sensitivity and energy expenditure (14).

Considering eWAT p85α abundance was decreased and BAT p55α was increased in the present study, we reason that abundance of these proteins may be influencing BAT mitochondrial oxygen consumption, similar to previous reports (14).

Mammalian target of rapamycin complex 2 (mTORC2), a protein recruited to lipid membrane bound phosphatidylinositol 3,4,5-triphosphate (PIP3), following PI3K activation of phosphatidylinositol 4,5-biphosphate (PIP2) to PIP3 (12), is necessary for cold-induced increases in adipose tissue thermogenesis and BAT glucose uptake (1). Furthermore, phosphorylated Akt2(S474), a downstream target of PI3K, is necessary for cold-induced increases in BAT uncoupling and fatty acid oxidation (16), through a ChREBP (Carbohydrate-repsonsive element-binding protein) mechanism.

Taken together, we have identified and begun to characterize a novel role of adipose tissue p55α in regulating glucose homeostasis and BAT thermogenesis. This study adds to the body the body of literature that suggests, rather than a single PI3K subunit alone, it is the molecular balance of PI3K subunits that plays a more critical role in regulating glucose homeostasis. Furthermore, interventions that enhance energy expenditure and glucose tolerance may be favorable for treating the metabolic diseases associated with obesity. Future studies are necessary to fully characterize the mechanism by which p55α regulates BAT thermogenesis and energy expenditure. Considering the differences in energy expenditure, it may be determined that adipo-p55OX mice are protected against diet induced obesity and/or obesity induced insulin resistance.

CHAPTER V

SHORT-TERM THERMONEUTRAL HOUSING ALTERS GLUCOSE METABOLISM AND MARKERS OF ADIPOSE TISSUE BROWNING IN RESPONSE TO HIGH FAT DIET IN LEAN MICE

Clayton ZS and McCurdy CE. Short-term thermonetural housing alters glucose metabolism and markers of adipose tissue browning in response to a high fat diet in lean mice. *American Journal of Physiology Regulatory, Integrative and Comparative Physiology* 23:doi 10.1152. 2018.
ZSC performed experiments; ZSC and CEM analyzed data; ZSC and CEM interpreted results from experiments; ZSC and CEM drafted manuscript; ZSC and CEM revised manuscript; ZSC and CEM approved final version of manuscript; ZSC and CEM conception and design of research; ZSC and CEM prepared figures.

Introduction

Obesity-induced insulin resistance is thought to occur secondary to the release of pro-inflammatory cytokines and chemokines, which may be secreted as an adaptive response to maintain adipose tissue function in the presence of expanding or hypoxic adipocytes (34). Adipose tissue-derived cytokines and chemokines have been shown to regulate insulin action in an autocrine, paracrine and endocrine manner (31) . However, the mechanism(s) that regulate and initiate the inflammatory response in obesity are not clearly understood. High fat diet induced glucose intolerance and insulin resistance have been observed in both lean rodents (23, 24, 27, 35 47) and humans (7) in as little as three days of high fat feeding. Interestingly, Lee and colleagues demonstrated in mice that inflammation is not necessary for the three day HFD- induced glucose intolerance and insulin resistance (27), despite a marked increase in pro-inflammatory gene expression in white adipose tissue (WAT). Recent studies have identified a relationship between housing temperature and inflammatory response (17); the mice in the study by Lee *et al* were

housed well below the murine thermoneutral zone (29-34°C) (27), which may confound these results. For example, Tian and colleagues demonstrated that long-term (9-10 weeks) thermoneutral housing of mice accelerates perivascular white adipose tissue (pvWAT) inflammation in response to HFD (42), and Giles and colleagues have shown that thermoneutral housing as compared to conventional housing exacerbates lipopolysaccharide induced inflammation (15).

In most laboratories, mice are housed at room temperature, between 20-26°C, which is recommended within the *Guide for the Care and Use of Laboratory Animals* (1). Mice housed at routine vivarium temperatures have been shown to have less adipose tissue inflammation relative to mice housed at thermoneutral temperatures, and have also been shown to have greater energy intake and expenditure (12). Together, these results may influence net energy balance and potentially lead to unpredictable outcomes in metabolic data. Considering the laboratory mouse is used as a preferred model system for the study of many metabolic diseases, due to the relative ease of creating genetic perturbations, it is imperative to understand the differences between mouse and human thermal physiology, to ensure the applicability of preclinical findings. Housing mice below their thermoneutral zone has been referred to as a subthermoneutral stress (17), which is not common in human dwellings of daily life.

Chronic subthermoneutral stress has been shown to promote non-shivering thermogenesis, which is achieved through mitochondria rich brown adipose tissue (BAT) (12). BAT contains uncoupling protein-1 (UCP-1), which serves to mediate heat generation by uncoupling of oxidative phosphorylation from ATP synthesis (18). Chronic cold exposure not only influences inflammation and energetics, but has been shown to

upregulate BAT mass, *Ucp1* gene expression in BAT, as well as induce "browning" of white adipose tissue (WAT), through increased *Ucp1* gene expression and an increase in multilocular cells within WAT (30). BAT activity has been estimated to account for 2.7%-5% of basal metabolic rate in humans, which could cumulatively promote more than 4 kg of fat loss per year (45, 46). Furthermore, increased BAT mass has been shown to regulate glucose homeostasis and improve insulin sensitivity in a mass dependent manner (37).

Currently, most studies comparing behavioral, metabolic and inflammatory responses to varying ambient temperatures have been long-term ($\geq$ 8 weeks). An acute response to changes in housing temperature on metabolic variables in the laboratory mouse has not been examined. Therefore, the purpose of this study was to investigate the effect of short-term thermoneutral housing (30°C) compared to standard vivarium housing temperature (22°C) on glucose tolerance, metabolism and behavior (food intake, activity) in response to HFD.

Methods

Experimental Design. All experiments were approved by Institutional Animal Care and Use Committee at the University of Oregon. Mice with a mixed B6/129S background and homozygous for *loxP* sites flanking exon 8 of the *Pik3r1* gene (*Pik3r1*^{tm1Lca}/J; Jackson Laboratory, #012871) were used in these studies. Mice with the targeted allele compared to wild type show no difference p85α abundance in the absence of recombinant cre (Fig. 1 *A,B*) **(2, 28)**) and were used in thermoneutral studies to complement ongoing work in this mouse line. All mice were housed at standard vivarium temperature (T_S; 22°C) with a 12:12-h light-dark cycles (Light Cycle: 6:00- 18:00; Dark Cycle: 18:00-6:00) and fed chow diet with 13% fat (Picolab Rodent Diet 20; LabDiet) until 10 weeks of age. At ten weeks of age, male mice were singly housed in standard-sized cages and placed within an environmental cabinet set at T_s and fed a control diet (CON: 10% Calories from fat; Research Diets, D1245OH) for one week. The 12h light /dark cycle remained the same throughout the study. After the cage acclimation period, mice remained on CON diet but were randomly assigned to murine thermoneutral temperature (T_N; 30°C) or remained at T_S for 1 week. At 12 weeks of age, mice either remained on CON diet or were switched to a HFD (45% Calories from fat; Research Diets, D12451) for 1d (1 full light:dark cycle) or 5d (5 full light:dark cycles). Both the CON and HF diets were matched for sucrose (17%). At the end of the diet period, mice were euthanized by cervical dislocation following isolfluorane anesthesia between 10am and 1pm and tissues (inguinal scWAT, interscapular BAT and perigonadal eWAT) were rapidly dissected, snap-frozen in liquid nitrogen and stored at -80°C until analysis.

Body Composition. Body composition (lean tissue, fat and free fluid) was measured by time domain (TD)-NMR using the Minispec LF50 mouse NMR (Bruker BioSpin, Billerica MA, state) in anaesthetized mice before and after the 1 and 5 day period. Percentages were calculated from body weight measured on a standard scale (Mettlor-Toledo, Columbus, OH) using the Minispec Software.

Food Intake and Total Energy Expenditure. Using a metabolic monitoring system (Promethion, Sable Systems, Las Vegas, NV), we measured cage behavior (food intake, water intake and activity), oxygen, carbon dioxide and water vapor during the 12:12-h light-dark cycles (Light Cycle: 6:00- 18:00; Dark Cycle: 18:00-6:00) following one and five full light and dark cycles. The metabolic cages were kept inside an environmental cabinet allowing temperature control throughout the study. Metascreen software (Sable Systems Inc.) was used for data collection and data was processed with ExpeData (Sable Systems Inc.) proprietary macros. Energy expenditure (kcals/hour) was calculated relative to bodyweight (kg). Food intake (g/day) was converted to kcals/day and made relative to bodyweight (kg).

Oral Glucose Tolerance Test. Glucose tolerance tests were performed in conscious mice following the 1d and 5d diet treatment. Mice were fasted for 4 h (6-10 AM) before testing to normalize glucose and insulin levels. Tails were nicked with a sterile scissors and ~2-5 µl of blood was analyzed with a handheld glucometer (Bayer Contour). After the fasting glucose measurements, the animals were given 5g dextrose/kg bodyweight by oral gavage. Glucose was measured from the tail blood at 10, 20, 30, 45, 60, 75, 90 and 120 minutes. Glucose area under the curve (AUC) was calculated from baseline glucose values using Graphpad Prism 7.0.

Insulin Tolerance Test. Insulin tolerance tests were performed in conscious mice following the 1d and 5d diet treatment. Mice were fasted for 4h (6-10 AM) before testing to normalize glucose and insulin levels. Tails were nicked with sterile scissors and ~2-5 µl of blood was analyzed with a handheld glucometer (Bayer Contour). After the fasting glucose measurements, the animals received an intraperitoneal (I.P.) injection of 0.25 U insulin (Humulin-R, Eli Lilly and Company, Indianapolis, IN)/kg bodyweight. Glucose was measured from tail blood again at 10, 20, 30, 40, 50 and 60 minutes.

RNA isolation and quantitative real-time PCR. Inguinal subcutaneous white adipose tissue (scWAT), perigonadal epididymal white adipose tissue (eWAT) and interscapular BAT were homogenized using the Bead Ruptor Elite, Bead Mill Homogenizer (OMNI International, Kennesaw, GA) at (5 m/second for 30 seconds x 2) in 100 mg/ 1mL Qiazol (Qiagen, Valencia, CA). Total RNA was isolated using a Pure Link RNA Kit (Invitrogen, Eugene, OR) according to the manufacturer's protocol and quantified with a nanodrop spectrophotometer. cDNA was synthesized from total RNA using iScript reverse transcriptase (BioRad) and gene expression was measured by quantitative real-time PCR in CFX384 instrument (BioRad). Gene expression was calculated as the $2^{-\Delta\Delta CT}$ with target genes normalized to beta actin and an internal reference sample (CON diet at 22°C). Mouse PCR primers (BioRad) were used for *Actb, Ucp1, Prdm16, Cidea, Cox8b, Pgc1a, Adipoq*, *Leptin, Il1b, Il4, Il6, Il10, Il13, Ifng*, and *Ccl2*.

Immunoblotting. scWAT, eWAT and BAT samples were homogenized with a BDC 2002 (Compact Digital, Caframo Lab Solutions, Ontario, Canada) at 100mg tissue/ 300µL of homogenization buffer (20mM Tris-HCl pH 7.4, 150mM NaCl, 1% Igepal/NP-40, 20mM NaF, 2mM EDTA pH 8.0, 2.5mM NaPP, 20mM β-glycerophosphate, 10% glycerol

with added protease inhibitors (1mg/mL Aprotinin, 1mg/mL Leupeptin, 1mg/mL Pepstatin, 6mg/mL Pefabloc SC, Phosphatase Inhibitor Cocktail 2 and 3 (Sigma Aldrich, San Jose, CA)). Samples were solubilized at 4°C for 1 hour with rotation and spun at 4°C at a speed of 12,000 x g for 15min. Protein abundance was measured by bicinchoninic acid (BCA) assay (Thermo Fisher Scientific, Eugene, OR). Target proteins were measured in tissue homogenates (1 mg/mL) by capillary electrophoresis using a Wes instrument (Protein Simple, Biotechne) with rabbit polyclonal antibodies for PRDM16 (1:25, PA5-20872; Thermo Fisher Scientific; Eugene, OR), UCP1 (1:50, PA1-24894; Thermo Fisher Scientific; Eugene, OR) or PI3-Kinase p85 (1:25, ABS233; EMD Millipore; Burlington, MA) and with GAPDH (1:1K, 25778; Santa Cruz Biotechnology; Santa Cruz, CA) as a loading control. Data was quantitated using Compass Software (Protein Simple, Biotechne) with target proteins expressed relative to the loading control.

In vivo ^{3}H-2-deoxy-d-glucose uptake. To measure tissue-specific glucose uptake after one day of diet treatment, mice were fasted for 4h (6-10 AM), and injected I.P with 2 g/kg cold glucose spiked with 0.5μCi/g ^{3}H-2-deoxy-d-glucose (Perkin Elmer, Waltham, MA). Tissues were harvested 30 minutes after the injection, weighed, and snap frozen in liquid nitrogen. Tissues were processed in 1 mL homogenizing buffer with glass on glass kontes tubes using a BDC 2002 homogenizer (Caframo, Compact Digital, Ontario, Canada). 50 μL of homogenate was counted on a scintillation counter. A BCA assay was ran on individual tissue lysates and counts per minute (CPM) were made relative to tissue weight.

Statistical Analysis. Data were analyzed by a two-way analysis of variance (ANOVA) for main effects of diet and temperature except for the oral glucose tolerance

test, which used a repeated measures 2-way ANOVA for main effects of group and temperature. A Sidak's multiple comparisons post hoc test was performed when significant main effect differences were detect using a *p*-value of ≤ 0.01. All data are presented as the mean ± standard error of the mean (SEM). Statistics were calculated using Graph Pad Prism version 7 (Graph Pad Software; La Jolla, CA). No differences were detected between 1 and 5d CON at each temperature for all physiological measures (data not shown). Herein, 1d CON data are reported.

Results

Short-term thermoneutral housing combined with acute HFD increases bodyweight and adiposity in male mice. Body weight was increased in male mice housed at 30°C for 8 days (d) compared to 22°C with CON or HFD; however, these temperature-mediated differences in body weight were ameliorated by a longer (5d) HFD exposure (Fig. 1*D*). Short-term T_N as compared to T_s housing also altered body composition. Percent fat mass increased independent of diet type (CON vs HFD) or duration of HFD (Fig. 1*E*). The percent lean mass was reduced in 30°C vs. 22°C with 1d CON and HFD but similar to body weight, temperature-mediated differences in lean mass were absent with 5d HFD. At 22°C, 5d HFD reduced the percent lean mass as compared to 1d CON and 1d HFD (Fig. 1*F*). The increase in percent fat mass with T_N housing is driven, in part, by an increase in scWAT (and eWAT mass with 1d CON and 1d HFD (Fig. 1, *G-H*). eWAT mass was not different between T_s and T_N housing with 5d HFD (Fig. 1*I*). BAT mass was reduced by in CON (100±3 mg vs. 85±3 mg), 1d HFD (100±5 mg vs. 77±4 mg) and 5d HFD (120±5 mg vs. 69±8 mg) with T_N housing (Fig. 1*G*).

Short-term thermoneutral housing alters the mouse behavior and the metabolic and circadian response to HFD. Mouse feeding behavior was changed by both diet and housing temperature. Specifically, T_N suppressed food intake on 1d CON diet (118±21 kcals vs. 57±14 kcals), but not 1 day and 5 day HFD, during the light cycle compared to 22°C (Fig. 2*A*). Additionally, HFD increased light cycle food intake at both temperatures and was greater with 5d HFD (22°C: 182±18 kcals vs. 118±21 kcals; 30°C: 160±9 kcals vs. 57±14 kcals) compared to 1d CON (Fig. 2*A*). During the dark cycle, HFD led to a stepwise increase in daily food intake (kcals/kg) only at T_s (CON: 223±18 kcals; 1d HFD:

274±22 kcals; 5d HFD: 312±18 kcals) and was significantly greater after 5d with HFD relative to CON diet (Fig. 2*B*). No difference in food intake between diet groups was observed at 30°C (Fig. 2*B*). There was a significant interaction of diet and housing temperature on measurements of RER in both the light and dark cycle (Fig. 2, *C-D*). RER was higher in mice on the 1d CON diet at 22°C vs. 30°C in both the light (0.92 vs. 0.82) and dark (0.92 vs. 0.84) cycle. At T_s housing, RER was lower with HFD as anticipated during the light and dark cycle (Fig. 2, *C-D*). In contrast, RER was not different between mice fed CON vs. HFD at T_N housing during the light cycle and the difference in dark cycle RER observed at 22°C with HFD was diminished at 30°C (Fig. 2, *C-D*). There were no differences in total activity during the light cycle by diet or temperature (Fig.2, E); however, there was a significant interaction of diet and housing temperature on measurements of total activity during the dark cycle (Fig. 2*F*). At 22°C, HFD (1 and 5d) increased dark cycle activity (1d HFD: 112±10; 5d HFD: 120±8 meters (m)) compared to CON (70±4 m). In contrast, dark cycle activity was not influenced by diet in mice housed at 30°C; activity of mice on CON diet was as great as mice on HFD (CON: 119±8; 1d HFD: 103±7; 5d HFD: 124±9 m). There was no additive effect of HFD on activity of mice at T_N (Fig.2*F*). Energy expenditure was lower with 30°C vs. 22°C independent of diet throughout the circadian cycle (Fig. 2, *G-H*).

Thermoneutral housing alters glucose metabolism and insulin sensitivity in response to a HFD. Fasting glucose increased with 5d HFD compared to CON and 1d HFD within each housing temperature; however, fasting glucose was lower in each diet group at 30°C housing (Fig. 3*A*). Glucose tolerance was reduced following 1d and 5d of HFD feeding and was only influenced by temperature at the 10min time-point at 22°C following

1d HFD (Fig. 3, B-D). There were no differences between all CON groups (data not shown) and all HFD groups (data not shown). There was no effect of diet or temperature on glucose disposal in response to an insulin bolus after 1d; however, a 5d HFD at 22°C but not 30°C significantly decreased insulin sensitivity (Fig. 3, *E-F*). Examining tissue-specific effects of temperature on glucose metabolism, we found that housing temperature shifted the distribution of glucose uptake during insulin-stimulated condition such that glucose uptake was highest in soleus muscle at 30°C while BAT had the greatest uptake at 22°C in mice on CON diet. With 1d HFD, we found tissue-specific reductions in glucose disposal by temperature. Specifically, 1d HFD decreased BAT glucose disposal by 63% at 22°C housing but not 30°C (Fig. 3, *G-H*). In contrast, at 30°C housing but not 22°C, soleus glucose disposal was reduced by 54% with 1d HFD feeding (Fig. 3, *E-F*).

Thermonetural housing reduces markers of adipose tissue thermogenesis in BAT. In addition to the decrease in BAT mass, T_N housing also decreased gene expression of key regulators of thermogenesis. Specifically, there was a main effect of temperature to decrease *Ucp1*, *Prdm16, Cox8b and Pgc1a* expression after 8 and 12d at 30°C compared to constant 22°C housing (Fig. 4, *A-D*). For *Ucp1* and *Pgc1a* (Fig. 4, *A, D*), the decrease in expression with 30°C was independent of diet type (CON vs. HFD) and time on diet (1d vs. 5d). *Prdm16* expression was decreased at 30°C after 1d, independent of diet; however, it was only decreased with HFD and not CON diet with longer exposure at 30°C (Fig. 4*B*) suggesting a transient effect of temperature on *Prdm16* expression in mice fed a CON diet. *Cox8b* expression was only decreased at 30°C with HFD independent of time on diet (Fig. 4*C*). As these are relatively small changes in gene expression, we sought to determine whether the differences were sufficient to alter protein abundance. PRDM16 protein

abundance was decreased at 30°C following 1d HFD treatment (Fig. 4, *E-F*), while no difference was detected for UCP1 (Fig. 4 *E, G*).

Diet and thermoneutral housing reduce some markers of adipose tissue browning in inguinal scWAT but not eWAT. In scWAT, there was a main effect of temperature to decrease *Ucp1, Cox8b and Pgc1a* expression with T_N compare to T_S housing. Specifically, *Ucp1* expression was decreased at 30°C compared to 22°C independent of diet type (CON vs. HFD) and time on diet (1d vs. 5d). *Cox8b* (Fig. *5B*), *Pgc1a* (Fig. *5D*) and *Prdm16* (data not shown) gene expression was decreased at 30°C compared to 22°C only after longer time (12d) in T_N conditions independent of diet type. Similar to the changes in *Ucp1* expression, *Cidea* expression was decreased at 30°C independent of diet type (CON vs. HFD) or length of time at T_N conditions (8 and 12d); additionally, 5d HFD feeding further reduced *Cidea* expression compared to 5d CON at 30°C (Fig. 5*C*). Thermoneutral housing did not decrease *Ucp1, Prdm16, Cidea, Cox8b or Pgc1a* gene expression in visceral eWAT tissue following 1d or 5d of diet (data not shown).

Thermal neutral housing augments the effect of high fat diet to reduce anti-inflammatory gene expression in inguinal scWAT. With 1d of HFD compared CON, there was no change in the gene expression of *Il4, Il10*, and *Il13* anti-inflammatory markers at either temperature in both scWAT and eWAT depots (Fig. 6, *A-F*). However, with longer diet exposure, there was a significant interaction between diet and temperature to reduce the gene expression of these key anti-inflammatory markers in scWAT. Specifically, *Il4, Il10*, and *Il13* were reduced with 5d of HFD diet feeding only at 30°C and not at 22°C(Fig. 6, *A, C, D*). In contrast, there was no change in the gene expression of *Il4, Il10*, and *Il13*

with temperature in eWAT following 5d diet treatment (Fig. 6, *B, D, F*). *Il13* expression was increased in eWAT with 5d HFD compared to CON at 22°C, but not at 30°C (Fig 6*F*)

Thermal neutral housing attenuates the effect of a high fat diet to increase pro-inflammatory gene expression in eWAT. Overall, expression of some pro-inflammatory genes were elevated by short –term HFD in eWAT at T_S housing but this effect was lost with T_N housing. Specifically, there was no effect of diet (1 or 5d) or temperature on *Tnfa* expression in eWAT (Fig. 7*A*). There was a transient effect of HFD to increase *Il1b* with 1d at 22°C, but not at 30°C, that was diminished by longer exposure to HFD in eWAT (Fig. 7*B*). *Il6* expression increased following 1d and 5d of HFD at 22°C and not 30°C in eWAT (Fig. 7*C*). Lastly, *Ccl2* expression was significantly higher at 30°C compared to 22°C with longer exposure to T_N housing; exposure to 5d HFD in mice at 22°C increased *Ccl2* expression to levels to mice at 30°C in eWAT (Fig. 7*D*). No differences were detected in *Tnfa*, *Il1b*, *Il6* or *Ccl2* gene expression in scWAT with short-term HFD diet or housing temperature (data not shown).

Discussion

The most salient findings of this study are that T_N housing altered the metabolic and cellular response to acute HFD in key pathways that have been implicated in HFD-induced insulin resistance. To our knowledge, this is the first study to assess the effect of T_N housing on *in vivo* glucose metabolism, adipose tissue browning and adipose tissue inflammatory gene expression after such a brief time domain (8 or 12 days total: 7-day acclimation + 1 or 5 day diet treatment).

Short-term T_N housing had a significant and rapid impact on the phenotype and metabolism of the mice. Specifically, T_N housing influenced food intake, activity, EE and RER resulting in altered fat accretion, adipose tissue distribution and substrate utilization. We found that T_N housing decreased food intake during the light cycle relative to mice housed at T_s, particularly in mice on the CON diet. This increase in food intake may be necessary to support the higher EE measured in T_S vs. T_N; These observations are in agreement with previous reports (10, 17) showing an inverse relationship between housing temperature and food intake in chronic conditions. For example, in a 20-week study that utilized a similar experimental design, mice housed at 30°C had increased WAT (scWAT and eWAT) mass and decreased BAT mass relative to mice housed at 22°C (10). Our data shows that these changes in adipose tissue (scWAT, eWAT and BAT) mass in the response to housing temperature occur very rapidly with as little as 8d acclimation. We also found that RER was higher at 22°C housing relative to 30°C across both the light and dark cycles with control diet feeding, which supports previous studies showing higher carbohydrate oxidation in mice on a standard chow diet housed at lower temperatures for longer periods of time (11, 13, 17). We did not observe temperature differences in RER during HFD

feeding likely reflecting the greater influence of the diet composition (i.e. higher fat) on metabolism and the overall decrease in glucose tolerance. We also found that BAT glucose uptake at 22°C during CON feeding was much higher relative to CON fed mice at 30°C. At the cellular level, increased glucose utilization by BAT at 22°C is supported by higher gene expression of *Ucp1*, *Pgc1a, Prdm16,* and PRDM16 protein abundance, which combined promote mitochondrial metabolism that is favorable for heat generation through uncoupled respiration (5). Although 1d exposure to 4°C) has shown to be sufficient to decrease BAT UCP1 protein abundance relative to 22°C (21), we did not see a difference in the present study with 8d acclimation likely due to the large variability in the measurement. Taken together, these data demonstrate that short-term thermoneutral housing is sufficient to alter energy intake, adipose tissue weight, substrate utilization and energy expenditure.

Fasting glucose is primarily regulated by hepatic glycogen stores (32) and is influenced by circulating catecholamines. Subthermoneutral stress increases sympathetic nervous system (SNS) activity and increases circulating norepinephrine (10). Although we do not have data regarding norepinephrine turnover, we speculate that the increase in fasting glucose measured at T_s housing may be due to elevated norepinephrine in response to subthermoneutral stress that results in increased hepatic glycogenolysis (19). After five days of HFD, we find that fasting glucose increased in mice housed at both 22°C and 30°C, but was higher in all conditions (CON and HFD) in mice at 22°C vs. 30°C. Although we observed differences by housing temperature in several factors that have been shown to influence glucose tolerance (energy expenditure (48), BAT mass (37) and upregulation of UCP1 in BAT and scWAT (38), no differences were detected in glucose tolerance between

mice housed at 22°C and 30°C . Additionally, we found a similar decrease in glucose tolerance with 1d and 5d HFD feeding at both housing temperatures. To our knowledge, this is the first rodent study to identify mild glucose intolerance following one day of HFD feeding. The magnitude of change in glucose AUC with 5 days of HFD and was not greater than at 1 day. Interestingly, when Cui and colleagues (10) pair fed mice housed at 22°C to match the reduced intake of mice at 30°C, mice housed at 22°C displayed improvements in glucose tolerance and insulin sensitivity. Thus, we may have seen temperature based differences in glucose tolerance across, if we had implemented pair-feeding.

Although systemic glucose tolerance was similar by temperature, we found tissue-specific differences in glucose clearance indicating that the cellular mechanisms that lead to reduced glucose tolerance with HFD acutely are different depending on housing temperature. Specifically, HFD-feeding reduced insulin-mediated BAT glucose uptake in mice at 22°C but reduced soleus muscle glucose uptake in mice at 30°C. The increase in BAT glucose uptake at T_s likely reflects the greater energy demand of BAT in mice housed at 22°C vs. 30°C, which is reflected by the decrease in BAT mass and EE in mice housed at T_N. These findings have significant implications for studies examining mechanisms that initiate insulin resistance in obesity as it suggests that mice living under conditions of chronic subthermoneutral stress respond differently to HFD challenges than those housed in T_N conditions.

Expansion of scWAT, even in the face of obesity, has been suggested to promote insulin sensitivity in both rodents and humans (25, 26, 29, 33, 36, 40). Implantation of scWAT, but not visceral WAT, into the abdominal cavity of mice improves whole body metabolism (20, 44). In further support that scWAT and eWAT depots are cell

autonomous, Stanford and colleagues (38) demonstrated that transplantation of scWAT, but not eWAT, from exercise trained mice, into the visceral or subcutaneous cavity of sedentary and HFD fed mice, significantly improved glucose tolerance and insulin sensitivity in recipient mice. The same study also observed an exercise induced increase in scWAT *Ucp1* and *Prdm16* expression, which was not seen in eWAT (38). Moreover, inguinal scWAT has been shown to be more susceptible to browning than eWAT (3, 6, 8, 9, 18). These data agree with our findings that scWAT responds more rapidly than eWAT to subthermoneutral stress by increasing markers of browning (*Ucp1*, *Cox8b, Cidea, Pgc1a*). An inverse relationship between periventricular WAT browning and inflammation at 30°C housing was recently shown by Tian and colleagues (43). The study found that although inflammation augmented the development of atherosclerosis, it did not influence insulin resistance, relative to 22°C. Thermoneutral housing has also been shown to exacerbate nonalcoholic fatty liver disease and the response to pro-inflammatory stimuli (16, 39) by influencing Toll-Like Receptor 4 (TLR4) responsiveness (16). Knockout of TLR4 in adipose tissue has been shown to protect against whole body insulin resistance following an acute lipid challenge (41); thus, a connection exists between housing temperature, inflammation and whole body glucose metabolism. We also observed subtle differences in some inflammatory gene markers following one and more so five day HFD feeding that was depot and temperature dependent. Specifically, there was a decrease in anti-inflammatory gene expression (*Il4*, *Il10* and *Il13*) in scWAT only in mice housed at 30°C after 5d HFD with no increase in pro-inflammatory gene expression. Together, these data suggests that a reduction in the anti-inflammatory cytokines in scWAT proceeds or initiates the shift to a pro-inflammatory state that is typically associated with obesity. In

eWAT, there were again subtle increases in some pro-inflammatory markers (*Il1b*, *Il6* and *Ccl2*) with HFD but only in mice housed at 22°C and not 30°C. The lack of an increase in eWAT inflammatory markers in mice housed at 30°C may be attributed to the overall greater eWAT and scWAT mass and perhaps greater potential for expansion. WAT expansion has been shown to reduced adipose tissue inflammation in obesity (22).

An increase in BAT mass has been proposed to be a protective mechanism against subthermoneutral stress, due to the capacity of BAT to generate heat through uncoupled respiration, via UCP1 (5). In a mass dependent manner, BAT has also been associated with an increase in energy expenditure and improvements in insulin sensitivity (38). In contrast, loss of UCP1 exacerbates HFD induced impairments in glucose metabolism (49) and results in obesity even in chow fed rodents (14). To our knowledge, we are the first to identify that changes in energy expenditure, BAT mass and downregulation of BAT browning genes occurs as rapidly as eight days of T_N housing. BAT has also been proposed to be a site of diet induced thermogenesis (reviewed in (4)), as a potential protective mechanism to enhance energy expenditure in the face of long-term abundant energy intake. Here, we observed reduced BAT *Ucp1* expression, decreased EE and increased adiposity in mice after short-term housing at 30°C relative to 22°C that was associated with greater insulin resistance when challenged with a 5d HFD in agreement with previous findings conducted over longer time course.

Herein, we have provided a detailed analysis of the acute metabolic and behavioral responses of mice housed at standard vivarium (22°C) and thermoneutral (30°C) temperatures, while consuming a HFD (45% Calories from fat) or CON (10% Calories from fat diet). We found that one day of HFD was sufficient to impair glucose tolerance

despite no evidence of a consistent parallel increase in immune response. Although housing temperature did not influence HFD induced glucose tolerance, the tissue-specific responses resulting in reduced glucose disposal were altered by housing temperature. Furthermore, short-term (8-12 days) thermoneutral housing decreases energy expenditure, BAT mass, fasting blood glucose and scWAT/BAT "browning" genes and scWAT anti-inflammatory genes. Considering the aforementioned variables have been implicated in mechanisms that initiate insulin resistance in obesity, it is important that housing conditions that alter the physiology of the model system be considered in interpretation of metabolic data.

CONCLUSION

Focus of this Discussion

This discussion will 1) summarize the key findings of each study, 2) describe how the findings advance the current understanding of how adipose tissue *Pik3r1* mediates changes in insulin sensitivity, 3) identify several new questions raised by the results in this dissertation, and 4) propose a follow up experiment to address one of these questions.

Summary of Key Findings

Results from this dissertation provide a number of novel insights into the role of adipose tissue *Pik3r1* in regulating glucose homeostasis, insulin sensitivity and thermogenic programming of adipose tissue. Previous research from our laboratory and others established a need to investigate the effect of *Pik3r1* in regulating glucose homoestasis and insulin sensitivity, specifically in adipose tissue. Accordingly, the studies in this dissertation focused on understanding the role of *Pik3r1* in regulating glucose tolerance following acute and long term HFD exposure. As imperative as it is to understand how the *in vivo* systems functions without a particular protein, it is also necessary to understand if there is a gain of function mechanism if the protein were to be over expressed; thus, we aimed to assess the role of adipose tissue p55α OX in regulating glucose homeostasis, insulin sensitivity and adipose tissue thermogenesis. A summary of the key findings is provided below.

Study 1. Heterozygous Knockout of Adipocyte Pik3r1 Protects Against Acute HFD Induced Glucose Intolerance and Induced Insulin Resistance

- In male cre negative pik3r1$^{flox/flox}$ (WT) mice, eWAT p85α abundance was increased 7.5-fold following three days of HFD exposure

- Increased eWAT p85α abundance was associated with decreased glucose tolerance and insulin sensitivity in WT mice
- Heterozygous knockout, but not homozygous knockout, of adipocyte *Pik3r1* protected against acute HFD induced glucose intolerance and insulin resistance, despite increased body weight and adiposity, relative to WT mice.
- Homozygous knockout of adipocyte *Pik3r1* resulted in exacerbated levels of glucose intolerance, relative to WT mice, insulin resistance and decreased energy expenditure

Study 2. Inducible heterozygous knockout of adipocyte *Pik3r1* reverses obesity induced glucose intolerance and enhances adipocyte insulin sensitivity

- Heterozygous knockout, but not homozygous KO, of adipocyte *Pik3r1* reversed obesity induced glucose intolerance
- Heterozygous knockout, but not homozygous KO, of adipocyte *Pik3r1* protected mice from obesity induced impairments in systemic and adipocyte insulin resistance

Study 3. Adipocyte specific overexpression of p55α enhances glucose tolerance, energy expenditure and markers of thermogenesis in brown adipose tissue

- Male mice with adipocyte specific overexpression of p55α enhanced glucose tolerance independent of body weight and adiposity, relative to male WT ($p55^{flox/flox}$) mice
- Male mice with adipocyte specific overexpression of p55α had increased BAT mass and enhanced energy expenditure, relative to male WT ($p55^{flox/flox}$) mice

- Male mice with adipocyte specific overexpression of p55α had increased markers (gene and protein levels of UCP1 and PRDM16) of thermogenic programming in BAT

Study 4. Short-term thermoneutral housing alters glucose metabolism and markers of adipose tissue browning in response to a high fat diet in lean mice

- Standard vivarium temperature resulted in decreased body weight, percent fat mass, inguinal subcutaneous WAT mass, perigonadal eWAT mass in 1d CON, 1d HFD and 5d HFD treated WT mice
- Standard vivarium temperature resulted in increased BAT mass and energy expenditure, independent of diet condition in WT mice
- One day of HFD was sufficient to decrease glucose tolerance, independent of housing temperature, and the observed phenotype was not made worse by five days of HFD
- BAT was the preferential tissue for glucose disposal under standard vivarium housing conditions, while skeletal muscle was the preferential tissue for glucose disposal under thermoneutral conditions
- Short-term (8 days) thermoneutral housing was sufficient to decrease markers of adipose tissue thermogenesis in BAT and inguinal subcutaneous white adipose tissue
- Thermoneutral housing increased proinflammatory gene expression in inguinal epididymal white adipose tissue following one day of HFD, relative to mice housed at standard vivarium temperature

How These Studies Fill Gaps in Current Understanding

The studies in this dissertation were designed to fill three main gaps in the understanding of how adipose tissue *Pik3r1* influences insulin sensitivity and glucose homeostasis. The major goal of study 1 was to evaluate the role of HZ knockout of adipocyte *Pik3r1* in regulating acute HFD induced impairments in glucose intolerance and insulin sensitivity. Lee et al. (8) recently demonstrated that three days of HFD was sufficient to drive glucose intolerance independent of changes in body weight and adiposity. Furthermore, our lab previously showed that obese mice with global HZ deletion of *Pik3r1* (αHZ) maintain adipose tissue PI3K activity, as well as adipocyte and systemic insulin sensitivity (9). Considering obesity is a progressive disease, and its associated comorbidities actually arise prior to a significant gain in body weight or adiposity (3), it was crucial to determine the role of adipose tissue *Pik3r1* in regulating the onset of glucose intolerance and insulin resistance. Study 1 established that increased eWAT p85α abundance occurs rapidly and is associated with decreased glucose tolerance and insulin sensitivity. Furthermore, by reducing *Pik3r1* expression prior to the onset of acute HFD treatment, mice maintain glucose tolerance and insulin sensitivity.

The major goal of study 2 was to investigate whether HZ knockout of adipocyte *Pik3r1* would reverse glucose intolerance following the development of obesity. Considering previous findings from our lab (9) demonstrate that αHZ mice are not resistant to obesity and protected against obesity induced impairments in adipocyte and systemic insulin sensitivity, it was crucial to determine whether HZ knockout of adipocyte *Pik3r1* following the development of obesity would reduce obesity induced impairments in glucose tolerance. This study demonstrates that the targeting the

metabolic diseases associated with obesity may be of greater importance to overall health than weight loss alone. Furthermore, study 2 demonstrates that adipocyte HZ knockout protects against obesity induced adipocyte and systemic insulin resistance, as well as insulin signaling upstream (p-IRS1 Y896) and downstream (p-AKT Ser473) of PI3K.

The major goal of study 3 was to determine the specific role of p55α OX, *in vivo*, on glucose metabolism and insulin sensitivity. To date, p55α OX has only been studied in cell culture systems, which is undoubtedly informative for establishing mechanism, but lacks translational potential for future clinical interventions. αHZ obese mice were protected from an obesity induced increase in eWAT p55α abundance (9), which was associated with enhanced adipocyte and systemic insulin sensitivity. Furthermore, global knockout of p50α/p55α enhanced adipocyte and systemic insulin sensitivity (5), thus we hypothesized that independent of diet, mice with adipocyte specific p55α OX (adipo-p55OX) would have decreased glucose tolerance and insulin sensitivity. Contrary to our hypothesis, we found that adipo-p55OX mice had a two-fold improvement in glucose tolerance, relative to $p55^{flox/flox}$ WT controls, which was associated with increased BAT mass and energy expenditure. In order to help explain the differences observed in energy expenditure, we found that adipo-p55OX mice had increased *Ucp1* and *Prdm16* (markers of thermogenesis) gene expression as well as protein abundance. This study has identified a novel role for adipose tissue p55α in regulating glucose homeostasis and adipose tissue browning.

The major goal of study 4 was to determine the effect standard vivarium housing conditions had on glucose metabolism, energy expenditure and adipose tissue browning. Considering mouse thermoneutral zone is 30°C and standard vivarium temperature (22-

23°C) is considered a thermal stress for mice (7), it was imperative to determine whether our primary outcome measures were influenced by housing conditions. To date, no studies have assessed the short-term effect of thermoneutral housing relative to standard vivarium temperature on glucose homeostasis, insulin sensitivity and adipose tissue browning. Here, we provide evidence that acute (one and five day) HFD induced glucose intolerance is not influenced by housing temperature; however; we did observe a divergence in site of glucose disposal, suggesting BAT is the primary site for glucose disposal at standard vivarium conditions while the soleus is the primary site for glucose disposal under thermoneutral conditions. Furthermore, we observed that eight days of thermoneutral housing was sufficient to decrease markers of adipose tissue thermogenesis in BAT and scWAT, relative to standard vivarium conditions, which agrees with similar findings in long-term thermoneutral exposure (6). Considering we are conducting mouse studies to ultimately improve human health, and humans do not typically live in thermal stressed conditions, it is imperative we are not biasing our findings by housing mice at inappropriate temperatures.

Future Experiments

To follow up on study 1, it is necessary to determine the immune-phenotype of the adipose tissue from mice with HZ knockout of adipocyte *Pik3r1*. Considering αHZ mice are protected from obesity induced AT macrophage infiltration (9), it is necessary to determine whether *Pik3r1* also influences immune cell abundance, immune cell chemotaxis and cytokine production. The current logic behind obesity induced insulin resistance is that inflammation is the primary driver of the insulin resistant phenotype; however, in the present study, WT mice had impaired glucose tolerance and insulin sensitivity following three days of HFD treatment independent of changes in body weight or adiposity.

To follow up on study 2, it is also necessary to determine the immune-phenotype of the adipose tissue from mice with HZ knockout of adipocyte *Pik3r1*. Findings from immune-phenotyping experiments in these mice would build on previous findings from αHZ mice (9), where the primary question was whether the adipocyte phenotype influenced the immune-phenotype. By using inducible HZ knockout of adipocyte *Pik3r1* following the development of obesity, we will able to determine whether the immune-phenotype of adipose tissue influences the adipocyte phenotype.

To follow up on study 3, it would be informative to perform hyperinsulinemic-euglycemic clamps on these mice, to determine how adipocyte specific OX of p55α influences other tissues (i.e. liver and skeletal muscle) responsible for maintaining glucose homeostasis (2). Considering the adipo-p55OX mouse is a novel mouse model, it is important to further pursue the mechanism as to how adipo-p55OX improves BAT thermogenesis, and whether these differences actually result in increased heat generation.

As described in figure 1, we propose that BAT PI3K plays a direct role in regulating BAT thermogenesis and increasing energy expenditure. Furthermore, it would be informative to determine if adipo-p55OX mice also have increased browning of WAT. Initially, we should determine whether adipo-p55OX mice have morphological changes (increased abundance of multilocular, brown adipocytes) in WAT. A third experiment to initially conduct to follow up on the findings in this dissertation is to determine whether adipo-p55OX mice are protected from obesity induced insulin resistance.

To follow up on study 4, we should assess morphological changes in scWAT to determine whether there is a unilocular to multilocular cell shift, which would be indicative of WAT browning. Furthermore, it would be important to determine whether a more long-term thermoneutural exposure, prior to the onset of HFD, would influence the metabolic response to HFD.

Conclusion

In conclusion, this dissertation has provided novel insights into the role of adipocyte *Pik3r1* in regulating acute and long term HFD induced insulin resistance. Furthermore, this dissertation has characterized glucose metabolic profile of a novel mouse model of adipocyte specific OX p55α. Moreover, studies in adipo-p55OX mice reveal a novel role for BAT p55α in regulating BAT thermogenesis and energy expenditure. Lastly, this dissertation provides evidence that short-term housing of mice within their thermoneutral zone has a rapid impact on adipose tissue thermogenesis and inflammation. In order to adequately translate preclinical findings to future clinical trials, it is critical that mouse researchers are not biasing their findings by inappropriately

housing their mice. Taken together, by identifying the roles of adipose tissue *Pik3r1* in regulating adipose tissue and systemic insulin sensitivity, the studies presented in this dissertation support the use of adipose tissue *Pik3r1* as a therapeutic target for attenuating metabolic disease.

APPENDIX A

FIGURES FOR CHAPTER I

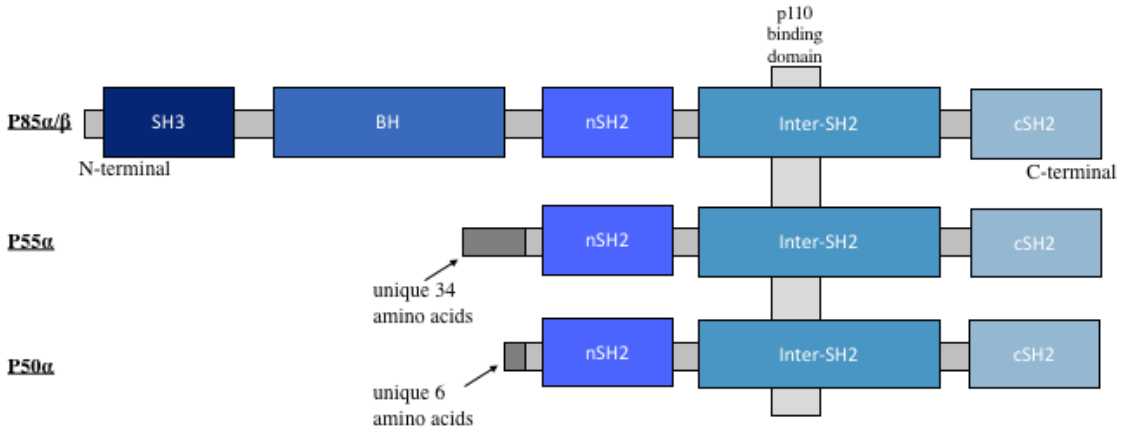

Figure 1. The protein domains of PI 3-Kinase regulatory subunits. The full length p85α gene products and p55α and p50α, contain the common SH2 carboxy-terminal domain, an internal SH2 domain and the p110 catalytic subunit binding domain. p50α and p55α lack the amino-terminal portion found in the full length p85α and p85β containing the SH3 domain, the proline-rich domains, and the BH domain, and in its place p55α and p50α have unique amino-terminal sequences consisting of 34 and 6 amino acids, respectively.

APPENDIX B

FIGURES FOR CHAPTER II

Figure 1.

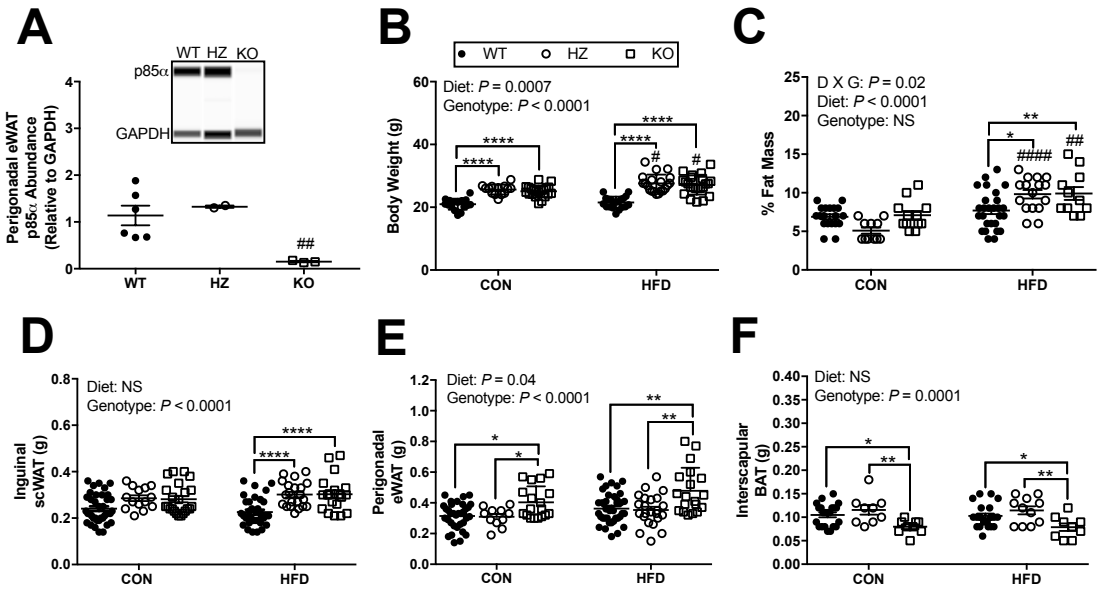

Figure 1. Model validation, body weight, body composition and tissue weights in WT, HZ and KO mice fed a control diet vs. high fat diet for 3d. (A) Immunoblot of PI3K p85α abundance in eWAT of WT, HZ and KO mice (n = 3-5/group). (B) Body weight and (C) percent fat mass following 3d of CON and HFD treatment (n =15-20/group). (D) Inguinal scWAT, (E) perigondal eWAT and (F) interscapular BAT mass following 3d of CON and HFD feeding (n = 15-20/group). Data reported as mean ± SEM. # differences within same genotype (# $P \leq 0.05$; ## $P < 0.01$; ### $P < 0.001$; #### $P < 0.0001$). * differences within same diet (* $P \leq 0.05$; ** $P < 0.01$; *** $P < 0.001$; **** $P < 0.0001$).

Figure 2.

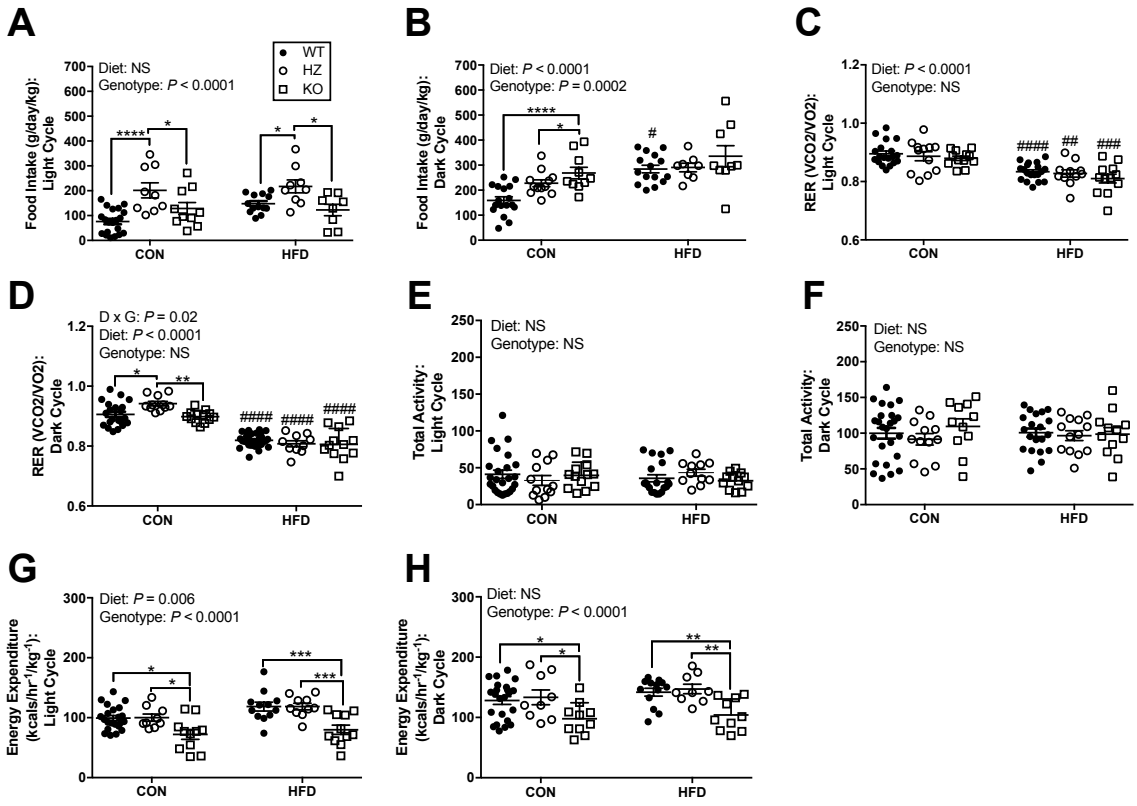

Figure 2. Metabolic phenotyping in WT, HZ and KO mice fed control diet vs. high fat diet for 3d. Food intake assessed during the (A) light and (B) dark cycles (n =10-15/group). (C) Respiratory exchange ratio (RER) assessed during the light and (D) dark cycles (n= 10-15/group). (E) Total activity assessed during the light and (F) dark cycles (n= 10-15/ group). (G) Energy expenditure assessed during the light and (H) dark cycles (n =10-15/ group). Data reported as mean ± SEM. # differences within same genotype (# $P \leq 0.05$; ## $P < 0.01$; ### $P < 0.001$; #### $P < 0.0001$). * differences within same diet (* $P \leq 0.05$; ** $P < 0.01$; *** $P < 0.001$; **** $P < 0.0001$).

Figure 3.

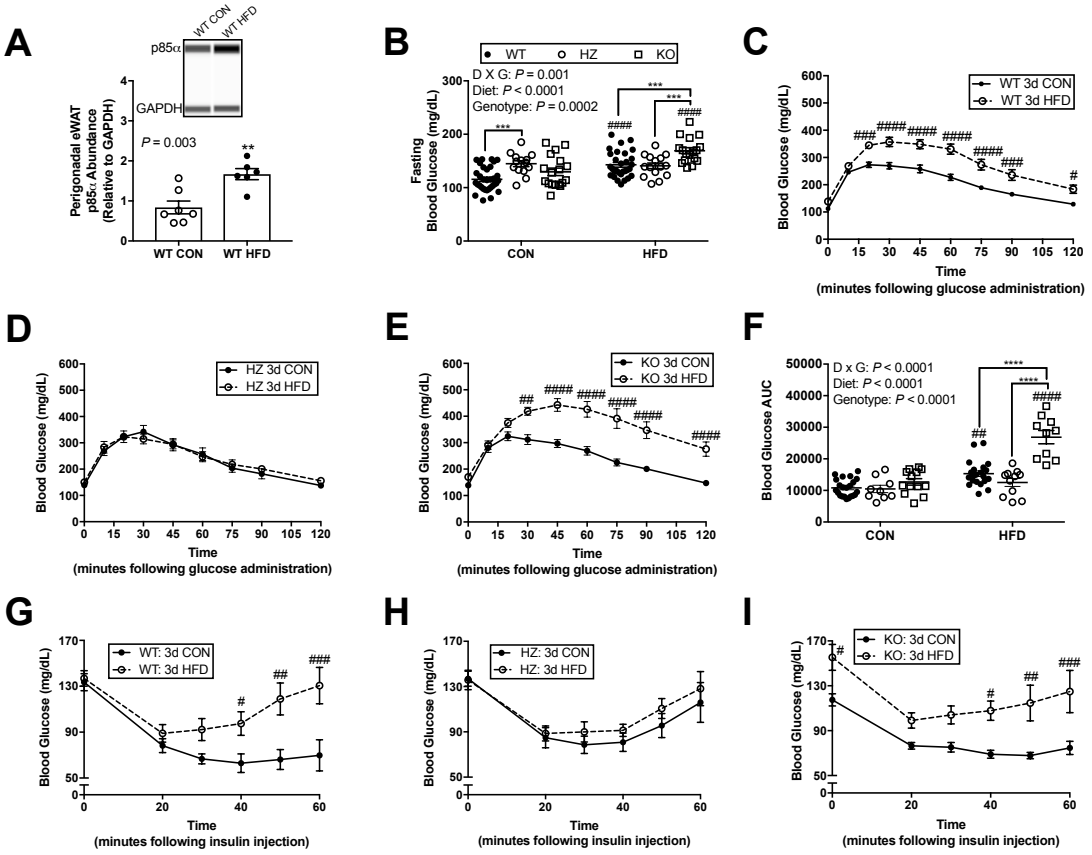

Figure 3. Perigonadal eWAT p85α abundance, glucose metabolism and insulin sensitivity in WT, HZ and KO mice fed control diet vs. high fat diet for 3d. (A) Perigonadal eWAT p85α abudance in WT mice fed CON or HFD for 3d (n = 6-7/group). (B) Fasting blood glucose in WT, HZ and KO mice fed CON or HFD for 3d (n = 20-30/group). Oral glucose tolerance tests in (C) WT, (D) HZ and (E) KO mice fed CON or HFD for 3d (n = 10-15/group). (F) Oral glucose toleranc AUC in WT, HZ and KO mice fed CON or HFD for 3d (n = 10-15/group). Insulin tolerance tests in (G) WT, (H) HZ and (I) KO mice fed CON or HFD for 3d (n = 5-10/group). Data reported as mean ± SEM. # differences within same genotype (# $P \leq 0.05$; ## $P < 0.01$; ### $P < 0.001$; #### $P < 0.0001$). * differences within same diet (* $P \leq 0.05$; ** $P < 0.01$; *** $P < 0.001$; **** $P < 0.0001$).

APPENDIX C

FIGURES FOR CHAPTER III

Figure 1.

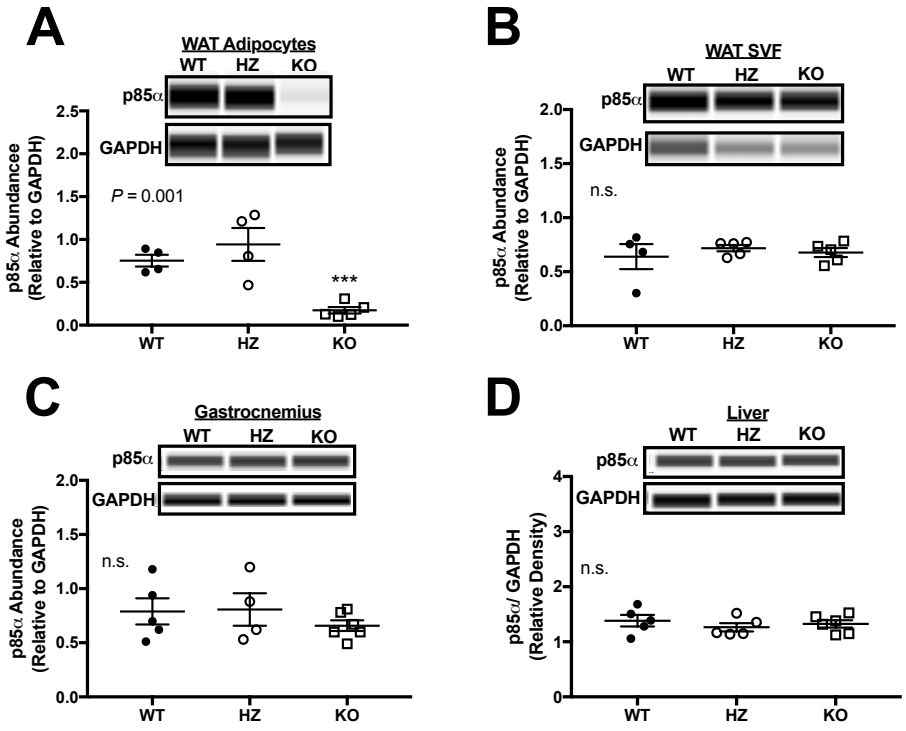

Figure 1. *Pik3r1* is knocked out strictly in adipocytes following administration of tamoxifen. p85 abundance from WT, HZ and KO mice in (A) WAT adipocytes, (B) WAT SVF, (C) gastrocnemius and (D) liver. Data reported as mean SEM. CON, control diet; HFD, high fat diet. Significant between genotype differences are expressed with * (* $P < 0.05$, ** $P<0.01$, *** $P<0.001$, **** $P<0.0001$).

Figure 2.

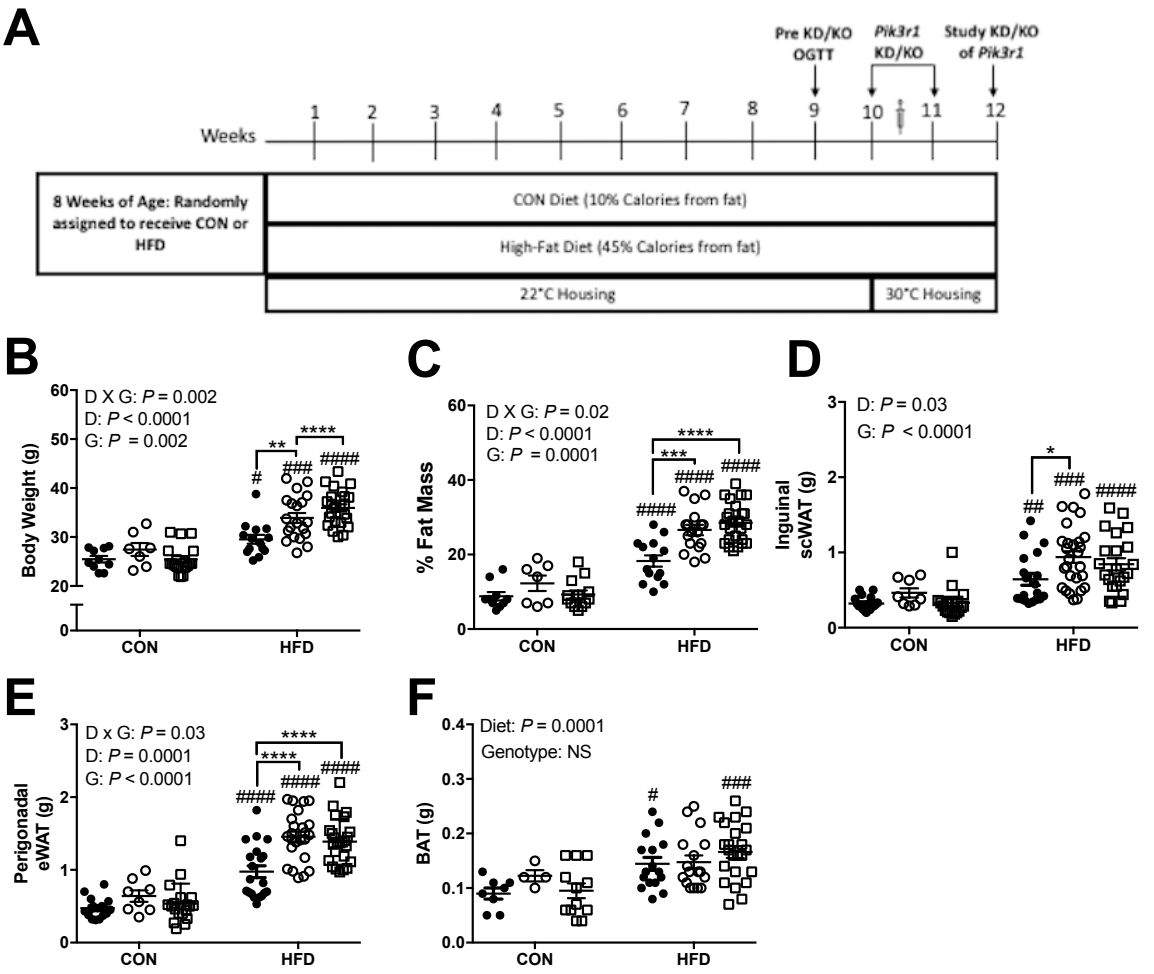

Figure 2. Body weight and adiposity are inversely associated with adipocyte *Pik3r1* expression following 12 weeks of HFD feeding. (A) Illustration of study design, (B) body weight, (C) percent fast mass, (D) inguinal scWAT mass, (E) gonadal eWAT mass and (F) interscapular BAT mass. Data reported as mean SEM. CON, control diet; HFD, high fat diet. Significant between diet differences are expressed with # (# $P< 0.05$, ## $P<0.01$, ### $P<0.001$, #### $P<0.0001$). Significant between genotype differences are expressed with * (* $P< 0.05$, ** $P<0.01$, *** $P<0.001$, **** $P<0.0001$).

Figure 3.

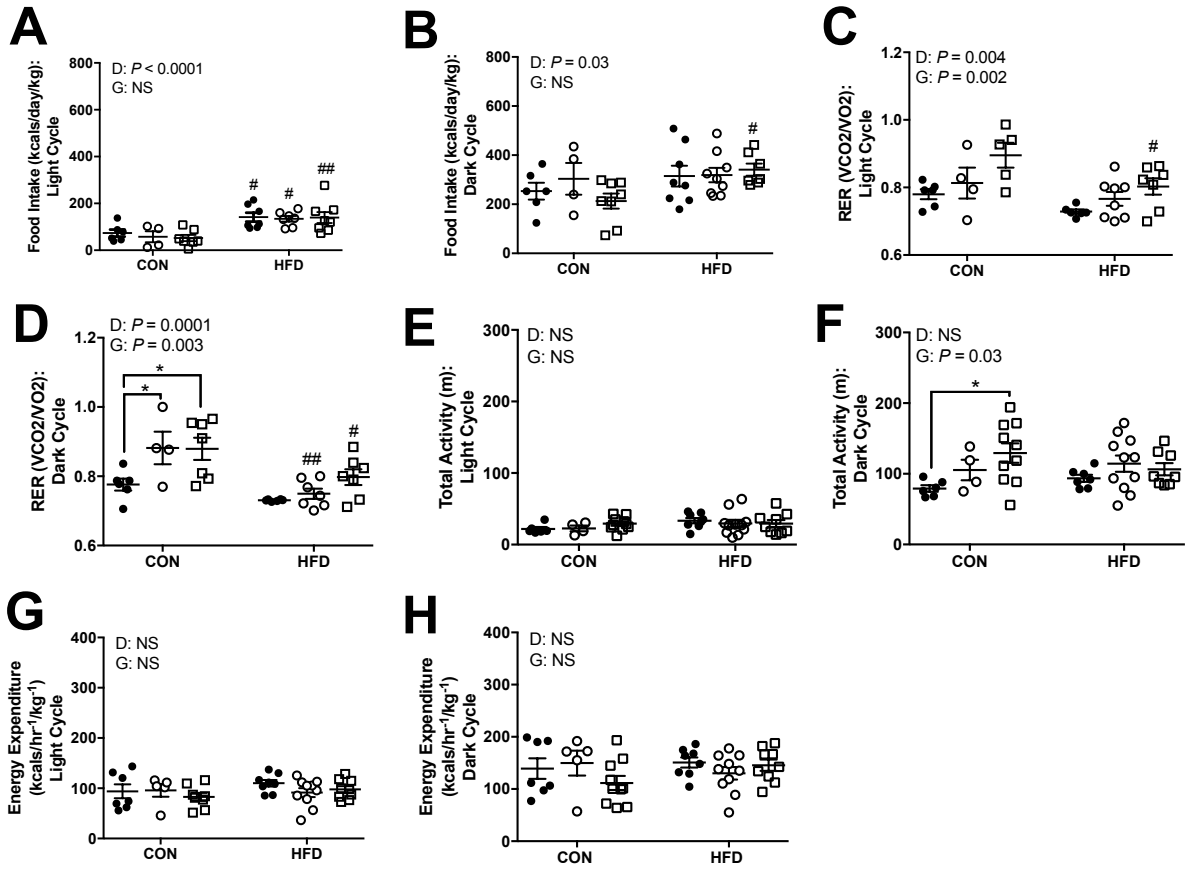

Figure 3. Metabolic phenotyping in WT, HZ and KO mice fed control diet vs. high fat . Food intake assessed during the (A) light and (B) dark cycles (n =10-15/group). (C) Respiratory exchange ratio (RER) assessed during the light and (D) dark cycles (n= 10-15/ group). (E) Total activity assessed during the light and (F) dark cycles (n= 10-15/group). (G) Energy expenditure assessed during the light and (H) dark cycles (n =10-15/group). Data reported as mean ± SEM. # differences within same genotype (# $P \leq 0.05$; ## $P < 0.01$; ### $P < 0.001$; #### $P < 0.0001$). * differences within same diet (* $P \leq 0.05$; ** $P < 0.01$; *** $P < 0.001$; **** $P < 0.0001$).

Figure 4.

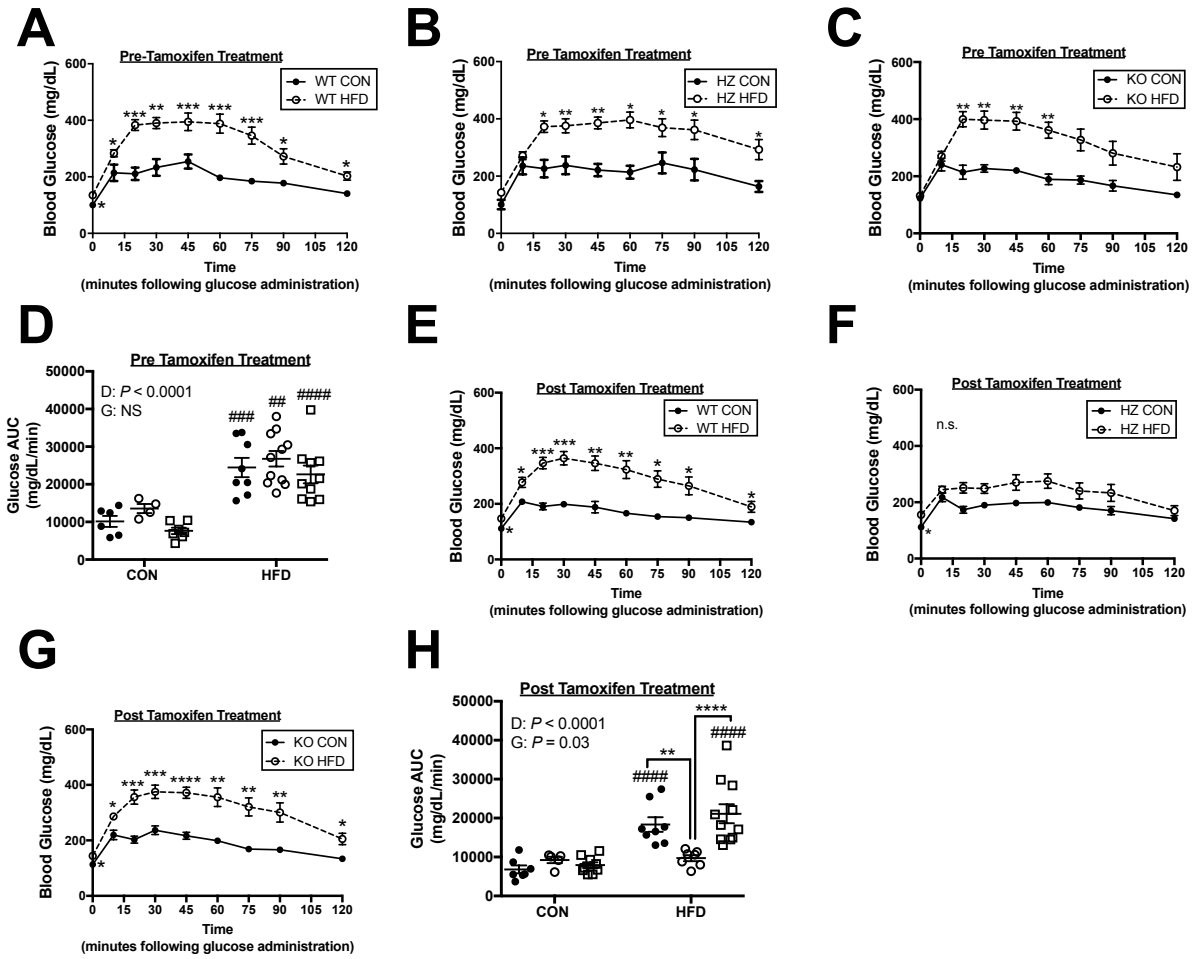

Figure 4. Glucose tolerance before and after heterozygous and homozygous *Pik3r1* knockout. Oral glucose tolerance tests in CON and HFD fed (A) WT, (B) HZ and (C) KO mice prior to tamoxifen treatment. (D) Glucose area under the curve in CON and HFD fed WT, HZ and KO mice prior to tamoxifen treatment. Oral glucose tolerance tests in CON and HFD fed (E) WT, (F) HZ and (G) KO mice prior to tamoxifen treatment. (H) Glucose area under the curve in CON and HFD fed WT, HZ and KO mice following tamoxifen treatment. Data reported as mean SEM. CON, control diet; HFD, high fat diet. Significant between diet differences are expressed with # (# $P < 0.05$, ## $P<0.01$, ### $P<0.001$, #### $P<0.0001$). Significant between genotype differences are expressed with * (* $P < 0.05$, ** $P<0.01$, *** $P<0.001$, **** $P<0.0001$).

Figure 5.

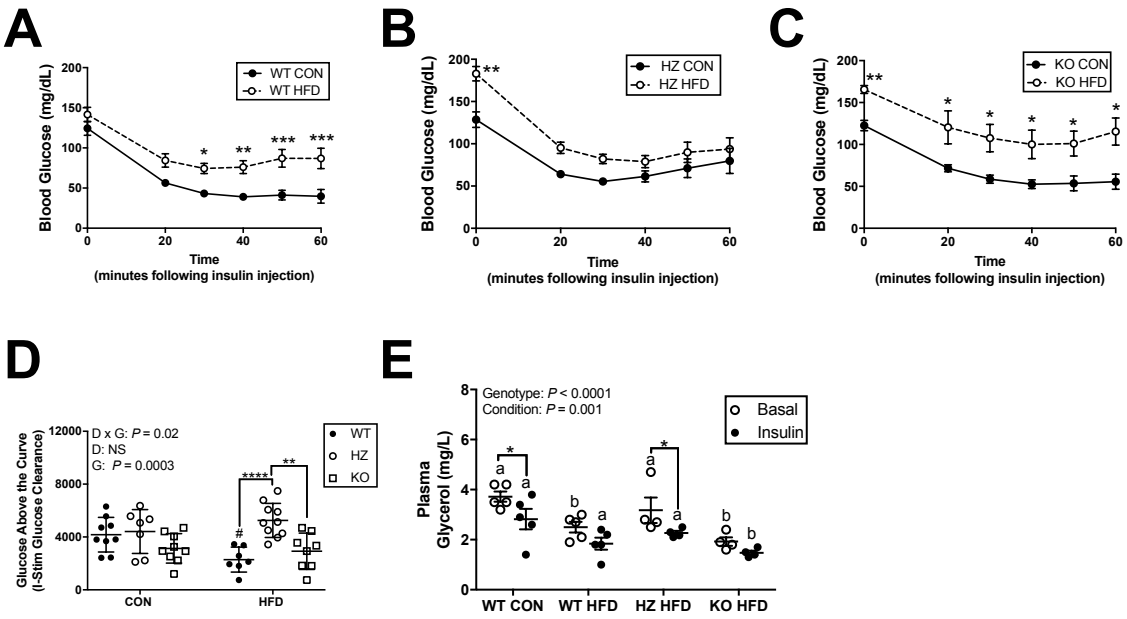

Figure 5. ***In vivo*** **insulin tolerance and insulin-stimulated suppression of plasma glycerol.** Insulin tolerance tests in CON and HFD fed (A) WT, (B) HZ and (C) KO mice following tamoxifen treatment, and I-stim glucose area above the curve (D) . (E) Insulin-stimulated suppression of plasma glycerol in WT CON, WT HFD, HZ HFD and KO HFD. Data reported as mean SEM. CON, control diet; HFD, high fat diet. Significant between diet differences are expressed with # (# $P< 0.05$, ## $P<0.01$, ### $P<0.001$, #### $P<0.0001$). Significant between genotype differences are expressed with * (* $P< 0.05$, ** $P<0.01$, *** $P<0.001$, **** $P<0.0001$).

Figure 6.

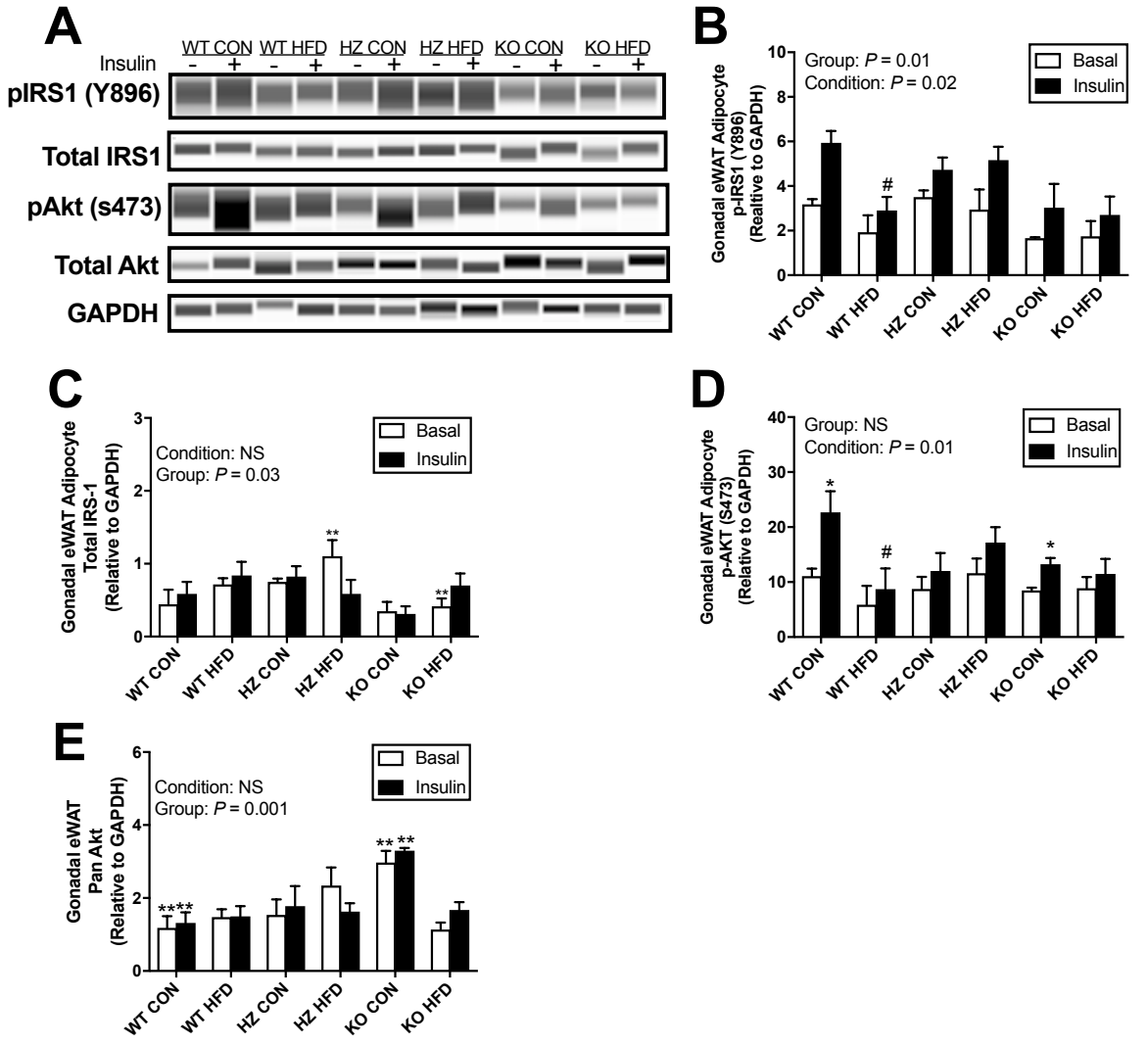

Figure 6. Adipocyte insulin signaling after heterozygous and homozygous KO of *Pik3r1*. (A) Representative immunoblots of pAKT(S473), pan AKT, pIRS1(Y896), total IRS1 and GAPDH. Quantification of (B) pIRS1(Y896), (C) total IRS1, (D) pAKT(S473) and (E) total Akt, quantified relative to GAPDH. Data reported as mean SEM. CON, control diet; HFD, high fat diet. Significant between diet differences are expressed with # (# $P \leq 0.05$, ## $P < 0.01$, ### $P < 0.001$, #### $P < 0.0001$) . Significant between genotype differences are expressed with * (* $P \leq 0.05$, ** $P < 0.01$, *** $P < 0.001$, **** $P < 0.0001$).

APPENDIX D

FIGURES FOR CHAPTER IV

Figure 1.

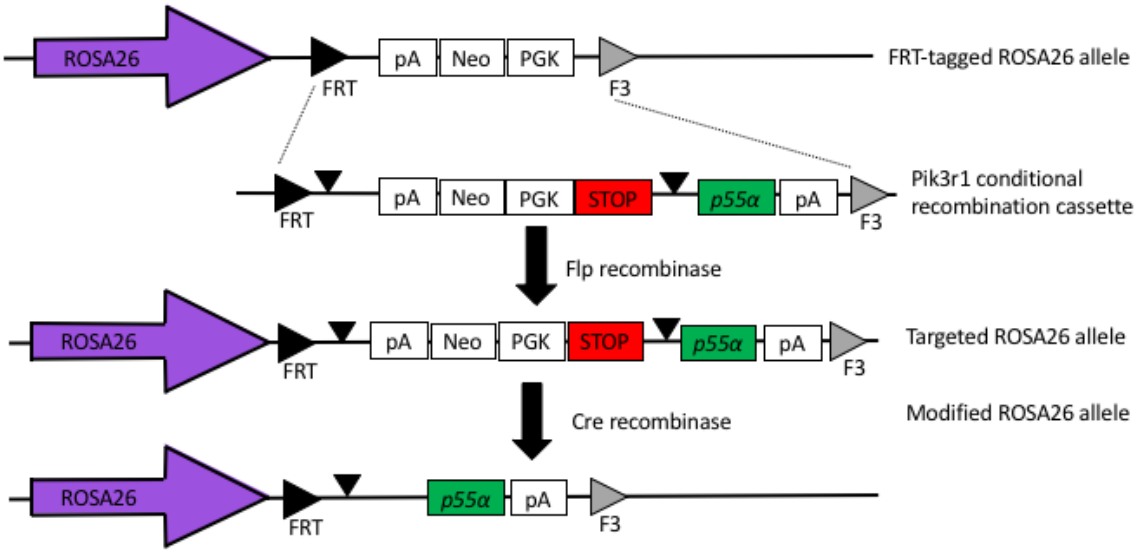

Figure 1. Design of adipocyte specific p55α OX mouse. Pik3r1 knock-in at the ROSA26 locus by recombinase-mediated cassette exchange (RMCE). A Pik3r1 recombination cassette was made by flanking the cDNA of Pik3r1 (p85a, p55a or p50a) and a floxed PGK-Puro selection marker followed by 4x SV40 polyA STOP signal with FRT and F3. This cassette together with pCAG-Flpe were electroporated into ROSA-FNF3-1F1 ES cells (an ES cell line targeted with FRT-PGK-neo-F3 at the ROSA26 locus). The exchange of neo for Pik3r1 at the ROSA26 locus was facilitated by Flp-recombinase mediated site specific recombination so that the recombinants would become G418 sensitive and Puro resistant. The correct exchange was confirmed by PCR. The 4x SV40 polyA STOP signal along with the selection marker PGK-Puro is removed by Cre recombinase. This puts the Pik3r1 cDNA under the expression of the endogenous ROSA26 promoter.

Figure 2.

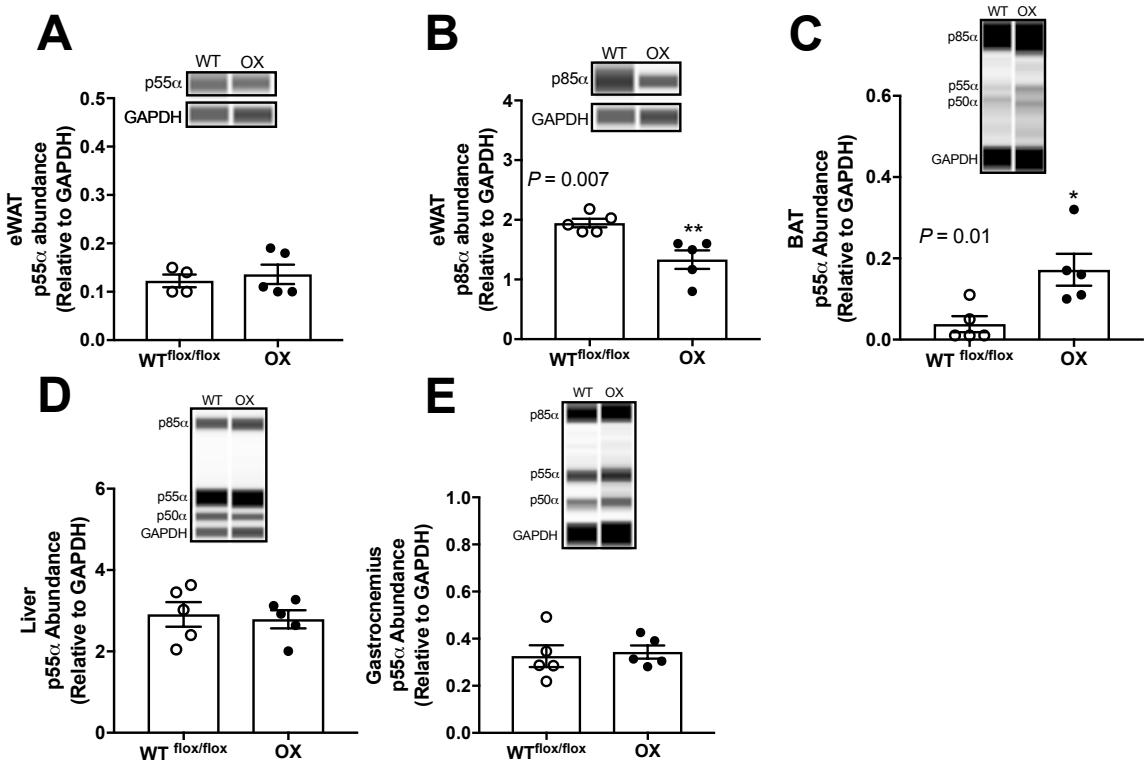

Figure 2. Validation of adipocyte specific OX of p55. Body weight, body composition and adipose tissue weight in WT and adipo-p55OX mice. Representative mmunoblot and quantification of (A) eWAT p55α, (B) eWAT p85α, (C) BAT p55α, (D) Liver p55α and (E) Gastrocnemius p55α in WT and adipo-p55 OX mice. Data are expressed as means ± SEM. * represent significant differences between groups (* $P < 0.05$, ** $P < 0.01$, *** $P < 0.001$, **** $P < 0.0001$). (n= 5-6/ group).

Figure 3.

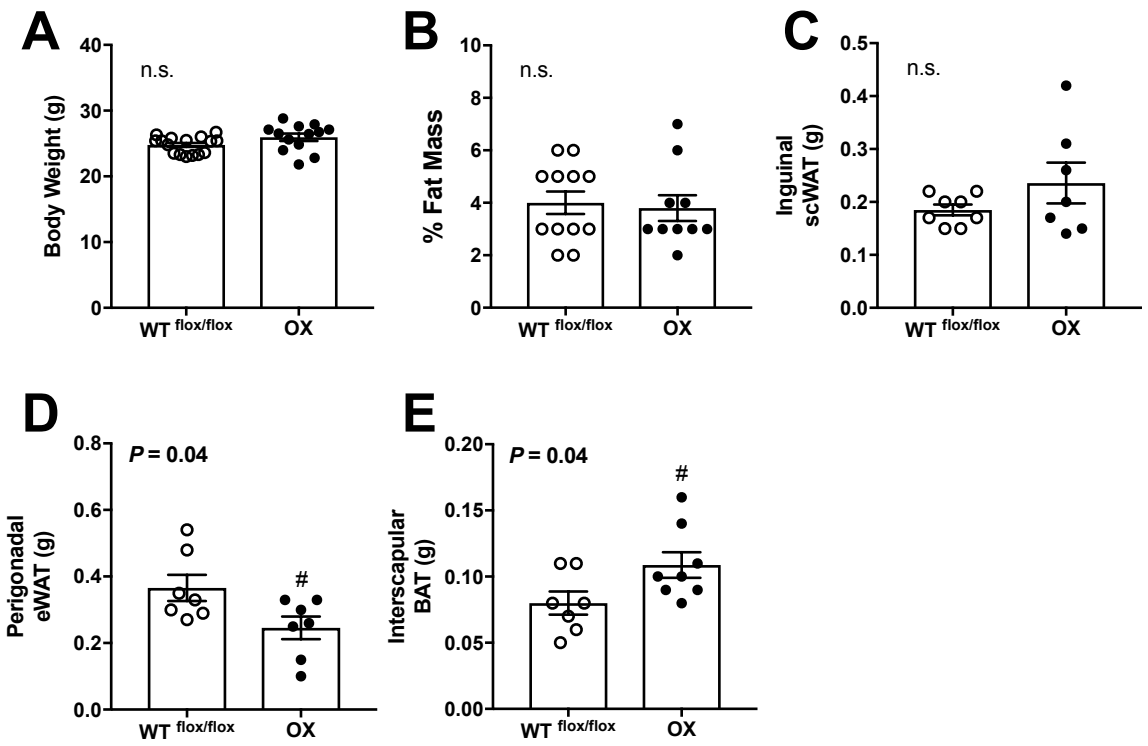

Figure 3. Body weight, body composition and adiposity in WT and p55α OX mice. (A) Body weight, (B) percent fat mass, (C) inguinal scWAT, (D) perigonadal eWAT, (E) interscapular BAT in male WT and adipo-p55OX mice. Data are expressed as means ± SEM. * represent significant differences between groups (* $P < 0.05$, ** $P < 0.01$, *** $P < 0.001$, **** $P < 0.0001$). (n= 10-15/ group).

Figure 4.

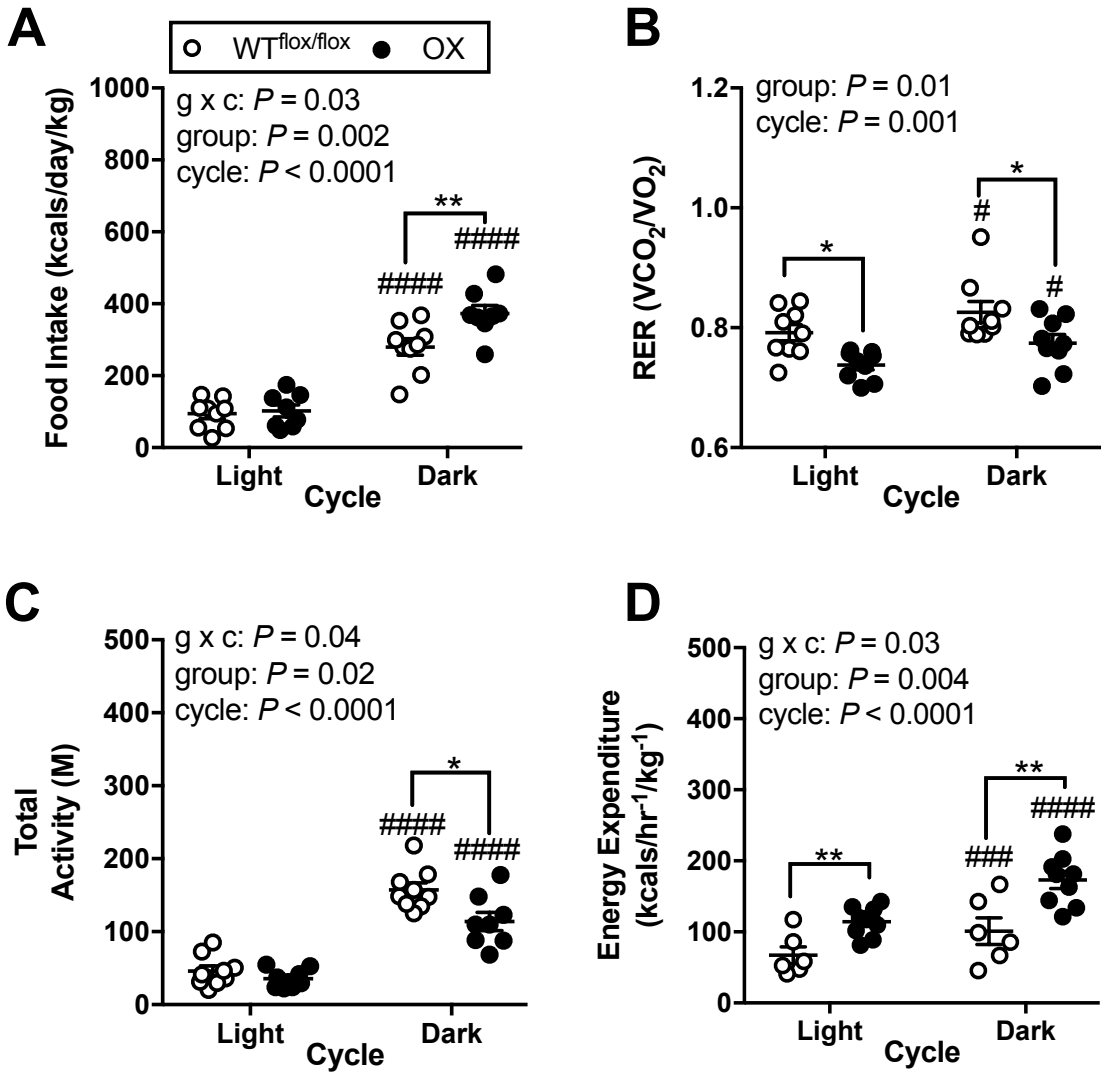

Figure 4. The effect of adipocyte specific p55 OX on Kilocalories consumed, substrate utilization, activity and energy expenditure in WT and adipo-p55 OX mice. (A) Food intake, (B) respiratory exchange ratio, (C) total activity and (D) energy expenditure during the light and dark cycles in male WT and adipo-p55OX mice. Data are expressed as means ± SEM. # represent between cycle differences (# $P < 0.05$, ## $P < 0.01$, ### $P < 0.001$, #### $P < 0.0001$). * represent significant differences between groups (* $P < 0.05$, ** $P < 0.01$, *** $P < 0.001$, **** $P < 0.0001$). (n= 10-12/ group).

Figure 5.

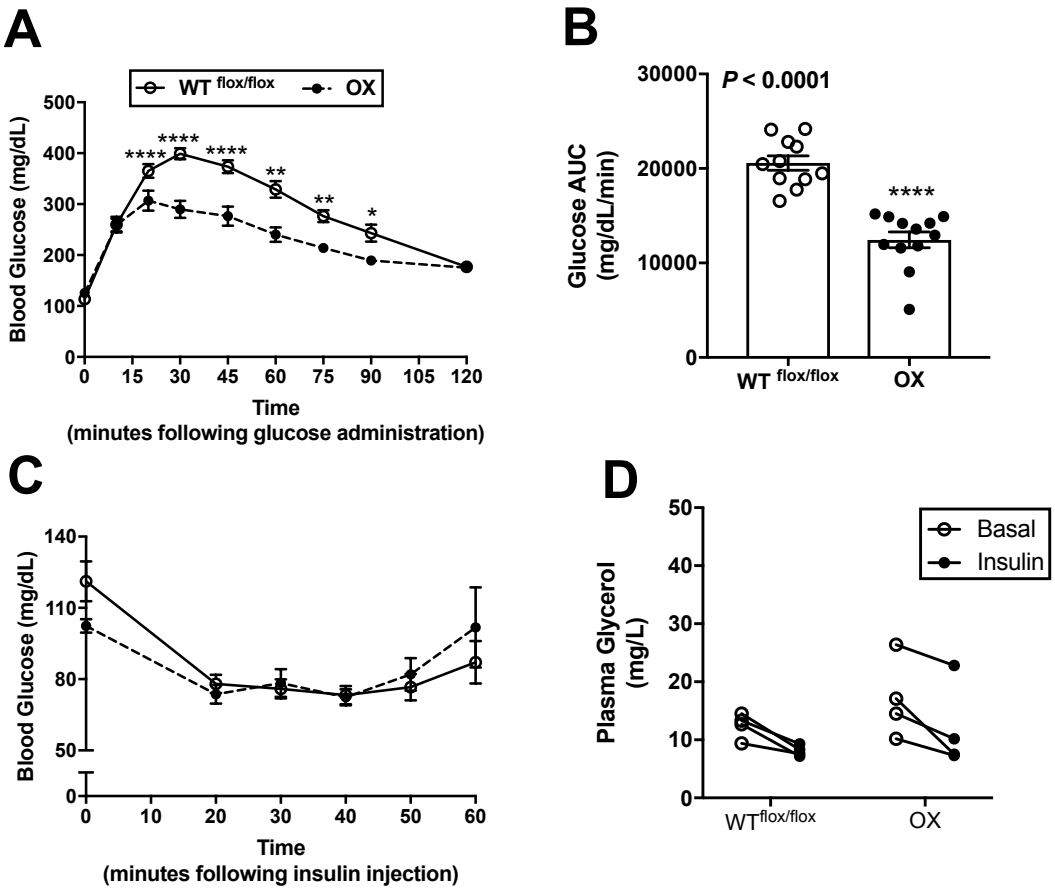

Figure 5. The effect of adipocyte specific p55 OX on glucose tolerance, systemic insulin sensitivity and adipocyte insulin sensitivity. (A) Oral glucose tolerance tests, (B) glucose area under the curve, (C) insulin tolerance tests and (D) insulin-stimulated suppression of plasma glycerol in WT and adipo-p55OX mice. Data are expressed as means ± SEM. * represent significant differences between groups (* $P < 0.05$, ** $P < 0.01$, *** $P < 0.001$, **** $P < 0.0001$)

Figure 6.

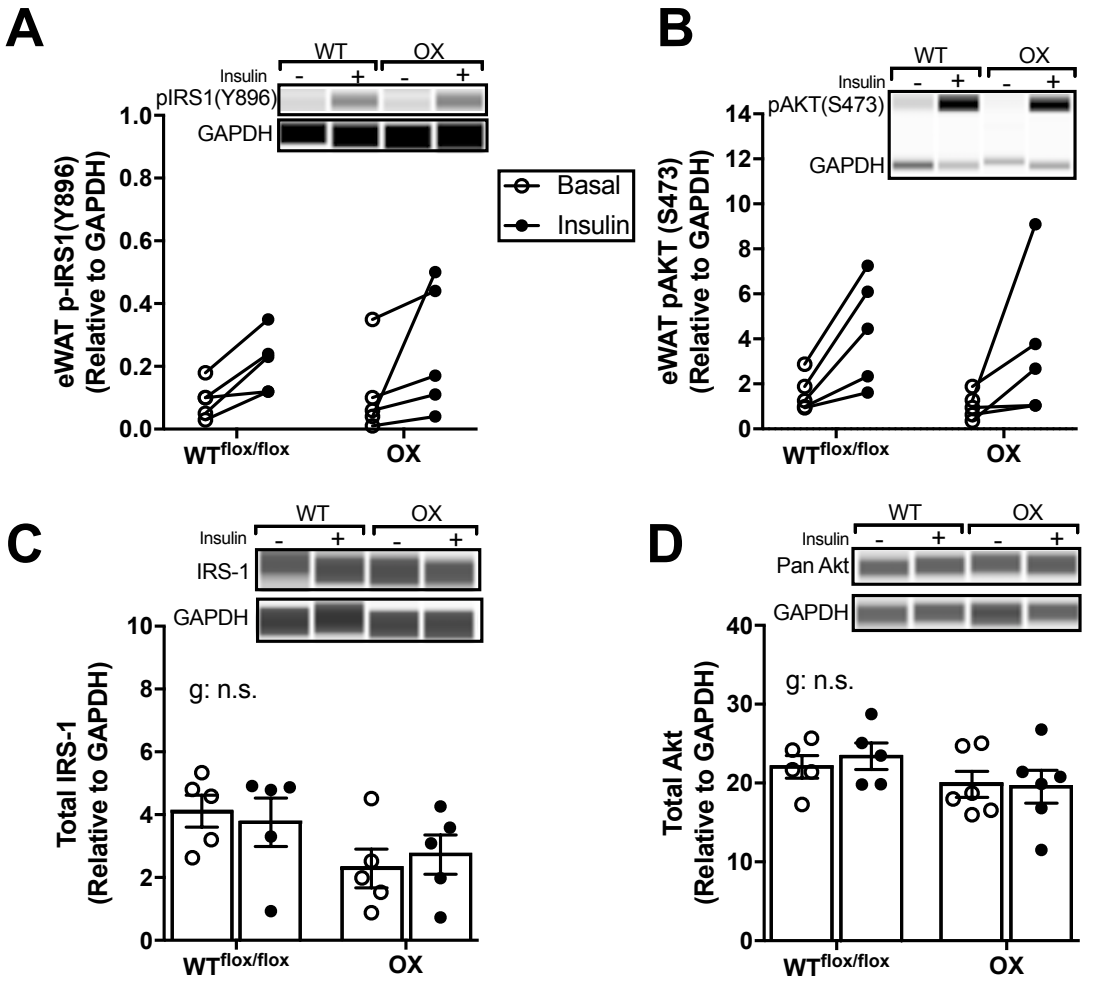

Figure 6. Perigonadal eWAT insulin signaling in WT and adipocyte specific p55 OX mice. Insulin stimulated (A) phospho-IRS1(Y896), (B) phospho-AKT(S473), (C) total IRS-1 and (D) Total Akt in basal and insulin stimulated perigondadal eWAT of WT and adipo-p55OX mice. Data reported as means ± SEM.

Figure 7.

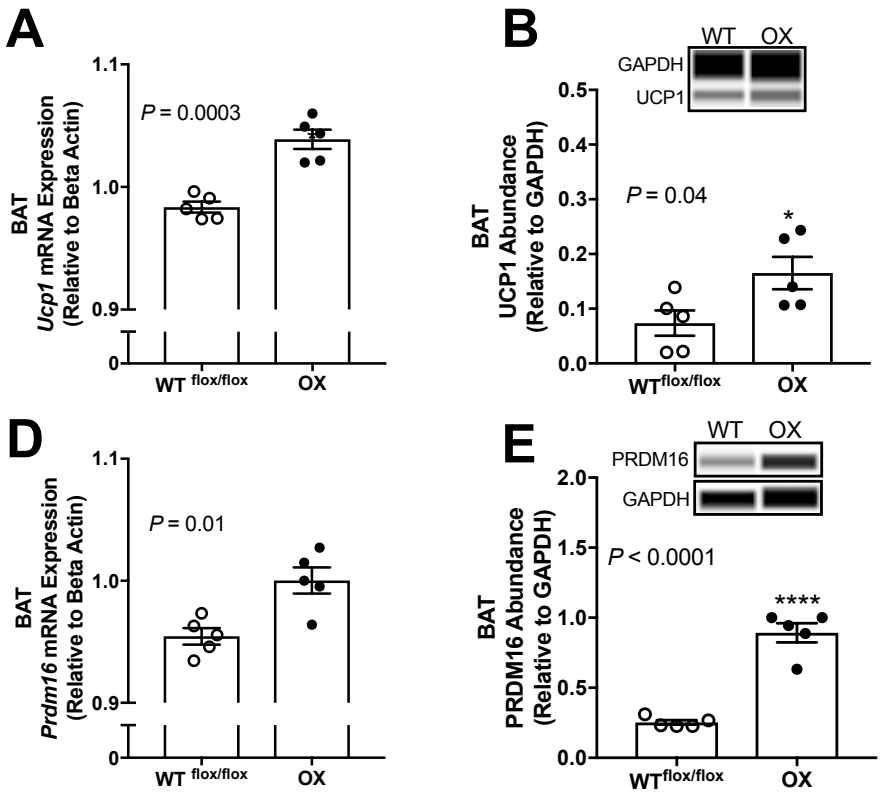

Figure 7. Thermogenic programming of BAT in WT and mice with adipocyte specific p55α OX. Brown adipose tissue (A) *Ucp1* gene expression, (B) UCP1 protein abundance, (C) *Prdm16* gene expression and (D) PRDM16 protein abundance. Data are expressed as means ± SEM. * represent between group differences (* $P < 0.05$, ** $P < 0.01$, *** $P < 0.001$, $P < 0.0001$.

APPENDIX E

FIGURES FOR CHAPTER V

Figure 1.

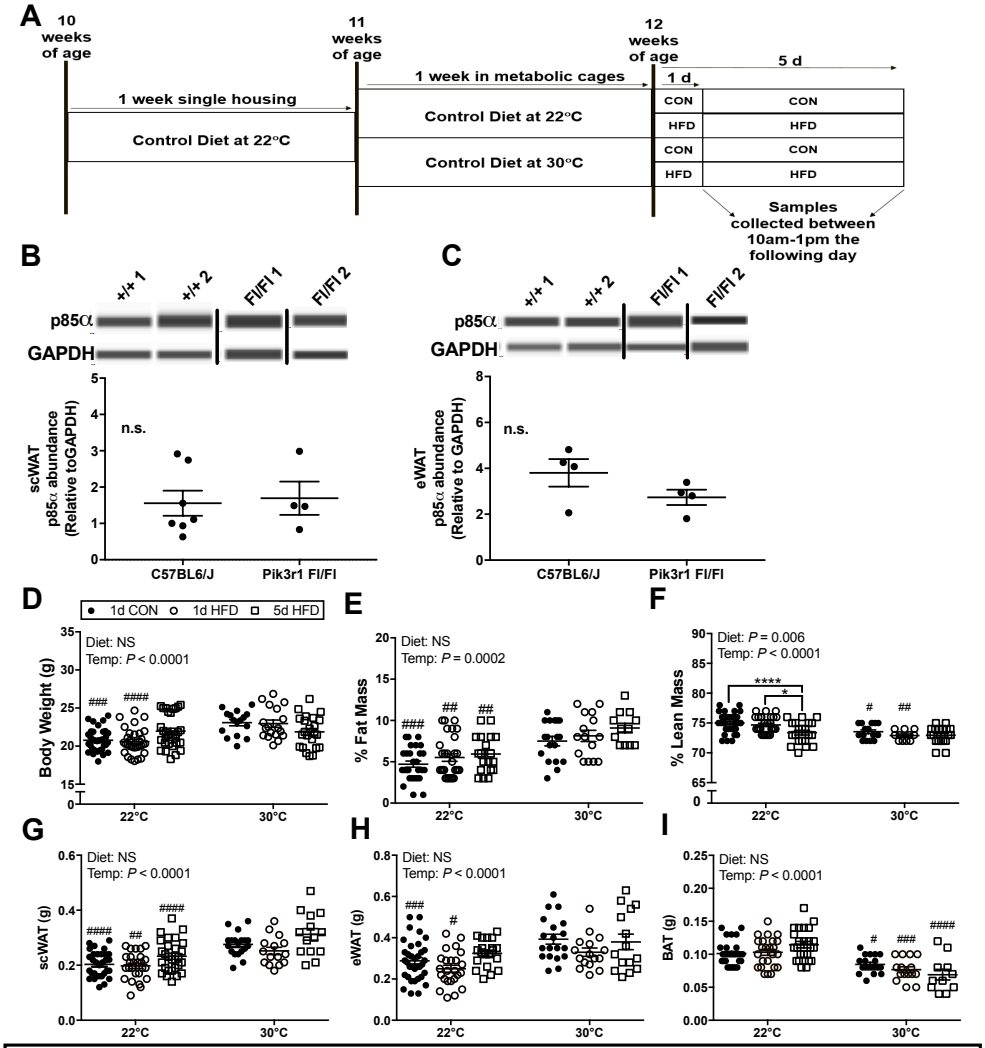

Fig. 1. Body weight and adiposity are increased in WT mice housed at murine thermoneutral temperature (30°C) vs. standard vivarium temperature (22°C) independent of diet. (A) Illustration of the study design. (B) p85 abundance in scWAT from Pik3r1$^{flox/flox}$ mice and C57BL6/J mice. (C) p85 abundance in eWAT from Pik3r1$^{flox/flox}$ mice and C57BL6/J mice. (D) Body weight and body composition before and after 1d CON, 1d HFD and 5d HFD treatment at standard vivarium temperature (22°C) (n=35/group) and murine thermoneutral temperature (30°C) (n =20/group). Inguinal scWAT (E), eWAT (F) and BAT (G) weight following 1 or 5d of CON and HFD feeding at 22°C (n = 35/group) and 30°C (n = 20/group). Data were analyzed by a 2-way ANOVA (diet x temperature) with a Sidak multiple comparison test. *p*-values for main effects ($p \leq 0.01$) are listed in each graph. Significant findings with multiple comparison test for temperature are indicated with # (# $p<0.05$, ## $p<0.01$, ### $p<0.001$, #### $p<0.0001$) and for diet are indicated with * (* $p< 0.05$, ** $p<0.01$, *** $p<0.001$, **** $p<0.0001$).

Figure 2.

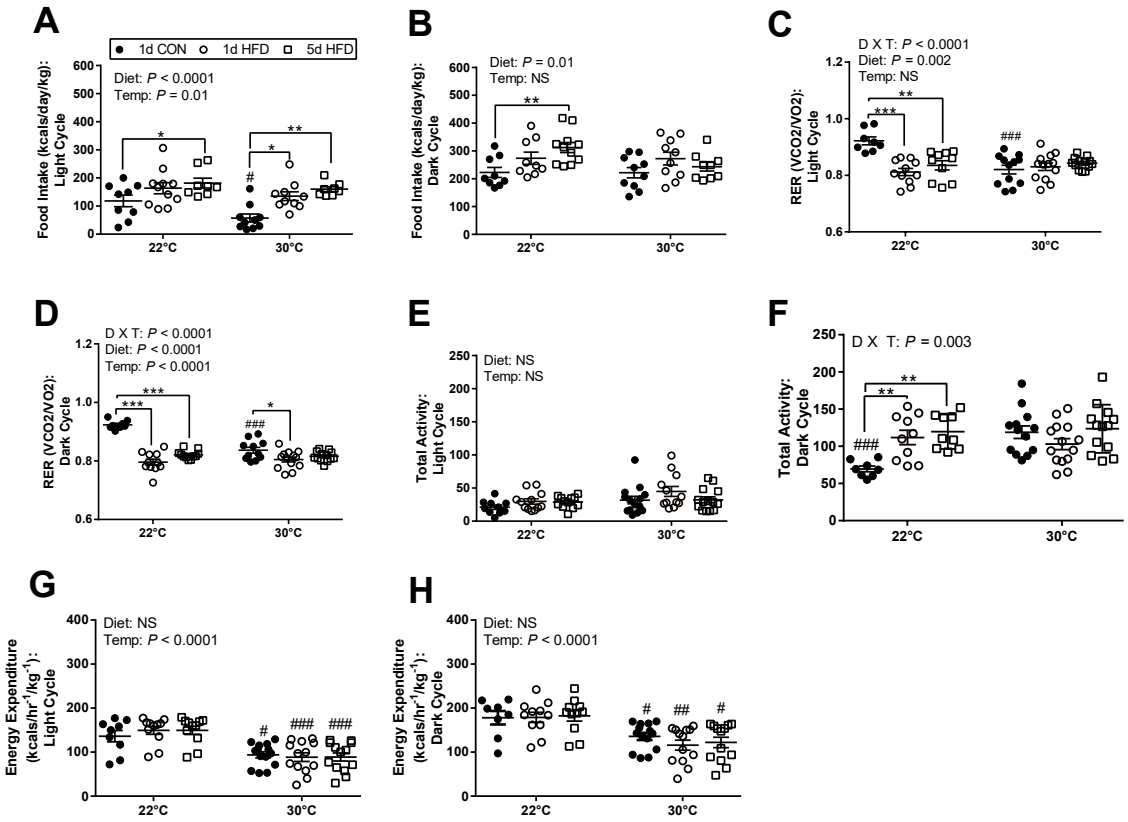

Fig. 2. Housing temperature alters the metabolic phenotype of mice on a control and high fat diet. Food intake assessed during the light (A) and dark cycles (B) during 1d CON, 1d HFD and 5d HFD at 22°C (n =10/group) and 30°C (n= 15/group). Respiratory exchange ratio (RER) assessed during the light (C) and dark cycles (D) during 1d CON, 1d HFD and 5d HFD at 22°C (n= 10/group) and 30°C (n= 15/group). Total activity assessed during the light (E) and dark (F) cycles during 1d CON, 1d HFD and 5d HFD at 22°C (n= 10/group) and 30°C (n= 15/group). Energy expenditure assessed during the light (G) and dark cycles (H) during 1d CON, 1d HFD and 5d HFD at 22°C (n =10/group) and 30°C (n =15/group). Data reported as mean ± SEM. CON, control diet; HFD, high fat diet. Data were analyzed by a 2-way ANOVA (diet x temperature) with a Sidak multiple comparison test. *p*-values for main effects ($p \leq 0.01$) are listed in each graph. Significant findings with multiple comparison test for temperature are indicated with # (# $p<0.05$, ## $p<0.01$, ### $p<0.001$, #### $p<0.0001$) and for diet are indicated with * (* $p< 0.05$, ** $p<0.01$, *** $p<0.001$, **** $p<0.0001$).

Figure 3.

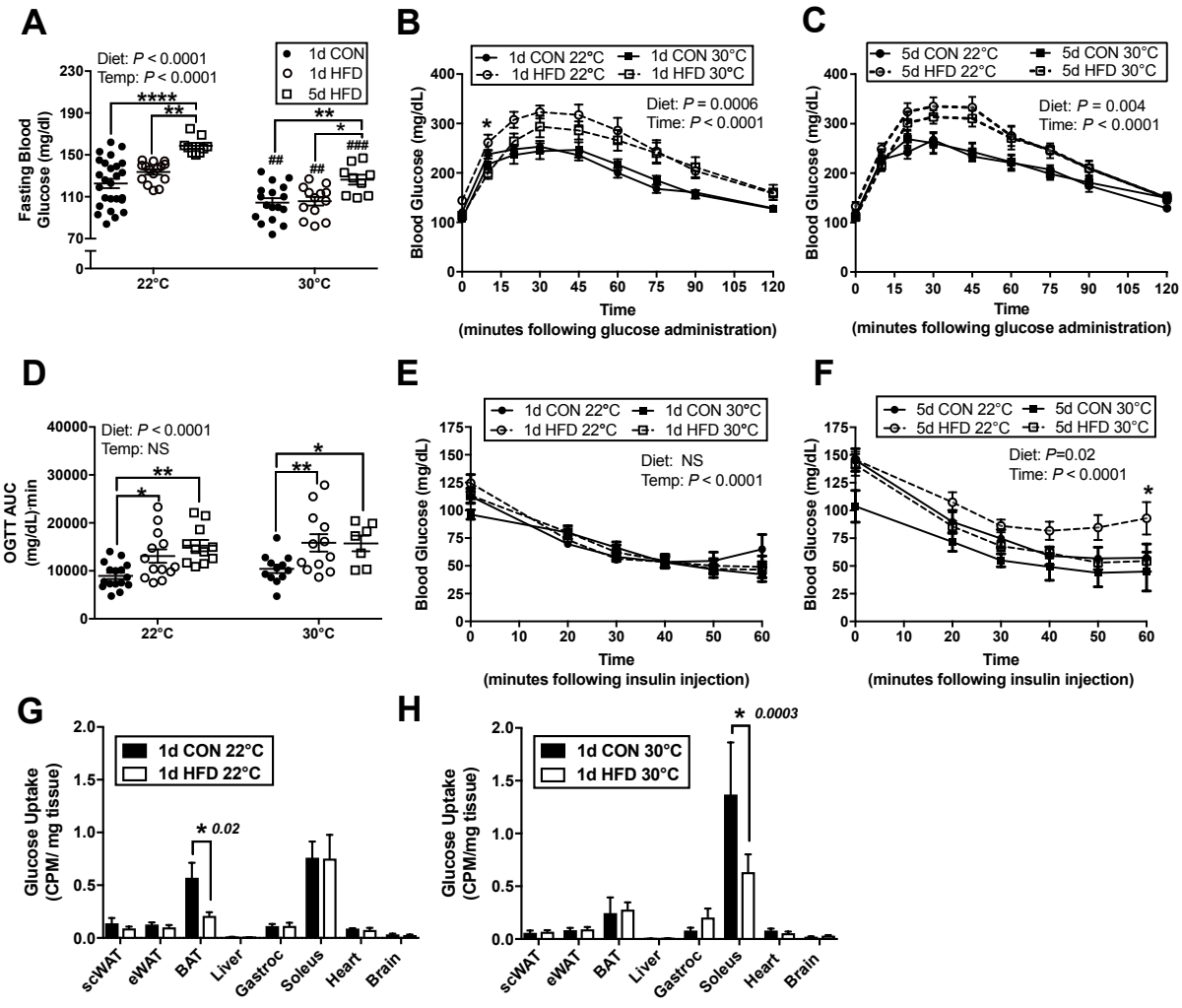

Fig. 3. Short-term thermoneutral housing alters on glucose homeostasis and insulin sensitivity in response to a high fat diet. (A) Fasting (4h) glucose following 1d CON, 1d HFD and 5d HFD treatment at standard vivarium temperature (22°C) (n = 20/group) and murine thermoneutral temperature (30°C) (n =15/group). (B-C) Oral glucose tolerance and glucose AUC (D) following 1d or 5d of CON and HFD treatment at standard vivarium temperature (22°C) (n= 17/group) and murine thermoneutral temperature (30°C) (n = 15/group). (E-F) Insulin tolerance tests following 1 (E) or 5d (F) of CON and HFD at 22°C (n =8/group) and 30°C (n=7/group) housing temperatures. (G-H) *In vivo* ^{3}H-2-deoxy-d-glucose uptake following 1d of CON or HFD diet at 22°C (n =5/group) (E) and 30°C (n = 5/group) housing temperatures. Data reported as mean ± SEM. CON, control diet; HFD, high fat diet. Data were analyzed by a 2-way ANOVA (diet x temperature) with a Sidak multiple comparison test. *p*-values for main effects ($p \leq 0.01$) are listed in each graph. Significant findings with multiple comparison test for temperature are indicated with # (# $p<0.05$, ## $p<0.01$, ### $p<0.001$, #### $p<0.0001$) and for diet are indicated with * (*$p< 0.05$, ** $p<0.01$, *** $p<0.001$, **** $p<0.0001$).

Figure 4.

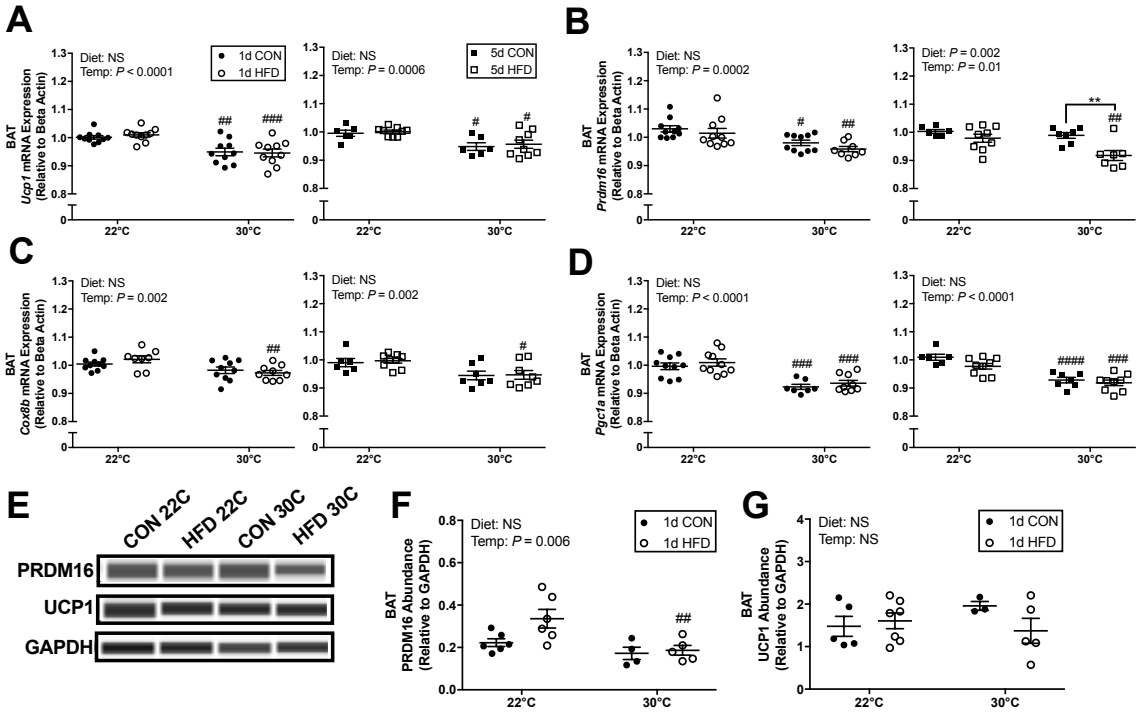

Fig. 4. Short-term thermoneutral housing reduces gene expression markers of thermogenesis in BAT. (A) *Ucp1*, (B) *Prdm16*, (C) *Cox8b*, and (D) *Pgc1a* following 1d CON, 1d HFD, 5d CON and 5d HFD treatment at standard vivarium temperature (22°C) and murine thermoneutral temperature (30°C). (E) Immunoblots and quantification of (F) PRDM16 and (G) UCP-1 abundance in BAT. Data reported as mean ± SEM. CON, control diet; HFD, high fat diet. Data were analyzed by a 2-way ANOVA (diet x temperature) with a Sidak multiple comparison test. *p*-values for main effects ($p \leq 0.01$) are listed in each graph. Significant findings with multiple comparison test for temperature are indicated with # (# $p<0.05$, ## $p<0.01$, ### $p<0.001$, #### $p<0.0001$) and for diet are indicated with * (* $p< 0.05$, ** $p<0.01$, *** $p<0.001$, **** $p<0.0001$).

Figure 5.

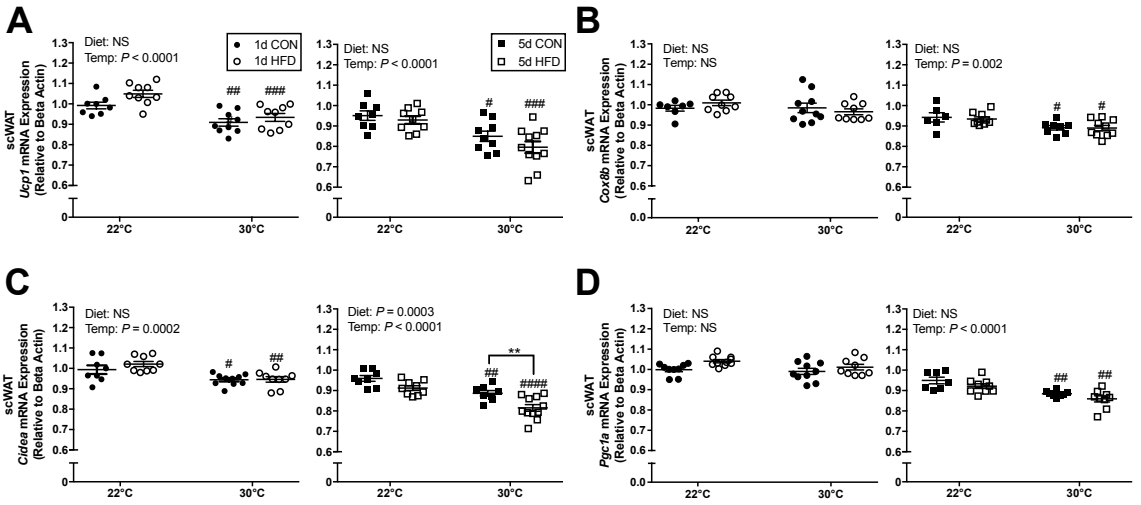

Fig. 5. Short-term thermoneutral housing reduces activation of browning genes in inguinal scWAT. (A) *Ucp1*, (B) *Cox8b,* (C) *Cidea*, and (D) *Pgc1a* following 1d CON, 1d HFD, 5d CON and 5d HFD treatment at standard vivarium temperature (22°C) and murine thermoneutral temperature (30°C). Data reported as mean ± SEM. CON, control diet; HFD, high fat diet. Data were analyzed by a 2-way ANOVA (diet x temperature) with a Sidak multiple comparison test. *p*-values for main effects ($p \leq 0.01$) are listed in each graph. Significant findings with multiple comparison test for temperature are indicated with # (# $p<0.05$, ## $p<0.01$, ### $p<0.001$, #### $p<0.0001$) and for diet are indicated with * (* $p< 0.05$, ** $p<0.01$, *** $p<0.001$, **** $p<0.0001$).

Figure 6.

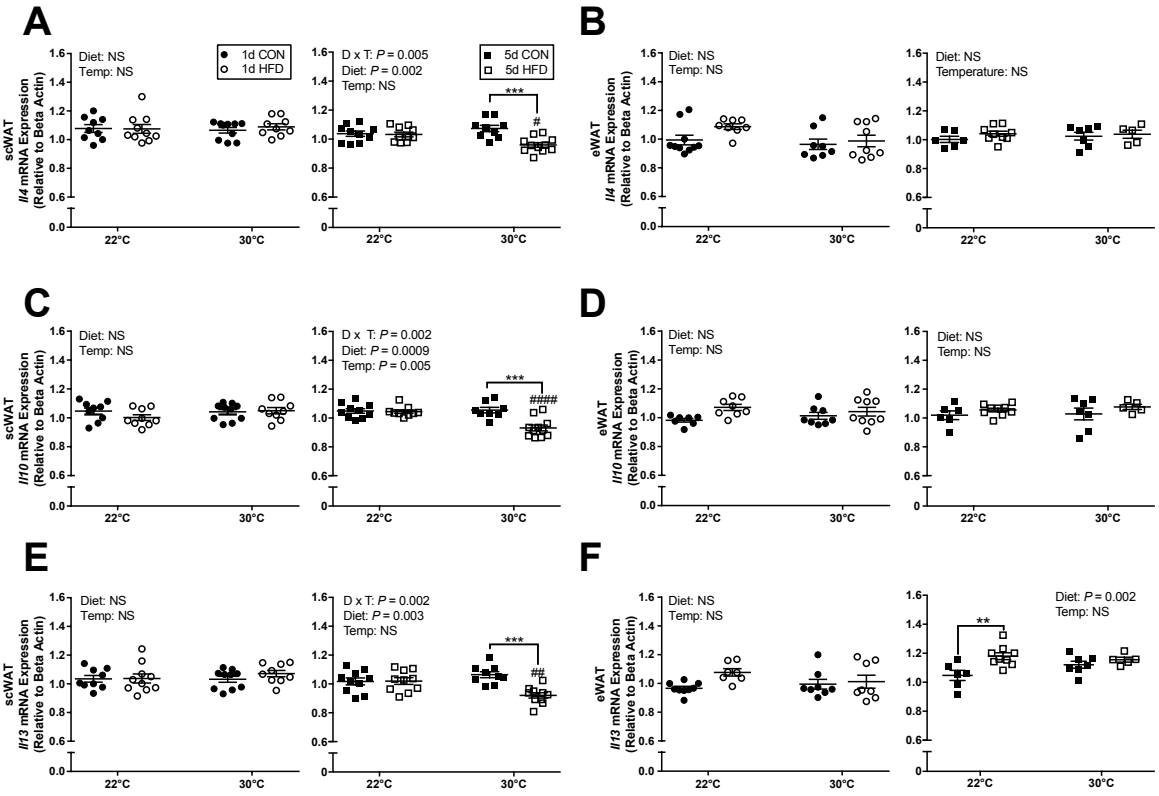

Fig. 6. Short-term thermoneutral housing reduces inguinal scWAT anti-inflammatory gene expression in response to high fat diet. scWAT (A) and eWAT (B) *Il4* gene expression, scWAT (C) and eWAT (D) *Il10* gene expression, and scWAT (E) and eWAT (F) *Il13* gene expression following 1d CON, 1d HFD, 5d CON and 5d HFD treatment at standard vivarium temperature (22°C) and murine thermoneutral temperature (30°C). Data reported as mean ± SEM. CON, control diet; HFD, high fat diet. Significant findings with multiple comparison test for temperature are indicated with # (# p<0.05, ## p<0.01, ### p<0.001, #### p<0.0001) and for diet are indicated with * (*p< 0.05, ** p<0.01, *** p<0.001, **** p<0.0001).

Figure 7.

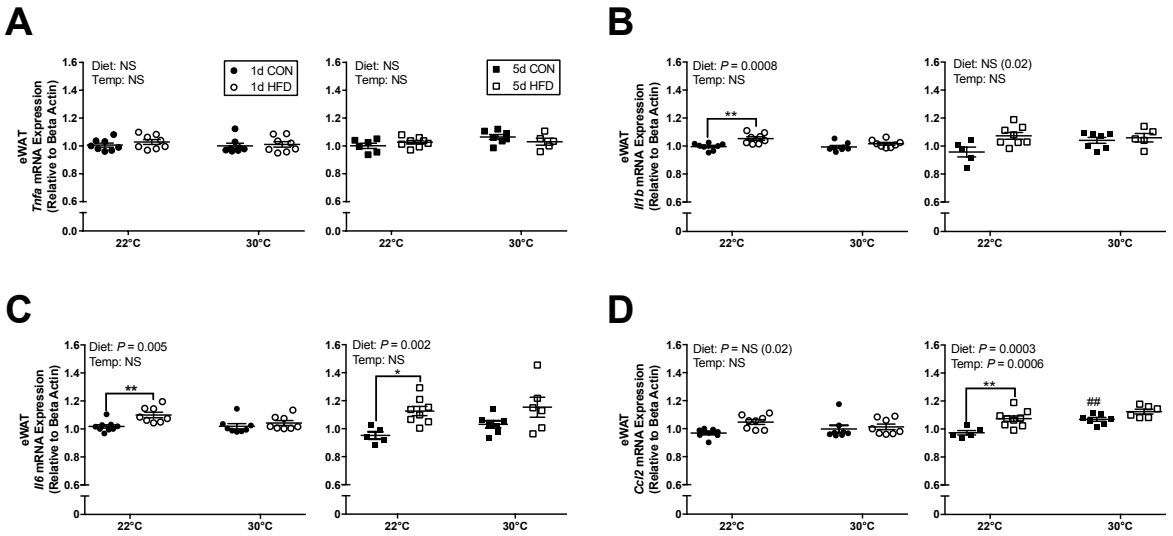

Fig. 7. Standard vivarium housing temperature (22°C) but not thermoneutral housing increases eWAT pro-inflammatory gene expression in response to a HFD. eWAT (A) *Tnfa,* (B) *Il1b*, (C) *Il6,* and (D) *Ccl2* gene expression following 1d CON, 1d HFD, 5d CON and 5d HFD at standard vivarium temperature (22°C) and murine thermoneutral temperature (30°C). Data reported as mean ± SEM. CON, control diet; HFD, high fat diet. Significant findings with multiple comparison test for temperature are indicated with # (# $p<0.05$, ## $p<0.01$, ### $p<0.001$, #### $p<0.0001$) and for diet are indicated with * (*$p< 0.05$, ** $p<0.01$, *** $p<0.001$, **** $p<0.0001$).

APPENDIX F

FIGURE FOR CONCLUSION

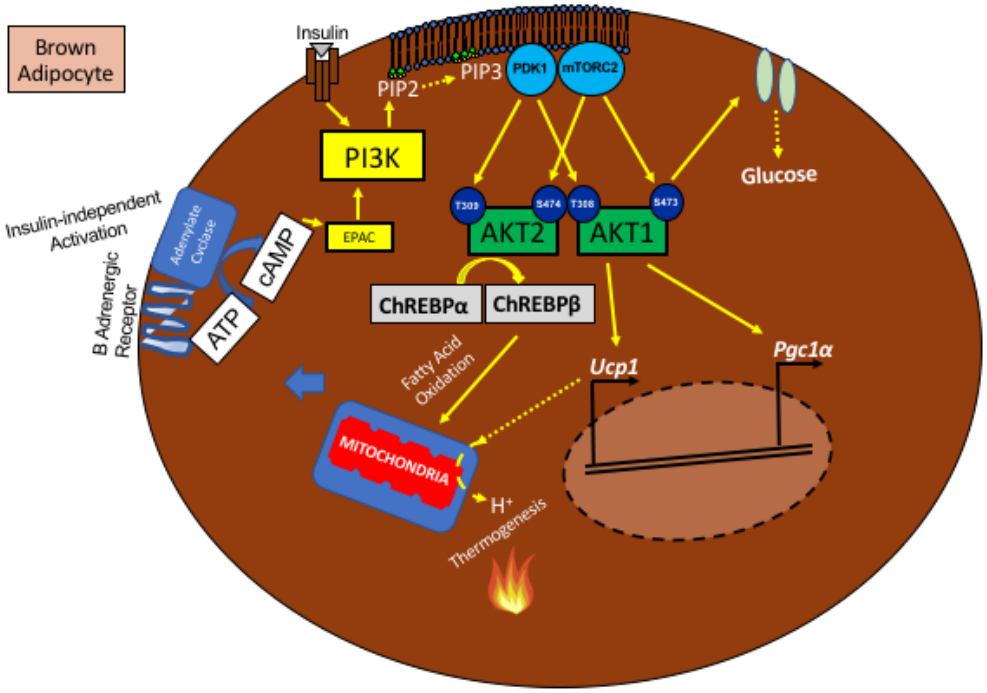

Figure 1. Proposed mechanism as to how PI3K is influencing thermogenesis in brown adipose tissue (BAT). PI3K catalyzes the reaction of phosphatidylinositol 4-5, bisphosphate (PIP2) to phosphatidylinositol 3,4,5-triphosphate (PIP3). Upon activation of PIP3, protein kinase 3-phosphoinositide dependent protein kinase-1 (PDK1) is recruited to the plasma membrane and activated, which phosphorylates AKT1 at Serine473 and AKT2 at Serine474. Upon PIP3 activation, mammalian target of rapamycin complex 2 (mTORC2) is also recruited to the plasma membrane and activated, and phosphorylates AKT1 at Threonine308 (4). mTORC2 activation of AKT1 phosphorylation has been shown to increase with cold exposure, and mice with adipose tissue specific knockout of mTORC2 have impaired cold-induced thermogenesis, upregulation of *Ucp1* and decreased BAT glucose uptake (1). Furthermore, BAT AKT2 phosphorylation is increased during thermal stress in mice, which activates Carbohydrate-responsive element binding protein (ChREBP), and its conversion from the α to β isoform enhances mitochondrial fatty acid oxidation in BAT (10).

REFERENCES CITED

Chapter I

1. Obesity: preventing and managing the global epidemic. Report of a WHO consultation. *World Health Organ Tech Rep Ser* 894: i-xii, 1-253, 2000.

2. **Bandyopadhyay GK, Yu JG, Ofrecio J, and Olefsky JM**. Increased p85/55/50 expression and decreased phosphotidylinositol 3-kinase activity in insulin-resistant human skeletal muscle. *Diabetes* 54: 2351-2359, 2005.

3. **Barbour LA, Mizanoor Rahman S, Gurevich I, Leitner JW, Fischer SJ, Roper MD, Knotts TA, Vo Y, McCurdy CE, Yakar S, Leroith D, Kahn CR, Cantley LC, Friedman JE, and Draznin B**. Increased P85alpha is a potent negative regulator of skeletal muscle insulin signaling and induces in vivo insulin resistance associated with growth hormone excess. *J Biol Chem* 280: 37489-37494, 2005.

4. **Brachmann SM, Ueki K, Engelman JA, Kahn RC, and Cantley LC**. Phosphoinositide 3-kinase catalytic subunit deletion and regulatory subunit deletion have opposite effects on insulin sensitivity in mice. *Mol Cell Biol* 25: 1596-1607, 2005.

5. **Cannon B, and Nedergaard J**. Brown adipose tissue: function and physiological significance. *Physiol Rev* 84: 277-359, 2004.

6. **Cantley LC**. The phosphoinositide 3-kinase pathway. *Science* 296: 1655-1657, 2002.

7. **Cartee GD, Kietzke EW, and Briggs-Tung C**. Adaptation of muscle glucose transport with caloric restriction in adult, middle-aged, and old rats. *Am J Physiol* 266: R1443-1447, 1994.

8. **Chen D, Mauvais-Jarvis F, Bluher M, Fisher SJ, Jozsi A, Goodyear LJ, Ueki K, and Kahn CR**. p50alpha/p55alpha phosphoinositide 3-kinase knockout mice exhibit enhanced insulin sensitivity. *Mol Cell Biol* 24: 320-329, 2004.

9. **Cornier MA, Bergman BC, and Bessesen DH**. The effects of short-term overfeeding on insulin action in lean and reduced-obese individuals. *Metabolism* 55: 1207-1214, 2006.

10. **Cornier MA, Bessesen DH, Gurevich I, Leitner JW, and Draznin B**. Nutritional upregulation of p85alpha expression is an early molecular manifestation of insulin resistance. *Diabetologia* 49: 748-754, 2006.

11. **Duncan RE, Ahmadian M, Jaworski K, Sarkadi-Nagy E, and Sul HS**. Regulation of lipolysis in adipocytes. *Annu Rev Nutr* 27: 79-101, 2007.

12. **El Sheikh SS, Domin J, Tomtitchong P, Abel P, Stamp G, and Lalani EN**. Topographical expression of class IA and class II phosphoinositide 3-kinase enzymes in normal human tissues is consistent with a role in differentiation. *BMC Clin Pathol* 3: 4, 2003.

13. **Feldmann HM, Golozoubova V, Cannon B, and Nedergaard J**. UCP1 ablation induces obesity and abolishes diet-induced thermogenesis in mice exempt from thermal stress by living at thermoneutrality. *Cell Metab* 9: 203-209, 2009.

14. **Flegal KM, Carroll MD, Kit BK, and Ogden CL**. Prevalence of obesity and trends in the distribution of body mass index among US adults, 1999-2010. *JAMA* 307: 491-497, 2012.

15. **Foukas LC, Berenjeno IM, Gray A, Khwaja A, and Vanhaesebroeck B**. Activity of any class IA PI3K isoform can sustain cell proliferation and survival. *Proc Natl Acad Sci U S A* 107: 11381-11386, 2010.

16. **Hedley AA, Ogden CL, Johnson CL, Carroll MD, Curtin LR, and Flegal KM**. Prevalence of overweight and obesity among US children, adolescents, and adults, 1999-2002. *JAMA* 291: 2847-2850, 2004.

17. **Jeffery E, Wing A, Holtrup B, Sebo Z, Kaplan JL, Saavedra-Peña R, Church CD, Colman L, Berry R, and Rodeheffer MS**. The Adipose Tissue Microenvironment Regulates Depot-Specific Adipogenesis in Obesity. *Cell Metab* 24: 142-150, 2016.

18. **Jiang G, and Zhang BB**. Pi 3-kinase and its up- and down-stream modulators as potential targets for the treatment of type II diabetes. *Front Biosci* 7: d903-907, 2002.

19. **Kelley DE, Wing R, Buonocore C, Sturis J, Polonsky K, and Fitzsimmons M**. Relative effects of calorie restriction and weight loss in noninsulin-dependent diabetes mellitus. *J Clin Endocrinol Metab* 77: 1287-1293, 1993.

20. **Kozak LP, Koza RA, and Anunciado-Koza R**. Brown fat thermogenesis and body weight regulation in mice: relevance to humans. *Int J Obes (Lond)* 34 Suppl 1: S23-27, 2010.

21. **Lee MJ, Wu Y, and Fried SK**. Adipose tissue heterogeneity: implication of depot differences in adipose tissue for obesity complications. *Mol Aspects Med* 34: 1-11, 2013.

22. **Lee YS, Li P, Huh JY, Hwang IJ, Lu M, Kim JI, Ham M, Talukdar S, Chen A, Lu WJ, Bandyopadhyay GK, Schwendener R, Olefsky J, and Kim JB**. Inflammation is necessary for long-term but not short-term high-fat diet-induced insulin resistance. *Diabetes* 60: 2474-2483, 2011.

23. **Macotela Y, Emanuelli B, Mori MA, Gesta S, Schulz TJ, Tseng YH, and Kahn CR**. Intrinsic differences in adipocyte precursor cells from different white fat depots. *Diabetes* 61: 1691-1699, 2012.

24. **Mauvais-Jarvis F, Ueki K, Fruman DA, Hirshman MF, Sakamoto K, Goodyear LJ, Iannacone M, Accili D, Cantley LC, and Kahn CR**. Reduced expression of the murine p85alpha subunit of phosphoinositide 3-kinase improves insulin signaling and ameliorates diabetes. *J Clin Invest* 109: 141-149, 2002.

25. **McCurdy CE, Davidson RT, and Cartee GD**. Calorie restriction increases the ratio of phosphatidylinositol 3-kinase catalytic to regulatory subunits in rat skeletal muscle. *Am J Physiol Endocrinol Metab* 288: E996-E1001, 2005.

26. **McCurdy CE, Schenk S, Holliday MJ, Philp A, Houck JA, Patsouris D, MacLean PS, Majka SM, Klemm DJ, and Friedman JE**. Attenuated Pik3r1 expression prevents insulin resistance and adipose tissue macrophage accumulation in diet-induced obese mice. *Diabetes* 61: 2495-2505, 2012.

27. **Moriarty MW, McCurdy CE, Janssen RC, Shaw T, Leitner JW, Friedman JE, and Draznin B**. In vivo knockdown of p85alpha with an antisense oligonucleotide improves insulin sensitivity in Lep(ob/ob) and diet-induced obese mice. *Horm Metab Res* 41: 757-761, 2009.

28. **Osborn O, and Olefsky JM**. The cellular and signaling networks linking the immune system and metabolism in disease. *Nat Med* 18: 363-374, 2012.

29. **Rabinovsky R, Pochanard P, McNear C, Brachmann SM, Duke-Cohan JS, Garraway LA, and Sellers WR**. p85 Associates with unphosphorylated PTEN and the PTEN-associated complex. *Mol Cell Biol* 29: 5377-5388, 2009.

30. **Reaven GM**. Banting lecture 1988. Role of insulin resistance in human disease. *Diabetes* 37: 1595-1607, 1988.

31. **Reaven GM, Scott EM, Grant PJ, Lowe GD, Rumley A, Wannamethee SG, Stratmann B, Tschoepe D, Blann A, Juhan-Vague I, Alessi MC, and Bailey C**. Hemostatic abnormalities associated with obesity and the metabolic syndrome. *J Thromb Haemost* 3: 1074-1085, 2005.

32. **Rosen ED, and Spiegelman BM**. What we talk about when we talk about fat. *Cell* 156: 20-44, 2014.

33. **Schenk S, McCurdy CE, Philp A, Chen MZ, Holliday MJ, Bandyopadhyay GK, Osborn O, Baar K, and Olefsky JM**. Sirt1 enhances skeletal muscle insulin sensitivity in mice during caloric restriction. *J Clin Invest* 121: 4281-4288, 2011.

34. **Seale P, Bjork B, Yang W, Kajimura S, Chin S, Kuang S, Scimè A, Devarakonda S, Conroe HM, Erdjument-Bromage H, Tempst P, Rudnicki MA, Beier DR, and Spiegelman BM**. PRDM16 controls a brown fat/skeletal muscle switch. *Nature* 454: 961-967, 2008.

35. **Seale P, Conroe HM, Estall J, Kajimura S, Frontini A, Ishibashi J, Cohen P, Cinti S, and Spiegelman BM**. Prdm16 determines the thermogenic program of subcutaneous white adipose tissue in mice. *J Clin Invest* 121: 96-105, 2011.

36. **Stanford KI, Middelbeek RJ, Townsend KL, An D, Nygaard EB, Hitchcox KM, Markan KR, Nakano K, Hirshman MF, Tseng YH, and Goodyear LJ**. Brown adipose tissue regulates glucose homeostasis and insulin sensitivity. *J Clin Invest* 123: 215-223, 2013.

37. **Stumvoll M, Goldstein BJ, and van Haeften TW**. Type 2 diabetes: principles of pathogenesis and therapy. *Lancet* 365: 1333-1346, 2005.

38. **Taniguchi CM, Kondo T, Sajan M, Luo J, Bronson R, Asano T, Farese R, Cantley LC, and Kahn CR**. Divergent regulation of hepatic glucose and lipid metabolism by phosphoinositide 3-kinase via Akt and PKClambda/zeta. *Cell Metab* 3: 343-353, 2006.

39. **Tchkonia T, Thomou T, Zhu Y, Karagiannides I, Pothoulakis C, Jensen MD, and Kirkland JL**. Mechanisms and metabolic implications of regional differences among fat depots. *Cell Metab* 17: 644-656, 2013.

40. **Tchoukalova YD, Votruba SB, Tchkonia T, Giorgadze N, Kirkland JL, and Jensen MD**. Regional differences in cellular mechanisms of adipose tissue gain with overfeeding. *Proc Natl Acad Sci U S A* 107: 18226-18231, 2010.

41. **Thirone AC, Huang C, and Klip A**. Tissue-specific roles of IRS proteins in insulin signaling and glucose transport. *Trends Endocrinol Metab* 17: 72-78, 2006.

42. **Tran TT, and Kahn CR**. Transplantation of adipose tissue and stem cells: role in metabolism and disease. *Nat Rev Endocrinol* 6: 195-213, 2010.

43. **Vázquez-Vela ME, Torres N, and Tovar AR**. White adipose tissue as endocrine organ and its role in obesity. *Arch Med Res* 39: 715-728, 2008.

44. **Wahren J, and Ekberg K**. Splanchnic regulation of glucose production. *Annu Rev Nutr* 27: 329-345, 2007.

45. **Wang J, Obici S, Morgan K, Barzilai N, Feng Z, and Rossetti L**. Overfeeding rapidly induces leptin and insulin resistance. *Diabetes* 50: 2786-2791, 2001.

46. **Wild S, Roglic G, Green A, Sicree R, and King H**. Global prevalence of diabetes: estimates for the year 2000 and projections for 2030. *Diabetes Care* 27: 1047-1053, 2004.

Chapter II

1. **Acosta-Martínez M, Luo J, Elias C, Wolfe A, and Levine JE**. Male-biased effects of gonadotropin-releasing hormone neuron-specific deletion of the phosphoinositide 3-kinase regulatory subunit p85alpha on the reproductive axis. *Endocrinology* 150: 4203-4212, 2009.

2. **Bandyopadhyay GK, Yu JG, Ofrecio J, and Olefsky JM**. Increased p85/55/50 expression and decreased phosphotidylinositol 3-kinase activity in insulin-resistant human skeletal muscle. *Diabetes* 54: 2351-2359, 2005.

3. **Cantley LC**. The phosphoinositide 3-kinase pathway. *Science* 296: 1655-1657, 2002.

4. **Chen D, Mauvais-Jarvis F, Bluher M, Fisher SJ, Jozsi A, Goodyear LJ, Ueki K, and Kahn CR**. p50alpha/p55alpha phosphoinositide 3-kinase knockout mice exhibit enhanced insulin sensitivity. *Mol Cell Biol* 24: 320-329, 2004.

5. **Cornier MA, Bessesen DH, Gurevich I, Leitner JW, and Draznin B**. Nutritional upregulation of p85alpha expression is an early molecular manifestation of insulin resistance. *Diabetologia* 49: 748-754, 2006.

6. **Facchini FS, Hua N, Abbasi F, and Reaven GM**. Insulin resistance as a predictor of age-related diseases. *J Clin Endocrinol Metab* 86: 3574-3578, 2001.

7. **Fruman DA, Cantley LC, and Carpenter CL**. Structural organization and alternative splicing of the murine phosphoinositide 3-kinase p85 alpha gene. *Genomics* 37: 113-121, 1996.

8. **Hales CM, Carroll MD, Fryar CD, and Ogden CL**. Prevalence of Obesity Among Adults and Youth: United States, 2015-2016. *NCHS Data Brief* 1-8, 2017.

9. **Lee YS, Li P, Huh JY, Hwang IJ, Lu M, Kim JI, Ham M, Talukdar S, Chen A, Lu WJ, Bandyopadhyay GK, Schwendener R, Olefsky J, and Kim JB**. Inflammation is necessary for long-term but not short-term high-fat diet-induced insulin resistance. *Diabetes* 60: 2474-2483, 2011.

10. **Luo J, McMullen JR, Sobkiw CL, Zhang L, Dorfman AL, Sherwood MC, Logsdon MN, Horner JW, DePinho RA, Izumo S, and Cantley LC**. Class IA phosphoinositide 3-kinase regulates heart size and physiological cardiac hypertrophy. *Mol Cell Biol* 25: 9491-9502, 2005.

11. **Mauvais-Jarvis F, Ueki K, Fruman DA, Hirshman MF, Sakamoto K, Goodyear LJ, Iannacone M, Accili D, Cantley LC, and Kahn CR**. Reduced expression of the murine p85alpha subunit of phosphoinositide 3-kinase improves insulin signaling and ameliorates diabetes. *J Clin Invest* 109: 141-149, 2002.

12. **McCurdy CE, Schenk S, Holliday MJ, Philp A, Houck JA, Patsouris D, MacLean PS, Majka SM, Klemm DJ, and Friedman JE**. Attenuated Pik3r1 expression prevents insulin resistance and adipose tissue macrophage accumulation in diet-induced obese mice. *Diabetes* 61: 2495-2505, 2012.

13. **Morishita Y, Miura D, and Kida S**. PI3K regulates BMAL1/CLOCK-mediated circadian transcription from the Dbp promoter. *Biosci Biotechnol Biochem* 80: 1131-1140, 2016.

14. **Nelson VL, Jiang YP, Dickman KG, Ballou LM, and Lin RZ**. Adipose tissue insulin resistance due to loss of PI3K p110α leads to decreased energy expenditure and obesity. *Am J Physiol Endocrinol Metab* 306: E1205-1216, 2014.

15. **Okada T, Kawano Y, Sakakibara T, Hazeki O, and Ui M**. Essential role of phosphatidylinositol 3-kinase in insulin-induced glucose transport and antilipolysis in rat adipocytes. Studies with a selective inhibitor wortmannin. *J Biol Chem* 269: 3568-3573, 1994.

16. **Terauchi Y, Matsui J, Kamon J, Yamauchi T, Kubota N, Komeda K, Aizawa S, Akanuma Y, Tomita M, and Kadowaki T**. Increased serum leptin protects from adiposity despite the increased glucose uptake in white adipose tissue in mice lacking p85alpha phosphoinositide 3-kinase. *Diabetes* 53: 2261-2270, 2004.

17. **Terauchi Y, Tsuji Y, Satoh S, Minoura H, Murakami K, Okuno A, Inukai K, Asano T, Kaburagi Y, Ueki K, Nakajima H, Hanafusa T, Matsuzawa Y, Sekihara H, Yin Y, Barrett JC, Oda H, Ishikawa T,**

18. **Akanuma Y, Komuro I, Suzuki M, Yamamura K, Kodama T, Suzuki H, Koyasu S, Aizawa S, Tobe K, Fukui Y, Yazaki Y, and Kadowaki T**. Increased insulin sensitivity and hypoglycaemia in mice lacking the p85 alpha subunit of phosphoinositide 3-kinase. *Nat Genet* 21: 230-235, 1999.

19. **Ueki K, Fruman DA, Brachmann SM, Tseng YH, Cantley LC, and Kahn CR**. Molecular balance between the regulatory and catalytic subunits of phosphoinositide 3-kinase regulates cell signaling and survival. *Mol Cell Biol* 22: 965-977, 2002.

20. **Vanhaesebroeck B, Ali K, Bilancio A, Geering B, and Foukas LC**. Signalling by PI3K isoforms: insights from gene-targeted mice. *Trends Biochem Sci* 30: 194-204, 2005.

21. **Wang J, Obici S, Morgan K, Barzilai N, Feng Z, and Rossetti L**. Overfeeding rapidly induces leptin and insulin resistance. *Diabetes* 50: 2786-2791, 2001.

Chapter III

1. **Brachmann SM, Ueki K, Engelman JA, Kahn RC, and Cantley LC**. Phosphoinositide 3-kinase catalytic subunit deletion and regulatory subunit deletion have opposite effects on insulin sensitivity in mice. *Mol Cell Biol* 25: 1596-1607, 2005.

2. **Cantley LC**. The phosphoinositide 3-kinase pathway. *Science* 296: 1655-1657, 2002.

3. **Chen D, Mauvais-Jarvis F, Bluher M, Fisher SJ, Jozsi A, Goodyear LJ, Ueki K, and Kahn CR**. p50alpha/p55alpha phosphoinositide 3-kinase knockout mice exhibit enhanced insulin sensitivity. *Mol Cell Biol* 24: 320-329, 2004.

4. **Facchini FS, Hua N, Abbasi F, and Reaven GM**. Insulin resistance as a predictor of age-related diseases. *J Clin Endocrinol Metab* 86: 3574-3578, 2001.

5. **Greenfield JR, and Campbell LV**. Insulin resistance and obesity. *Clin Dermatol* 22: 289-295, 2004.

6. **Hales CM, Carroll MD, Fryar CD, and Ogden CL**. Prevalence of Obesity Among Adults and Youth: United States, 2015-2016. *NCHS Data Brief* 1-8, 2017.

7. **Karlsson EA, Sheridan PA, and Beck MA**. Diet-induced obesity impairs the T cell memory response to influenza virus infection. *J Immunol* 184: 3127-3133, 2010.

8. **Lee YS, Li P, Huh JY, Hwang IJ, Lu M, Kim JI, Ham M, Talukdar S, Chen A, Lu WJ, Bandyopadhyay GK, Schwendener R, Olefsky J, and Kim JB**. Inflammation is necessary for long-term but not short-term high-fat diet-induced insulin resistance. *Diabetes* 60: 2474-2483, 2011.

9. **Luo J, Sobkiw CL, Hirshman MF, Logsdon MN, Li TQ, Goodyear LJ, and Cantley LC**. Loss of class IA PI3K signaling in muscle leads to impaired muscle growth, insulin response, and hyperlipidemia. *Cell Metab* 3: 355-366, 2006.

10. **Majka SM, Miller HL, Helm KM, Acosta AS, Childs CR, Kong R, and Klemm DJ**. Analysis and isolation of adipocytes by flow cytometry. *Methods Enzymol* 537: 281-296, 2014.

11. **McCurdy CE, Schenk S, Holliday MJ, Philp A, Houck JA, Patsouris D, MacLean PS, Majka SM, Klemm DJ, and Friedman JE**. Attenuated Pik3r1 expression prevents insulin resistance and adipose tissue macrophage accumulation in diet-induced obese mice. *Diabetes* 61: 2495-2505, 2012.

12. **Meigs JB, Wilson PW, Fox CS, Vasan RS, Nathan DM, Sullivan LM, and D'Agostino RB**. Body mass index, metabolic syndrome, and risk of type 2 diabetes or cardiovascular disease. *J Clin Endocrinol Metab* 91: 2906-2912, 2006.

13. **Okada T, Kawano Y, Sakakibara T, Hazeki O, and Ui M**. Essential role of phosphatidylinositol 3-kinase in insulin-induced glucose transport and antilipolysis in rat adipocytes. Studies with a selective inhibitor wortmannin. *J Biol Chem* 269: 3568-3573, 1994.

14. **Okada T, Sakuma L, Fukui Y, Hazeki O, and Ui M**. Blockage of chemotactic peptide-induced stimulation of neutrophils by wortmannin as a result of selective inhibition of phosphatidylinositol 3-kinase. *J Biol Chem* 269: 3563-3567, 1994.

15. **Osborn O, and Olefsky JM**. The cellular and signaling networks linking the immune system and metabolism in disease. *Nat Med* 18: 363-374, 2012.

16. **Sassmann A, Offermanns S, and Wettschureck N**. Tamoxifen-inducible Cre-mediated recombination in adipocytes. *Genesis* 48: 618-625, 2010.

17. **Stumvoll M, Goldstein BJ, and van Haeften TW**. Type 2 diabetes: principles of pathogenesis and therapy. *Lancet* 365: 1333-1346, 2005.

18. **Taniguchi CM, Aleman JO, Ueki K, Luo J, Asano T, Kaneto H, Stephanopoulos G, Cantley LC, and Kahn CR**. The p85alpha regulatory subunit of phosphoinositide 3-kinase potentiates c-Jun N-terminal kinase-mediated insulin resistance. *Mol Cell Biol* 27: 2830-2840, 2007.

19. **Taniguchi CM, Kondo T, Sajan M, Luo J, Bronson R, Asano T, Farese R, Cantley LC, and Kahn CR**. Divergent regulation of hepatic glucose and lipid metabolism by phosphoinositide 3-kinase via Akt and PKClambda/zeta. *Cell Metab* 3: 343-353, 2006.

20. **Tremmel M, Gerdtham UG, Nilsson PM, and Saha S**. Economic Burden of Obesity: A Systematic Literature Review. *Int J Environ Res Public Health* 14: 2017.

21. **Winnay JN, Boucher J, Mori MA, Ueki K, and Kahn CR**. A regulatory subunit of phosphoinositide 3-kinase increases the nuclear accumulation of X-box-binding protein-1 to modulate the unfolded protein response. *Nat Med* 16: 438-445, 2010.

22. **Yao F, Zhang M, and Chen L**. Adipose Tissue-Specialized Immunologic Features Might Be the Potential Therapeutic Target of Prospective Medicines for Obesity. *J Diabetes Res* 2017: 4504612, 2017.

Chapter IV

1. **Albert V, Svensson K, Shimobayashi M, Colombi M, Muñoz S, Jimenez V, Handschin C, Bosch F, and Hall MN**. mTORC2 sustains thermogenesis via Akt-induced glucose uptake and glycolysis in brown adipose tissue. *EMBO Mol Med* 8: 232-246, 2016

2. **Antonetti DA, Algenstaedt P, and Kahn CR**. Insulin receptor substrate 1 binds two novel splice variants of the regulatory subunit of phosphatidylinositol 3-kinase in muscle and brain. *Mol Cell Biol* 16: 2195-2203, 1996.

3. **Barbour LA, Mizanoor Rahman S, Gurevich I, Leitner JW, Fischer SJ, Roper MD, Knotts TA, Vo Y, McCurdy CE, Yakar S, Leroith D, Kahn CR, Cantley LC, Friedman JE, and Draznin B**. Increased P85alpha is a potent negative regulator of skeletal muscle insulin signaling and induces in vivo insulin resistance associated with growth hormone excess. *J Biol Chem* 280: 37489-37494, 2005.

4. **Brachmann SM, Ueki K, Engelman JA, Kahn RC, and Cantley LC**. Phosphoinositide 3-kinase catalytic subunit deletion and regulatory subunit deletion have opposite effects on insulin sensitivity in mice. *Mol Cell Biol* 25: 1596-1607, 2005.

5. **Cantley LC**. The phosphoinositide 3-kinase pathway. *Science* 296: 1655-1657, 2002.

6. **Cheatham B, Vlahos CJ, Cheatham L, Wang L, Blenis J, and Kahn CR**. Phosphatidylinositol 3-kinase activation is required for insulin stimulation of pp70 S6 kinase, DNA synthesis, and glucose transporter translocation. *Mol Cell Biol* 14: 4902-4911, 1994.

7. **Chen D, Mauvais-Jarvis F, Bluher M, Fisher SJ, Jozsi A, Goodyear LJ, Ueki K, and Kahn CR**. p50alpha/p55alpha phosphoinositide 3-kinase knockout mice exhibit enhanced insulin sensitivity. *Mol Cell Biol* 24: 320-329, 2004.

8. **Dhand R, Hara K, Hiles I, Bax B, Gout I, Panayotou G, Fry MJ, Yonezawa K, Kasuga M, and Waterfield MD**. PI 3-kinase: structural and functional analysis of intersubunit interactions. *EMBO J* 13: 511-521, 1994.

9. **Fruman DA, Cantley LC, and Carpenter CL**. Structural organization and alternative splicing of the murine phosphoinositide 3-kinase p85 alpha gene. *Genomics* 37: 113-121, 1996.

10. **Inukai K, Anai M, Van Breda E, Hosaka T, Katagiri H, Funaki M, Fukushima Y, Ogihara T, Yazaki Y, Kikuchi, Oka Y, and Asano T**. A novel 55-kDa regulatory subunit for phosphatidylinositol 3-kinase structurally similar to p55PIK Is generated by alternative splicing of the p85alpha gene. *J Biol Chem* 271: 5317-5320, 1996.

11. **Inukai K, Funaki M, Ogihara T, Katagiri H, Kanda A, Anai M, Fukushima Y, Hosaka T, Suzuki M, Shin BC, Takata K, Yazaki Y, Kikuchi M, Oka Y, and Asano T**. p85alpha gene generates three isoforms of regulatory subunit for phosphatidylinositol 3-kinase (PI 3-Kinase), p50alpha, p55alpha, and p85alpha, with different PI 3-kinase activity elevating responses to insulin. *J Biol Chem* 272: 7873-7882, 1997.

12. **Liu P, Gan W, Chin YR, Ogura K, Guo J, Zhang J, Wang B, Blenis J, Cantley LC, Toker A, Su B, and Wei W**. PtdIns(3,4,5)P3-Dependent Activation of the mTORC2 Kinase Complex. *Cancer Discov* 5: 1194-1209, 2015.

13. **McCurdy CE, Schenk S, Holliday MJ, Philp A, Houck JA, Patsouris D, MacLean PS, Majka SM, Klemm DJ, and Friedman JE**. Attenuated Pik3r1 expression prevents insulin resistance and adipose tissue macrophage accumulation in diet-induced obese mice. *Diabetes* 61: 2495-2505, 2012.

14. **Nelson VL, Jiang YP, Dickman KG, Ballou LM, and Lin RZ**. Adipose tissue insulin resistance due to loss of PI3K p110α leads to decreased energy expenditure and obesity. *Am J Physiol Endocrinol Metab* 306: E1205-1216, 2014.

15. **Okada T, Kawano Y, Sakakibara T, Hazeki O, and Ui M**. Essential role of phosphatidylinositol 3-kinase in insulin-induced glucose transport and antilipolysis in rat adipocytes. Studies with a selective inhibitor wortmannin. *J Biol Chem* 269: 3568-3573, 1994.

16. **Sanchez-Gurmaches J, Tang Y, Jespersen NZ, Wallace M, Martinez Calejman C, Gujja S, Li H, Edwards YJK, Wolfrum C, Metallo CM, Nielsen S, Scheele C, and Guertin DA**. Brown Fat AKT2 Is a Cold-Induced Kinase that Stimulates ChREBP-Mediated De Novo Lipogenesis to Optimize Fuel Storage and Thermogenesis. *Cell Metab* 27: 195-209.e196, 2018.

17. **Seale P, Conroe HM, Estall J, Kajimura S, Frontini A, Ishibashi J, Cohen P, Cinti S, and Spiegelman BM**. Prdm16 determines the thermogenic program of subcutaneous white adipose tissue in mice. *J Clin Invest* 121: 96-105, 2011.

18. **Shepherd PR, Withers DJ, and Siddle K**. Phosphoinositide 3-kinase: the key switch mechanism in insulin signalling. *Biochem J* 333 (Pt 3): 471-490, 1998.

19. **Terauchi Y, Tsuji Y, Satoh S, Minoura H, Murakami K, Okuno A, Inukai K, Asano T, Kaburagi Y, Ueki K, Nakajima H, Hanafusa T, Matsuzawa Y, Sekihara H, Yin Y, Barrett JC, Oda H, Ishikawa T, Akanuma Y, Komuro I, Suzuki M, Yamamura K, Kodama T, Suzuki H, Koyasu S, Aizawa S, Tobe K, Fukui Y, Yazaki Y, and Kadowaki T**. Increased insulin sensitivity and hypoglycaemia in mice lacking the p85 alpha subunit of phosphoinositide 3-kinase. *Nat Genet* 21: 230-235, 1999.

20. **Ueki K, Algenstaedt P, Mauvais-Jarvis F, and Kahn CR**. Positive and negative regulation of phosphoinositide 3-kinase-dependent signaling pathways by three different gene products of the p85alpha regulatory subunit. *Mol Cell Biol* 20: 8035-8046, 2000.

Chapter V

1. The Guide for the Care and Use of Laboratory Animals. *ILAR J* 57: NP, 2016.

2. **Acosta-Martínez M, Luo J, Elias C, Wolfe A, and Levine JE**. Male-biased effects of gonadotropin-releasing hormone neuron-specific deletion of the phosphoinositide 3-kinase regulatory subunit p85alpha on the reproductive axis. *Endocrinology* 150: 4203-4212, 2009.

3. **Barbatelli G, Murano I, Madsen L, Hao Q, Jimenez M, Kristiansen K, Giacobino JP, De Matteis R, and Cinti S**. The emergence of cold-induced brown adipocytes in mouse white fat depots is determined predominantly by white to brown adipocyte transdifferentiation. *Am J Physiol Endocrinol Metab* 298: E1244-1253, 2010.

4. **Bonet ML, Mercader J, and Palou A**. A nutritional perspective on UCP1-dependent thermogenesis. *Biochimie* 134: 99-117, 2017.

5. **Cannon B, and Nedergaard J**. Brown adipose tissue: function and physiological significance. *Physiol Rev* 84: 277-359, 2004.

6. **Collins S, Daniel KW, Petro AE, and Surwit RS**. Strain-specific response to beta 3-adrenergic receptor agonist treatment of diet-induced obesity in mice. *Endocrinology* 138: 405-413, 1997.

7. **Cornier MA, Bergman BC, and Bessesen DH**. The effects of short-term overfeeding on insulin action in lean and reduced-obese individuals. *Metabolism* 55: 1207-1214, 2006.

8. **Cousin B, Casteilla L, Dani C, Muzzin P, Revelli JP, and Penicaud L**. Adipose tissues from various anatomical sites are characterized by different patterns of gene expression and regulation. *Biochem J* 292 (Pt 3): 873-876, 1993.

9. **Cousin B, Cinti S, Morroni M, Raimbault S, Ricquier D, Pénicaud L, and Casteilla L**. Occurrence of brown adipocytes in rat white adipose tissue: molecular and morphological characterization. *J Cell Sci* 103 (Pt 4): 931-942, 1992.

10. **Cui X, Nguyen NL, Zarebidaki E, Cao Q, Li F, Zha L, Bartness T, Shi H, and Xue B**. Thermoneutrality decreases thermogenic program and promotes adiposity in high-fat diet-fed mice. *Physiol Rep* 4: 2016.

11. **David JM, Chatziioannou AF, Taschereau R, Wang H, and Stout DB**. The hidden cost of housing practices: using noninvasive imaging to quantify the metabolic demands of chronic cold stress of laboratory mice. *Comp Med* 63: 386-391, 2013.

12. **DeRuisseau LR, Parsons AD, and Overton JM**. Adaptive thermogenesis is intact in B6 and A/J mice studied at thermoneutrality. *Metabolism* 53: 1417-1423, 2004.

13. **Even PC, and Blais A**. Increased Cost of Motor Activity and Heat Transfer between Non-Shivering Thermogenesis, Motor Activity, and Thermic Effect of Feeding in Mice Housed at Room Temperature - Implications in Pre-Clinical Studies. *Front Nutr* 3: 43, 2016.

14. **Feldmann HM, Golozoubova V, Cannon B, and Nedergaard J**. UCP1 ablation induces obesity and abolishes diet-induced thermogenesis in mice exempt from thermal stress by living at thermoneutrality. *Cell Metab* 9: 203-209, 2009.

15. **Giles DA, Moreno-Fernandez ME, Stankiewicz TE, Graspeuntner S, Cappelletti M, Wu D, Mukherjee R, Chan CC, Lawson MJ, Klarquist J, Sünderhauf A, Softic S, Kahn CR, Stemmer K, Iwakura Y, Aronow BJ, Karns R, Steinbrecher KA, Karp CL, Sheridan R, Shanmukhappa SK, Reynaud D, Haslam DB, Sina C, Rupp J, Hogan SP, and Divanovic S**. Thermoneutral housing exacerbates nonalcoholic fatty liver disease in mice and allows for sex-independent disease modeling. *Nat Med* 23: 829-838, 2017.

16. **Giles DA, Moreno-Fernandez ME, Stankiewicz TE, Graspeuntner S, Cappelletti M, Wu D, Mukherjee R, Chan CC, Lawson MJ, Klarquist J, Sünderhauf A, Softic S, Kahn CR, Stemmer K, Iwakura Y, Aronow BJ, Karns R, Steinbrecher KA, Karp CL, Sheridan R, Shanmukhappa SK, Reynaud D, Haslam DB, Sina C, Rupp J, Hogan SP, and Divanovic S**. Thermoneutral housing exacerbates nonalcoholic fatty liver disease in mice and allows for sex-independent disease modeling. *Nat Med* 2017.

17. **Gordon CJ**. The mouse thermoregulatory system: Its impact on translating biomedical data to humans. *Physiol Behav* 179: 55-66, 2017.

18. **Guerra C, Koza RA, Yamashita H, Walsh K, and Kozak LP**. Emergence of brown adipocytes in white fat in mice is under genetic control. Effects on body weight and adiposity. *J Clin Invest* 102: 412-420, 1998.

19. **Hartmann H, Beckh K, and Jungermann K**. Direct control of glycogen metabolism in the perfused rat liver by the sympathetic innervation. *Eur J Biochem* 123: 521-526, 1982.

20. **Hocking SL, Chisholm DJ, and James DE**. Studies of regional adipose transplantation reveal a unique and beneficial interaction between subcutaneous adipose tissue and the intra-abdominal compartment. *Diabetologia* 51: 900-902, 2008.

21. **Jankovic A, Golic I, Markelic M, Stancic A, Otasevic V, Buzadzic B, Korac A, and Korac B**. Two key temporally distinguishable molecular and cellular components of white adipose tissue browning during cold acclimation. *J Physiol* 593: 3267-3280, 2015.

22. **Kim J-Y, van de Wall E, Laplante M, Azzara A, Trujillo ME, Hofmann SM, Schraw T, Durand JL, Li H, Li G, Jelicks LA, Mehler MF, Hui DY, Deshaies Y, Shulman GI, Schwartz GJ, and Scherer PE**. Obesity-associated improvements in metabolic profile through expansion of adipose tissue. *The Journal of Clinical Investigation* 117: 2621-2637, 2007.

23. **Kim JK, Fillmore JJ, Sunshine MJ, Albrecht B, Higashimori T, Kim DW, Liu ZX, Soos TJ, Cline GW, O'Brien WR, Littman DR, and Shulman GI**. PKC-theta knockout mice are protected from fat-induced insulin resistance. *J Clin Invest* 114: 823-827, 2004.

24. **Kim JK, Kim YJ, Fillmore JJ, Chen Y, Moore I, Lee J, Yuan M, Li ZW, Karin M, Perret P, Shoelson SE, and Shulman GI**. Prevention of fat-induced insulin resistance by salicylate. *J Clin Invest* 108: 437-446, 2001.

25. **Kim JY, van de Wall E, Laplante M, Azzara A, Trujillo ME, Hofmann SM, Schraw T, Durand JL, Li H, Li G, Jelicks LA, Mehler MF, Hui DY, Deshaies Y, Shulman GI, Schwartz GJ, and Scherer PE**. Obesity-associated improvements in metabolic profile through expansion of adipose tissue. *J Clin Invest* 117: 2621-2637, 2007.

26. **Klein S, Fontana L, Young VL, Coggan AR, Kilo C, Patterson BW, and Mohammed BS**. Absence of an effect of liposuction on insulin action and risk factors for coronary heart disease. *N Engl J Med* 350: 2549-2557, 2004.

27. **Lee YS, Li P, Huh JY, Hwang IJ, Lu M, Kim JI, Ham M, Talukdar S, Chen A, Lu WJ, Bandyopadhyay GK, Schwendener R, Olefsky J, and Kim JB**. Inflammation is necessary for long-term but not short-term high-fat diet-induced insulin resistance. *Diabetes* 60: 2474-2483, 2011.

28. **Luo J, McMullen JR, Sobkiw CL, Zhang L, Dorfman AL, Sherwood MC, Logsdon MN, Horner JW, DePinho RA, Izumo S, and Cantley LC**. Class IA phosphoinositide 3-kinase regulates heart size and physiological cardiac hypertrophy. *Mol Cell Biol* 25: 9491-9502, 2005.

29. **Miyazaki Y, Mahankali A, Matsuda M, Mahankali S, Hardies J, Cusi K, Mandarino LJ, and DeFronzo RA**. Effect of pioglitazone on abdominal fat distribution and insulin sensitivity in type 2 diabetic patients. *J Clin Endocrinol Metab* 87: 2784-2791, 2002.

30. **Nedergaard J, and Cannon B**. The browning of white adipose tissue: some burning issues. *Cell Metab* 20: 396-407, 2014.

31. **Osborn O, and Olefsky JM**. The cellular and signaling networks linking the immune system and metabolism in disease. *Nat Med* 18: 363-374, 2012.

32. **Petersen MC, Vatner DF, and Shulman GI**. Regulation of hepatic glucose metabolism in health and disease. *Nat Rev Endocrinol* 2017.

33. **Porter SA, Massaro JM, Hoffmann U, Vasan RS, O'Donnel CJ, and Fox CS**. Abdominal subcutaneous adipose tissue: a protective fat depot? *Diabetes Care* 32: 1068-1075, 2009.
34. **Saltiel AR, and Olefsky JM**. Inflammatory mechanisms linking obesity and metabolic disease. *J Clin Invest* 127: 1-4, 2017.

35. **Shi H, Kokoeva MV, Inouye K, Tzameli I, Yin H, and Flier JS**. TLR4 links innate immunity and fatty acid-induced insulin resistance. *J Clin Invest* 116: 3015-3025, 2006.

36. **Snijder MB, Visser M, Dekker JM, Goodpaster BH, Harris TB, Kritchevsky SB, De Rekeneire N, Kanaya AM, Newman AB, Tylavsky FA, Seidell JC, and Study HA**. Low subcutaneous thigh fat is a risk factor for unfavourable glucose and lipid levels, independently of high abdominal fat. The Health ABC Study. *Diabetologia* 48: 301-308, 2005.

37. **Stanford KI, Middelbeek RJ, Townsend KL, An D, Nygaard EB, Hitchcox KM, Markan KR, Nakano K, Hirshman MF, Tseng YH, and Goodyear LJ**. Brown adipose tissue regulates glucose homeostasis and insulin sensitivity. *J Clin Invest* 123: 215-223, 2013.

38. **Stanford KI, Middelbeek RJ, Townsend KL, Lee MY, Takahashi H, So K, Hitchcox KM, Markan KR, Hellbach K, Hirshman MF, Tseng YH, and Goodyear LJ**. A novel role for subcutaneous adipose tissue in exercise-induced improvements in glucose homeostasis. *Diabetes* 64: 2002-2014, 2015.

39. **Stemmer K, Kotzbeck P, Zani F, Bauer M, Neff C, Muller TD, Pfluger PT, Seeley RJ, and Divanovic S**. Thermoneutral housing is a critical factor for immune function and diet-induced obesity in C57BL/6 nude mice. *Int J Obes (Lond)* 39: 791-797, 2015.

40. **Tankó LB, Bagger YZ, Alexandersen P, Larsen PJ, and Christiansen C**. Peripheral adiposity exhibits an independent dominant antiatherogenic effect in elderly women. *Circulation* 107: 1626-1631, 2003.

41.**Tao C, Holland WL, Wang QA, Shao M, Jia L, Sun K, Lin X, Kuo YC, Johnson JA, Gordillo R, Elmquist JK, and Scherer PE**. Short-Term vs. Long-Term Effects of Adipocyte Toll-like Receptor 4 Activation on Insulin Resistance in Male Mice. *Endocrinology* 2017.

42. **Tian XY, Ganeshan K, Hong C, Nguyen KD, Qiu Y, Kim J, Tangirala RK, Tonotonoz P, and Chawla A**. Thermoneutral Housing Accelerates Metabolic Inflammation to Potentiate Atherosclerosis but Not Insulin Resistance. *Cell Metab* 23: 165-178, 2016.

43. **Tian XY, Ganeshan K, Hong C, Nguyen KD, Qiu Y, Kim J, Tangirala RK, Tontonoz P, Tonotonoz P, and Chawla A**. Thermoneutral Housing Accelerates Metabolic Inflammation to Potentiate Atherosclerosis but Not Insulin Resistance. *Cell Metab* 23: 165-178, 2016.

44. **Tran TT, Yamamoto Y, Gesta S, and Kahn CR**. Beneficial effects of subcutaneous fat transplantation on metabolism. *Cell Metab* 7: 410-420, 2008.

45. **van Marken Lichtenbelt WD, Vanhommerig JW, Smulders NM, Drossaerts JM, Kemerink GJ, Bouvy ND, Schrauwen P, and Teule GJ**. Cold-activated brown adipose tissue in healthy men. *N Engl J Med* 360: 1500-1508, 2009.

46. **Virtanen KA, Lidell ME, Orava J, Heglind M, Westergren R, Niemi T, Taittonen M, Laine J, Savisto NJ, Enerbäck S, and Nuutila P**. Functional brown adipose tissue in healthy adults. *N Engl J Med* 360: 1518-1525, 2009.

47. **Wang J, Obici S, Morgan K, Barzilai N, Feng Z, and Rossetti L**. Overfeeding rapidly induces leptin and insulin resistance. *Diabetes* 50: 2786-2791, 2001.

48. **Weiss EP, Racette SB, Villareal DT, Fontana L, Steger-May K, Schechtman KB, Klein S, Holloszy JO, and Group WUSoMC**. Improvements in glucose tolerance and insulin action induced by increasing energy expenditure or decreasing energy intake: a randomized controlled trial. *Am J Clin Nutr* 84: 1033-1042, 2006.

49. **Winn NC, Vieira-Potter VJ, Gastecki ML, Welly RJ, Scroggins RJ, Zidon TM, Gaines TL, Woodford ML, Karasseva NG, Kanaley JA, Sacks HS, and Padilla J**. Loss of UCP1 exacerbates Western diet-induced glycemic dysregulation independent of changes in body weight in female mice. *Am J Physiol Regul Integr Comp Physiol* 312: R74-R84, 2017.

Chapter VI

1. **Albert V, Svensson K, Shimobayashi M, Colombi M, Muñoz S, Jimenez V, Handschin C, Bosch F, and Hall MN**. mTORC2 sustains thermogenesis via Akt-induced glucose uptake and glycolysis in brown adipose tissue. *EMBO Mol Med* 8: 232-246, 2016.

2. **Ayala JE, Bracy DP, Malabanan C, James FD, Ansari T, Fueger PT, McGuinness OP, and Wasserman DH**. Hyperinsulinemic-euglycemic clamps in conscious, unrestrained mice. *J Vis Exp* 2011.

3. **Brøns C, Jensen CB, Storgaard H, Hiscock NJ, White A, Appel JS, Jacobsen S, Nilsson E, Larsen CM, Astrup A, Quistorff B, and Vaag A**. Impact of short-term high-fat feeding on glucose and insulin metabolism in young healthy men. *J Physiol* 587: 2387-2397, 2009.

4. **Cantley LC**. The phosphoinositide 3-kinase pathway. *Science* 296: 1655-1657, 2002.
5. **Chen D, Mauvais-Jarvis F, Bluher M, Fisher SJ, Jozsi A, Goodyear LJ, Ueki K, and Kahn CR**. p50alpha/p55alpha phosphoinositide 3-kinase knockout mice exhibit enhanced insulin sensitivity. *Mol Cell Biol* 24: 320-329, 2004.

6. **Cui X, Nguyen NL, Zarebidaki E, Cao Q, Li F, Zha L, Bartness T, Shi H, and Xue B**. Thermoneutrality decreases thermogenic program and promotes adiposity in high-fat diet-fed mice. *Physiol Rep* 4: 2016.

7. **Ganeshan K, and Chawla A**. Warming the mouse to model human diseases. *Nat Rev Endocrinol* 13: 458-465, 2017.

8. **Lee YS, Li P, Huh JY, Hwang IJ, Lu M, Kim JI, Ham M, Talukdar S, Chen A, Lu WJ, Bandyopadhyay GK, Schwendener R, Olefsky J, and Kim JB**. Inflammation is necessary for long-term but not short-term high-fat diet-induced insulin resistance. *Diabetes* 60: 2474-2483, 2011.

9. **McCurdy CE, Schenk S, Holliday MJ, Philp A, Houck JA, Patsouris D, MacLean PS, Majka SM, Klemm DJ, and Friedman JE**. Attenuated Pik3r1 expression prevents insulin resistance and adipose tissue macrophage accumulation in diet-induced obese mice. *Diabetes* 61: 2495-2505, 2012.

10. **Sanchez-Gurmaches J, Tang Y, Jespersen NZ, Wallace M, Martinez Calejman C, Gujja S, Li H, Edwards YJK, Wolfrum C, Metallo CM, Nielsen S, Scheele C, and Guertin DA**. Brown Fat AKT2 Is a Cold-Induced Kinase that Stimulates ChREBP-Mediated De Novo Lipogenesis to Optimize Fuel Storage and Thermogenesis. *Cell Metab* 27: 195-209.e196, 2018.